CZECH TECHNICAL UNIVERSITY IN PRAGUE

Faculty of Mechanical Engineering

Department of Energy Engineering

Low-temperature adsorption for post-combustion CO_2 capture from fossil fuel combustion

by

Ing. Marek Nedoma

Programme type:	Doctoral
Study Programme:	Energy and Process Engineering
Supervisor:	prof. Ing. Jan Hrdlička, Ph.D.
Co-supervisor:	Ing. Matěj Vodička, Ph.D.

Prague 2023

Abstract

This thesis investigated the application of low-temperature adsorption for CO_2 separation in post-combustion CO_2 capture (PCC) applications, focusing on both technical and economic aspects. Adsorption is a well-documented process that remains limited to laboratory-scale applications and requires a theoretical approach to assess industrial applications. Decentralised energy systems with CO_2-lean emissions were selected for such an assessment. These systems are often overlooked at the expense of large-scale coal power generation and lack CO_2 capture solutions. The key contribution of the thesis is the development of mathematical model in *MATLAB* to predict various breakthrough experiments at elevated pressure and continuous operation of vacuum-swing adsorption (VSA) cycle to assess the design and economics of PCC in urban-scale cogeneration and heat plant (CHP).

The modelling first focused on simulating CO_2 breakthrough curves on zeolite 13X in a fixed-bed adsorber, which were successfully predicted, and model validated. The subsequent sensitivity analysis helped to understand the robustness of mathematical modelling, numerical principles, and the impact of key parameters on prediction accuracy. Furthermore, combining the model with empirical process-design criteria and literature review findings allowed for the initial proposal of a VSA system to capture CO_2 from emissions produced by a 4.3 MW natural gas-fired CHP, which was selected as a representative of an industrial application. The model was then refined to simulate a continuous 4-step VSA process under non-isothermal and non-isobaric conditions and bring the initial proposal closer to reality. As a consequence, a ready-to-operate CO_2 capture plant capable of recovering highly pure CO_2 was theoretically designed. The design procedure adhered to the real operating conditions and consisted of selective catalytic reduction, two-step dehydration combining condenser with 3-step temperature-swing adsorption using zeolite 5A, 4-step VSA using zeolite 13X, and a series of auxiliary components. Finally, an economic assessment was carried out for all sub-systems and components found in the CO_2 capture plant, providing valuable end-user insights.

Keywords

Adsorption, Breakthrough experiments, Economic assessment, Finite-volume method, Post-combustion carbon dioxide capture, Process modelling, Vacuum-swing adsorption.

Abstrakt

Tato disertační práce se zabývá využitím nízkoteplotní adsorpce pro post-combustion záchyt CO_2 (PCC) se zaměřením na technické a ekonomické aspekty. Adsorpce je dobře zdokumentovaný proces, který je však omezen na laboratorní aplikace, což v rámci studia průmyslových aplikací vyžaduje teoretický přístup. Decentralizované spalovací energetické systémy produkující spaliny s nízkou koncentrací CO_2 byly vybrány, protože představují často přehlíženou oblast na úkor velkých uhelných elektráren, která postrádá řešení záchytu CO_2. Hlavní přínos práce spočívá ve vývoji matematického modelu v prostředí *MATLAB* s cílem predikovat experimentálně změřené průrazové křivky při zvýšeném tlaku a kontinuální provoz vacuum-swing adsorpčního cyklu (VSA) se střídavým tlakem pro návrh a ekonomickou analýzu PCC v malokapacitní kogenerační jednotce (CHP).

Modelování bylo nejprve použito pro simulaci průrazových křivek CO_2 na zeolitu 13X v adsorbéru s pevným ložem, které byly úspěšně predikovány a model validován. Následná citlivostní analýza pomohla lépe porozumět matematickému modelování, numerickým principům a míře vlivu klíčových parametrů na přesnost predikce. Zkombinování modelu s návrhovými empirickými kritérii a poznatky z literatury umožnilo počáteční návrh VSA systému pro záchyt CO_2 ze spalin 4.3 MW kogenerační jednotky na zemní plyn, která byla vybrána jako zástupce průmyslové aplikace. Model byl následně upraven do podoby umožňující simulovat kontinuální 4-kroký VSA proces za neizotermických a neizobarických podmínek, což posunulo počáteční návrh blíže k realitě. Důsledkem byl teoretický procesní návrh záchytu CO_2 v elektrárně, která je schopna získávat CO_2 s vysokou čistotou. Návrhový postup uvažoval reálné provozní podmínky a zahrnoval selektivní katalytickou redukci, dvou stupňovou dehydrataci pomocí kondenzátoru a 3-krokové adsorpce se střídáním teploty (TSA) používající zeolit 5A, 4-krokovou VSA se zeolitem 13X a sérii pomocných komponent. Nakonec byla provedena ekonomická analýza všech dílčích systémů a komponent v tomto procesu, což koncovému uživateli poskytuje cenné informace.

Klíčová slova

Adsorpce, Metoda konečných objemů, Ekonomická analýza, Numerické procesní modelování, Post-combustion záchyt oxidu uhličitého, Vacuum-swing adsorpce.

Acknowledgment

My thanks go first to my supervisor, ***Professor Jan Hrdlička***, for his mentorship and valuable research guidance, and financial support throughout my Ph.D. and internship abroad. Second, to ***my family*** for making this journey easier and more enjoyable. Third, to ***Dr. Michal Netušil*** for his continuous cooperation on various topics and to ***Professor Pavel Ditl*** for his encouragement and consultation on my work, both from the Department of Process Engineering; to ***Dr. Marek Staf*** for conducting experimental breakthrough measurements at the University of Chemistry and Technology in Prague, and to ***Professor Jiří Fürst*** from the Department of Technical Mathematics for his advice on numerical mathematics. Finally, I am grateful to ***Dr. Olga Šolcová*** and ***Dr. Karel Soukup*** from the Catalysis and Reaction Engineering Research Group at the Institute of Chemical Process Fundamentals of the ASCR in Prague for their assistance with material characterisation at their laboratory.

My research was financially supported by the Student Grant Competition of CTU, under Grant No. *SGS19/103/OHK2/2T/12* and by the Technology Agency of the Czech Republic (TACR) within the project *TK03030167* "Low emission technologies of energy conversion of biomass and alternative fuels", which is gratefully acknowledged.

Declaration of Authorship

I hereby declare that this thesis is my own work, developed independently under the guidance of my supervisor. I have acknowledged all sources of information in the literature references. Unauthorised third-party services have not been employed in the creation of this thesis.

I understand that my work relates to the rights and obligations under the *Act No. 121/2000 Sb.*, the Copyright Act, as amended, in particular the fact that the Czech Technical University in Prague has the right to conclude a license agreement on the use of this work as a school-work pursuant to *Section 60 paragraph 1* of the Copyright Act.

In Prague, ...

Table of Content

List of Figures

List of Tables

Nomenclature

ROMAN LETTERS

A	area	m^3
b	adsorption isotherm parameter (Langmuir, Sips, Tóth)	$\mathrm{m}^3_{\mathrm{gas}}.\mathrm{mol}^{-1}_{\mathrm{gas}}$
b_0	Langmuir isotherm parameter	$\mathrm{m}^3_{\mathrm{gas}}.\mathrm{mol}^{-1}_{\mathrm{gas}}$
Bi	Biot number (mass transfer)	$-$
c	gas phase concentration	$\mathrm{m}^3_{\mathrm{gas}}.\mathrm{mol}^{-1}_{\mathrm{gas}}$
C	cost function	\$, €
$C_{p,a}$	heat capacity of adsorbed gas phase (adsorbate)	$\mathrm{J}.(\mathrm{mol}.\mathrm{K})^{-1}$
$C_{p,g}$	heat capacity of gas phase	$\mathrm{J}.(\mathrm{mol}.\mathrm{K})^{-1}$
$C_{p,s}$	heat capacity of solid phase (adsorbent)	$\mathrm{J}.(\mathrm{kg}.\mathrm{K})^{-1}$
$C_{p,w}$	heat capacity of column wall	$\mathrm{J}.(\mathrm{kg}.\mathrm{K})^{-1}$
d	Langmuir isotherm parameter	$\mathrm{m}^3_{\mathrm{gas}}.\mathrm{mol}^{-1}_{\mathrm{gas}}$
d_0	Langmuir isotherm parameter	$\mathrm{m}^3_{\mathrm{gas}}.\mathrm{mol}^{-1}_{\mathrm{gas}}$
d_{in}	inner diameter of adsorption column wall	m
d_p	adsorbent particle diameter	m
d_{pore}	adsorbent pore diameter	m
d_{out}	outer diameter of adsorption column wall (Figure 8)	m
D_{ax}	axial dispersion coefficient (gas)	$\mathrm{m}^2.\mathrm{s}^{-1}$
D_K	Knudsen diffusion coefficient (gas), $D_K = \left(\frac{y_{CO_2}}{D_{K,CO_2}} + \frac{y_{N_2}}{D_{K,N_2}}\right)^{-1}$	$\mathrm{m}^2.\mathrm{s}^{-1}$
D_m	molecular diffusion coefficient (gas)	$\mathrm{m}^2.\mathrm{s}^{-1}$
D_p	adsorbent pore diffusion coefficient (gas)	$\mathrm{m}^2.\mathrm{s}^{-1}$
$D_{p,eff}$	adsorbent pore effective diffusion coefficient (gas)	$\mathrm{m}^2.\mathrm{s}^{-1}$
e	Euler number, $\mathrm{e} \approx 2.7183$	$-$
f	conserved quantity (unit is a state variable dependent)	varies
F_M	material factor	$-$
F_P	pressure factor	$-$
g	acceleration due to gravity, $g \approx 9.81$	$\mathrm{m}.\mathrm{s}^{-2}$
h_{in}	inside heat transfer coefficient	$\mathrm{W}.(\mathrm{m}^2.\mathrm{K})^{-1}$
h_{out}	outside heat transfer coefficient	$\mathrm{W}.(\mathrm{m}^2.\mathrm{K})^{-1}$

k	Freundlich isotherm parameter (Table 1)	$-$
	mass transfer coefficient into the particle	s^{-1}
k_f	external mass transfer rate	s^{-1}
K_{ax}	effective axial thermal conductivity coefficient (gas)	$\mathrm{W.(m.K)^{-1}}$
K_w	thermal conductivity of column wall	$\mathrm{W.(m.K)^{-1}}$
L	column length	m
m	mass (adsorbent) / weight	kg
M	molar weight	$\mathrm{mol.kg^{-1}}$
n	adsorption isotherm parameter (Freundlich, Sips)	$-$
P	pressure	Pa, bar
	power	kW
Pe	Péclet number, $Pe = d_p v_0 / D_{ax}$ (Pe_∞ = limiting value)	$-$
PROD	productivity (cycle)	$\mathrm{mol_{gas}.\left(m^3_{ads}.s\right)^{-1}}$
PUR	purity (gas species)	%
q	gas concentration in the solid phase (adsorbed amount)	$\mathrm{mol_{gas}.kg^{-1}_{ads}}$
q^*	gas concentration in the solid phase at equilibrium	$\mathrm{mol_{gas}.kg^{-1}_{ads}}$
q_s	single-site adsorption isotherm equilibrium constant (saturation state)	$\mathrm{m^3_{gas}.mol^{-1}_{gas}}$, $\mathrm{mol_{gas}.kg^{-1}_{ads}}$
q_{sb}	Langmuir constant for adsorption of site "b"	$\mathrm{m^3_{gas}.mol^{-1}_{gas}}$
q_{sd}	Langmuir constant for adsorption of site "d"	$\mathrm{m^3_{gas}.mol^{-1}_{gas}}$
q	gas concentration in the solid phase (adsorbed amount)	$\mathrm{m^3_{gas}.mol^{-1}_{gas}}$
r	successive slope ratio	$-$
r_p	adsorbent particle radius	m
r_{in}	inner radius of adsorption column wall	m
r_{out}	inner radius of adsorption column wall	m
R_g	universal gas constant = 8.314	$\mathrm{(Pa.m^3).(mol.K)^{-1}}$
Re_p	Reynolds number for particle, $Re_p = \rho_g v_0 d_p / \mu_g$	$-$
REC	recovery (gas species or cycle)	%
S_b	adsorbent bed area	$\mathrm{m^2}$
S_{BET}	BET surface area	$\mathrm{m^2.g^{-1}_{ads}}$
Sc	Schmidt number, $Sc = \mu_g / \rho_g D_m$	$-$
Sh	Sherwood number, $Sh = f(Re_p, Sc)$	$-$

	Tóth isotherm parameter (Table 1)	$-$
t	time ("a measure of time", duration of step in adsorption system)	s
	thickness (column wall)	m
T	temperature (gas)	K
v	interstitial velocity (gas), $v = v_0/\varepsilon_b$	$\mathrm{m.\,s^{-1}}$
v_0	superficial velocity (gas)	$\mathrm{m.\,s^{-1}}$
v_f	fluidisation velocity (gas)	$\mathrm{m.\,s^{-1}}$
V	control volume (finite volume scheme)	$\mathrm{m^3}$
V_m	material volume (column packing) (Figure 8)	$\mathrm{m^3}$
V_p	adsorbent particle volume	$\mathrm{m^3}$
V_{pore}	adsorbent pore volume	$\mathrm{m^3.\,kg_{ads}^{-1}}$
W	work	W *or* J
y	concentration molar fraction (gas components), $y_i = c_i/c$	$-$
z	axial coordinate (column)	m

GREEK LETTERS

α	rate of pressure change	$\mathrm{s^{-1}}$
β	coefficient in Equation (17)	$-$
β_{mass}	dimensionless parameter in Equations (27) and (29)	$-$
γ	Poisson constant = 1.4,	$-$
	coefficient in Equation (17)	$-$
Δ	measure of change	$-$
ΔH	change of adsorption enthalpy (heat of adsorption)	$\mathrm{J.\,mol^{-1}}$
ΔU	change of adsorption internal energy	$\mathrm{J.\,mol^{-1}}$
δ	constant value = 10^{-10} (successive slope ratio)	$-$
ε_b	bed voidage	$-$
$\overline{\varepsilon}_b$	mean value of bed voidage	$-$
ε_p	adsorbent particle voidage	$-$
η_{pump}	vacuum pump efficiency	$-$
μ_g	dynamic viscosity	$\mathrm{kg.\,(m.\,s)^{-1}}$
ν	molar volume of gas	$\mathrm{m^3.\,mol^{-1}}$
π_1	$\pi - 1$ factor, $\pi_1 = (v_0 \varepsilon_p d_p^2 \varepsilon_b)/\,(4\,L_{col} D_{p,eff}(1\,-\,\varepsilon_b))$	$-$

π_2	$\pi - 2$ factor	$-$
ρ_b	adsorbent bed density	$\mathrm{kg.\,m^{-3}}$
ρ_g	gas density	$\mathrm{kg.\,m^{-3}}$
ρ_p	adsorbent particle density, $\rho_p = \rho_b/(\varepsilon_b - 1)$	$\mathrm{kg.\,m^{-3}}$
τ_p	tortuosity factor (adsorbent particle)	$-$
ϕ	flux limiter function	$-$

SUBSCRIPTS

0	initial (value)
$13X$	zeolite 13X
a	ambient
ads	adsorbent
ax	axial (coordinate, direction of gas flow)
A	adsorption (step)
AV	axial vane (flue gas fan)
b	adsorbent bed, site "b" of adsorbing gas
BD	blowdown (step)
col	column
$cond$	condenser
CR	centrifugal radial (flue gas fan)
emp	empty space
Ev	evacuation (step)
fan	flue gas fan
$feed$	inlet state (column or gas)
g	gas, gauge (pressure)
H	high (pressure boundary in adsorption cycle)
$H-E$	heat exchanger
i	*i*-th component (gas)
in	inner / internal (diameter)
I	intermediate (pressure boundary in adsorption cycle)
j	control volume spatial index (finite volume scheme)
L	low (pressure boundary in adsorption cycle)

max	maximum value (interstitial gas velocity)
out	outer / external (diameter)
p	adsorbent particle
$pore$	adsorbent particle pore
s	saturation state (adsorbent)
SV	switching valve (solenoid valve)
TSA	temperature swing adsorption
VP	vacuum pump
VSA	vacuum swing adsorption
w	column wall
WP	water pump
WT	water tank

ACRONYMS

AC	Activated carbon
ads	Adsorbent
ASU	Air separation unit (Figure 2)
AV	Axial vane (flue gas fan) (*Table 13*)
BEM	Bonnet one-pass shell fixed type (condenser / heat exchanger geometry)
CaL	Calcium looping (combustion)
CAPEX	Capital expenditures
CCS	Carbon capture and storage
CEPCI	Chemical engineering plant cost index
CHP	Combined heat and power
CLC	Chemical looping combustion
CR	Centrifugal radial (flue gas fan) (*Table 13*)
CRF	Capital recovery factor
CS	Carbon steel
CSS	Cyclic steady state
CW	Cooling water (*Figure 16*)
deNOx	Removal of nitric oxides (technology)
DR-VPSA	Dual-reflux vacuum-pressure swing adsorption (*Table 5*)
DSL	Dual-site Langmuir (isotherm model)

G ⇋ G	Gas-gas (heat exchanger) (*Figure 16*)
EU	European Union
FVM	Finite volume method
H-E	Heat exchanger (*Figure 16*)
IR	Infrared
IUPAC	International Union of Pure and Applied Chemistry
k€, k$	1000 €, $1000 (*Table 13*)
L ⇋ G	Liquid-gas (heat exchanger) (*Figure 16*)
LDF	Linear driving force (model)
MEA	Monoethanolamine
MOF	Metal-organic framework
NIST	National Institute of Standards and Technology
ODE	Ordinary differential equations
OPEX	Operating expenditures
P&ID	Piping and instrumentation diagram
PCC	Post-combustion CO_2 capture
PDE	Partial differential equations
PE	Pressure equalisation
PI	Performance indicator (adsorption process)
PSA	Pressure swing adsorption
PTSA	Pressure-temperature swing adsorption
RH	Relative humidity
RPSA	Rapid-pressure swing adsorption
RTSA	Rapid-temperature swing adsorption
SCR	Selective catalytic reduction
SS316	Stainless-steel S316 (high-grade steel)
SSL	Single-site Langmuir (isotherm model)
STP	Standard temperature and pressure: 273.15 K and 101325 Pa (*Figure 16*)
TAC	Total annualised cost
TDC	Total direct cost
TEA	Techno-economic analysis
TEMA	Tubular Exchanger Manufacturers Association
TMBE	Total mass balance error
TRL	Technology readiness level

TSA	Temperature swing adsorption
UCT	University of Chemistry and Technology
VPSA	Vacuum-pressure swing adsorption
VSA	Vacuum swing adsorption

Chapter 1

1 Introduction

Ongoing climate change is often associated with a strong reliance on the fossil fuel industry to satisfy the energy demand of the growing population and increasing gross domestic product per capita. Today, most of the energy is generated from carbon-containing fossil fuels, whereas the highest emissions are observed from burning coal. The emissions produced contain several heat-trapping gases, however, particular attention is paid to carbon dioxide (CO_2), whose concentration in the atmosphere increased from 280 ppm and exceeded 400 ppm for the first time, from the preindustrial era [1-3]. This called for the setting of a global target of carbon neutrality through the *Paris Climate Agreement* [4] and gave rise to the *European Green Deal*, with the aim of making Europe the first climate-neutral continent by 2050. Within its scope, reducing the carbon footprint is one of many goals to be met and addressed in a wide range of areas [5].

Meeting this goal in the power generation sector requires a rapid but smooth transition to renewable energy, making immediate diversion from fossil fuels difficult, thus promoting the urgent need to develop CO_2 capture technologies. So far, various CO_2 capture technologies have been developed onshore: *i)* single-process flue gas treatment technologies, *ii)* multi-process (*i.e.* hybrid) flue gas treatment technologies combining two or more separation techniques, *iii)* oxy-fuel combustion, and *iv)* "other technologies", for example, electrochemical separation (*i.e.* fuel cell conversion), or inherent CO_2 capture (*e.g.* chemical-looping combustion) [6]. In addition, offshore CO_2 capture focusing on reducing the carbon footprint of cargo ship engines is already being studied [7]. None of these technologies has reached full commercial-scale deployment, however, absorption, adsorption, and cryogenic separation onshore are at the threshold of technology readiness levels (TRL) 9 [6, 8]. CO_2 capture from power plants or other energy resources can be divided according to their location relative to the combustion process.

CO_2 capture in industrial combustion processes

CO_2 capture technologies for the combustion processes can be divided into three basic categories: *1)* post-combustion and *2)* pre-combustion technologies, and *3)* oxy-fuel combustion, as presented in Figure 1. Regardless of the technology used, it is the most expensive part of carbon capture and storage (CCS) processes, accounting for about 70 - 80 % of total CO_2 capture costs consisting of CO_2 capture, transport, and storage [9].

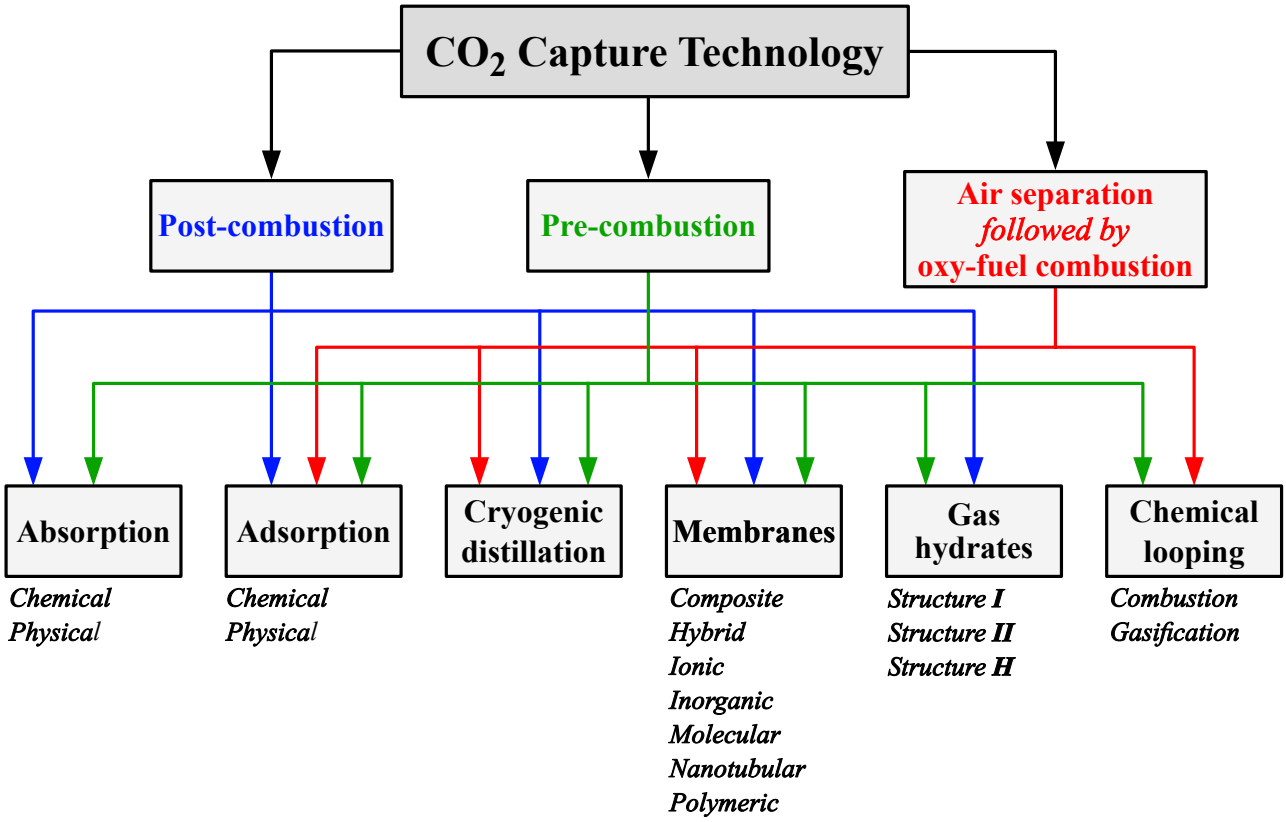

Figure 1. CO_2 capture technologies [10, 11].

1) Post-combustion

CO_2 capture takes place downstream of the combustion process. The processed gas is characterised by relatively low pressure and temperature, close to ambient conditions. A technology of choice for PCC is chemical absorption with amine-based solvents such as monoethanolamine (MEA) or ammonia and alkali-based, but its feasibility strongly depends on the CO_2 concentration in the processed gas and its volumetric flow. The most common alternatives studied are physical absorption, adsorption on solids, membrane and cryogenic separations, mineralisation, and recently hybrid systems consisting of more than two different processes. These technologies found great application in retrofitting already built coal and gas power plants, because their direct integration does not affect the power plant concept. PCC unit is usually placed at the end of the flue gas cleaning process due to the requirement of flue gas pre-treatment to remove reactive gases and particulate matter and, depending on the technology used, water vapor. The main disadvantage lies in the low CO_2 concentration in the processed gas, ranging, in traditional power plants, from 3 - 5 % for natural gas to 10 - 15% for pulverised coal, mainly diluted by the combustion-persistent N_2. This dilution increases the volume of processed gas, thereby increasing the separation technology size and the energy cost per unit of CO_2 captured. Consequently, highly selective separation methods are preferred. In comparison to other technologies, PCC is the most mature and promising technology, being closest to large-scale deployment [3].

2) Pre-combustion

CO_2 capture takes place upstream of the combustion process. The process involves two subsequent steps. First, a fuel is gasified by a steam-oxygen mixture to produce syngas (mixture of CO, CO_2, and H_2), followed by a water-gas shift reaction to convert CO to CO_2 and H_2. Following step is CO_2 separation, leaving hydrogen as a carbon-free fuel. Examples of CO_2 separation from syngas in the pre-combustion methods include physical absorption using solvents such as *Estasolvan*, *Fluor Solvent*, *Purisol*, *Rectisol*, or *Selexol*. Recent attention has been paid to the development of membrane separation, physical and chemical adsorption processes. Compared to PCC, pre-combustion processes have about an equal energy penalty, however, a highly complex integration into existing power plants makes them unsuitable for retrofitting [3, 12].

3) Oxy-fuel combustion

Oxy-fuel is a combustion technology replacing air (*i.e.* a gas mixture), used as an oxidiser in conventional combustion processes, with high-purity O_2 (higher than 90 %). The flue gas produced contains mainly CO_2, water vapour, and oxygen given by the oxidiser stoichiometry. Additionally, it contains trace pollutants, such as SO_2 or NO_X, similar to the conventional air combustion. The N_2 content is negligible and depends mainly on oxygen purity and intake of false air from the surroundings. Gaseous pollutants and particles are removed using conventional technologies, followed by water vapour condensation. Finally, the dry flue gas, containing up to 98 % CO_2, must be processed to remove non-condensable components (*e.g.* oxygen) and then is compressed for transport. On the positive side, oxy-fuel provides process integration ease, has a small footprint, and conventional techniques for flue gas processing can be applied. On the negative side, the high cost of separating O_2 from air makes oxy-fuel commercially less attractive, with its energy intensity comparable to the cost of PCC integration and operation. Cryogenic distillation is the preferred method for obtaining O_2 in large-scale applications, while alternatives under development include membrane separation, adsorption, and chemical-looping techniques [3, 13]. Currently, the majority of experimental studies are carried out using easy-to-operate laboratory-scale oxy-fuel boilers (*e.g.* analyses of design and materials, combustion regimes, or fuels) with thermal power in the range of 0.1 - 3 MW_{th}. Larger systems with limited duration of operation include pilot-scale oxy-fuel plants without CCS technology, typically about 10 MW_{th}, and oxy-fuel plants with CCS, having thermal power in the range of about 30 - 200 MW_{th}, demonstrating full-scale commercial deployment [14].

Another emerging combustion technology with fluidised reactors is chemical looping combustion. Unlike oxy-fuel combustion, it operates at lower temperatures and does not require prior oxygen separation; oxygen is carried by metal oxides that undergo a redox cycle to continuously bond and

release oxygen in the oxidising and fuel reactors, respectively [3]. The schematic representation of CO_2 capture in industrial point sources is shown in Figure 2.

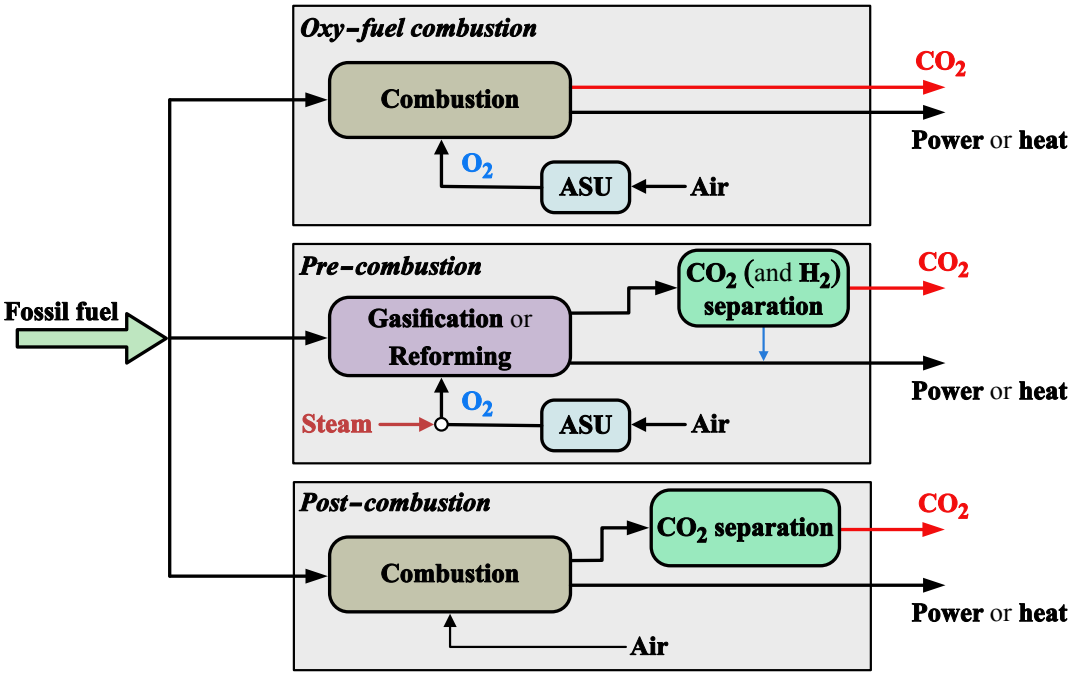

Figure 2. Scheme of CO_2 capture in industrial point sources [3].

The technological advancement of PCC and the advantage of easy integration into an operating fossil fuel power plant, whose deployment in the future is unexpected due to their gradual elimination from the power generation sector, are the motivations to address their topic in more detail.

Post-combustion CO_2 capture: Technology principle

The fundamental principles of prevalent and emerging technologies applicable for PCC can be described in a brief manner as follows using an example of a CO_2-rich flue gas:

- **Chemical absorption**: CO_2 is separated by entering a liquid phase (solvent) that triggers an exothermic chemical reaction. This separation takes place in an absorption column (tray or structured packing) interconnected with a stripping column, serving for solvent regeneration through the release of the absorbed CO_2 into a gas phase. Amine-based solutions are the most established solvents; other examples include, for example, ammonium-based solvents [3, 15].

- **Physical adsorption**: CO_2 is selectively separated by deposition on the surface of a porous solid adsorbent without triggering a chemical reaction, whereas releasing heat. This process occurs in an adsorption column (fixed, moving, or fluidised bed), serving also for sorbent regeneration.

Several columns are often interconnected to allow continuous operation. Both non-carbonaceous and carbonaceous adsorbents can be considered for CO_2 separation [3, 15].

- **Membrane separation**: CO_2 is separated by preferential permeation of other species across the membrane, leaving CO_2 molecules behind. This process is driven by a pressure difference and does not involve any significant heat exchange or phase change. Membrane is a thin, polymeric, or microporous film, enabling continuous operation without regeneration needs. Organic polymeric materials include polyimide or polysulfone; inorganic microporous membranes are often made of carbon, silica, zeolite, or alumina [3, 15].

- **Cryogenic distillation**: CO_2 is separated due to the different boiling points and volatilities of gas species, requiring cooling and compression to achieve CO_2 liquefaction (*i.e.* a phase change). It takes place in a distilling column (packed or trayed), resembling an absorption column. Although no separate agent is needed, auxiliary systems such as pumps, blowers, or chillers are required to facilitate a series of compression and refrigeration [3].

- **Gas hydrates**: CO_2 is separated based on the various phase equilibria of other gas species (N_2) by forming gas hydrates. This slow process occurs at high pressure and slightly sub-ambient temperatures. Gas hydrates are crystalline substances, necessitating promotion to be formed, which is carried out by using chemical additives or mechanical methods. Chemical additives include, *e.g.* tetrahydrofuran, cyclopentane, or dodecyl sulfonate; mechanical methods involve stirring, spraying, or ultrasonic waves [11].

- **Calcium looping (CaL)**: CO_2 is separated by a reversible exothermic chemical reaction with limestone (CaO), forming $CaCO_3$. Like adsorption, CaL uses solid sorbents and alternates CO_2 separation and regeneration processes (carbonation and decarbonation), however, operates at a higher temperature and limestone requires frequent replenishment. Two interconnected reactors, a carbonator and a calciner, separate CO_2 at 800 - 950 K and regenerate limestone at 1150 - 1250 K, respectively. Currently studied materials include a variety of calcium-based wastes [16].

For simplicity and relevance, CO_2 separations by cryogenic distillation, gas hydrates, and CaL are excluded from further consideration.

Post-combustion CO_2 capture: A state of the art

When selecting a PCC process, several factors must be considered, including fuel composition, combustion method, power plant size, and the required quality and quantity of CO_2 captured. The first two factors determine the concentration of CO_2 and other impurities in the flue gas. For many processes,

these impurities must be removed prior to CO_2 capture. The power plant size defines the gas volume to be processed and, consequently, the size of the tail-end CO_2 capture process. The latter factor is case-specific and may exceed the technical limits of individual processes. A more straightforward relationship is between the total process costs, the CO_2 concentration in the flue gas, CO_2 purity and recovery. Separation efficiency declines with decreasing CO_2 concentration, resulting in higher process costs. Similarly, these costs increase with the growing demands for CO_2 purity and recovery.

At present, chemical absorption is the cornerstone of PCC processes tested for commerce, with MEA-based aqueous amines reaching the highest TRL 9. Absorption-based PCC power plants are already being deployed, for example, *Alstom* (France), *Petra Nova* (USA), *SaskPower's Boundary Dam* (Canada), *Norcem AS (Aker Solution's ACC* process*)* and *SINTEF Energi* (both in Norway), and *Haifeng Carbon Capture Test Platform* and *Guohua Power Carbon Capture* (both in China). The most significant barriers to commercialisation are the high toxicity, degradability and corrosiveness of amine-based solvents, poor stability, and energy-intensive regeneration. Addressing these issues requires not only improving these solvents, but also modifying the process configuration and its integration within the power plant [11, 17-20].

Among the currently tested PCC processes, membranes are at TRL 6 - 7. However, conventional single-stage membranes require CO_2-rich streams above ambient pressure for efficient operation, where they can exploit their full potential of high selectivity towards CO_2 and excellent thermal and chemical stabilities. Since these conditions are not often met in PCC, membranes are more suitable for hybrid systems, for example, absorption-membranes or adsorption-membranes, with membranes being the second process [21]. Common challenges with membranes are clogging, mediocre permeability, implying larger surface area, and slow development due to material and technology costs. The potential of multistage membrane systems for processing CO_2-lean streams is yet to be explored [22, 23]. Examples of advanced pilot projects are not known; *Norcem CO_2 capture* and *MemCCC* (both Norway) projects reached TRL 4 [24].

The last typical PCC process, low-temperature adsorption, is at TRL 7. It offers several advantages, such as high selectivity and adsorbent regenerability, as well as more efficient processing of CO_2-lean gases on a scale of small- to medium size plants, where the process remains relatively simple. On the contrary, the treated gas must be free of any impurities and for most adsorbents also free of water, which is costly and calls urgently for the development of better materials. Furthermore, the complexity and footprint of the process increase with the size of the emission source [22, 25-27]. Examples of advanced adsorption processes include a rotary temperature swing adsorption (TSA) system from *Svante Inc.* [28], considered to be at the threshold of TRL 7 - 8 [29] (pilot demonstration was part of the *CO_2MENT* project [30]), the

rotating zeolite TSA wheel *C-SAVE* from *Seibu Giken Inc.* [31], and vacuum-temperature swing adsorption process from *RITE Chemical Research Group* [32]. A steam-reiterated concentration swing adsorption process with rotary adsorber from *ExxonMobil Corp.*, patented in 2017, has not been deployed or developed since [33]. A high-temperature adsorption process (*i.e.* CaL) is at TRL 7. The specific nature of the sorbents limits the versatility for PCC, as it integrates particularly well in the cement industry [34]. Advantages include low-cost sorbents (especially those made of calcium-based waste), utilisation of calcination-generated heat, and reusing degraded sorbents for clinker production, or within the steel and iron industries. Conversely, rapid degradation of the sorbent performance and a limited area of viable application, including conventional fossil fuel plants, must be addressed. Notable pilot-scale testing facilities with capacities ranging from hundreds of kW_{th} to units of MW_{th} have been developed in research institutes such as *Industrial Technology Research Institute* (Taiwan) or *INCAR-CSIC* (Spain), and universities in *Darmstadt* and *Stuttgart* (both in Germany), *Cranfield* (England), or *Ohio* (USA) [16].

In terms of CO_2 separation efficiency, absorption, adsorption, and membranes can produce high purity CO_2, regardless of economic and technical justifications. With decades of experience in absorption for PCC, its progress may have reached a plateau in many areas, demanding radical changes in the concept or solvent type to achieve further improvements, leaving room for other separation techniques to be looked into. Membranes are in the material and technological stages of development, and current types seem most apt for processing highly concentrated CO_2 flue gases as a single or combined processes. Both low- and high- temperature adsorption processes are at a more advanced stage in these areas, and therefore they are potential candidates for PCC, albeit with various areas of potential application. These areas are more constrained for high-temperature adsorption (CaL), and therefore attention is paid to the low-temperature adsorption process.

Chapter 2

2 Low-temperature adsorption technologies

2.1 Fundamentals of adsorption phenomena

Adsorption is a separation process taking place in a multicomponent system at the interface of two phases, where the concentration of one or more components in the gas phase changes by a transition to a solid phase. In this process, the molecules of separated component (adsorbate) are physically or chemically bound to the surface of a solid, typically a porous media in the form of powder, granules, or larger densified structures. Physical adsorption is more significant at low temperatures, less selective than chemical adsorption, reversible, and driven by van der Waals forces. On the other hand, chemical adsorption is less temperature-dependent, thermodynamically irreversible, and characterised by mononuclear chemical bonds between adsorbent and adsorbate. Low-temperature adsorption of CO_2 is a physical phenomenon, and therefore chemical adsorption is no longer considered [35].

This phenomenon is generally spontaneous, shifting toward adsorption equilibrium, and quantitatively described by adsorption isotherm. The rate of this shift is determined by the adsorption kinetics depending, for example, on the thermodynamic state of the system (temperature and pressure), the size and concentration of the adsorbate molecules, and morphology and selectivity of the adsorbent. The mechanisms involved in this process are momentum (flow around the adsorbent particles and gas flow through the column), enthalpy, and mass transfers within the adsorbent particles and within the column. The adsorbate mass transfer stops at adsorption equilibrium, indicating a full saturation of adsorbent with adsorbate. The maximum saturated amount of gas species (in moles or grams) at equilibrium per unit mass of adsorbent is expressed by the adsorption isotherm at a given temperature. The most widely accepted classification of adsorption isotherms by *IUPAC* is based on their shape (Figure 3), reflecting the morphological structure of the porous media where each pore of a characteristic size (micropores: 0 - 2 nm, mesopores: 2 - 50 nm, and macropores: over 50 nm) exhibits different adsorption behaviour [36]. In microporous materials (< 2 nm), the adsorbing gas generally forms a monolayer and desorption does not show hysteresis, simplifying it to a reversible process (isotherm Types I-III). The hysteresis loop, found in larger pores, is accompanied by condensation and irreversibility.

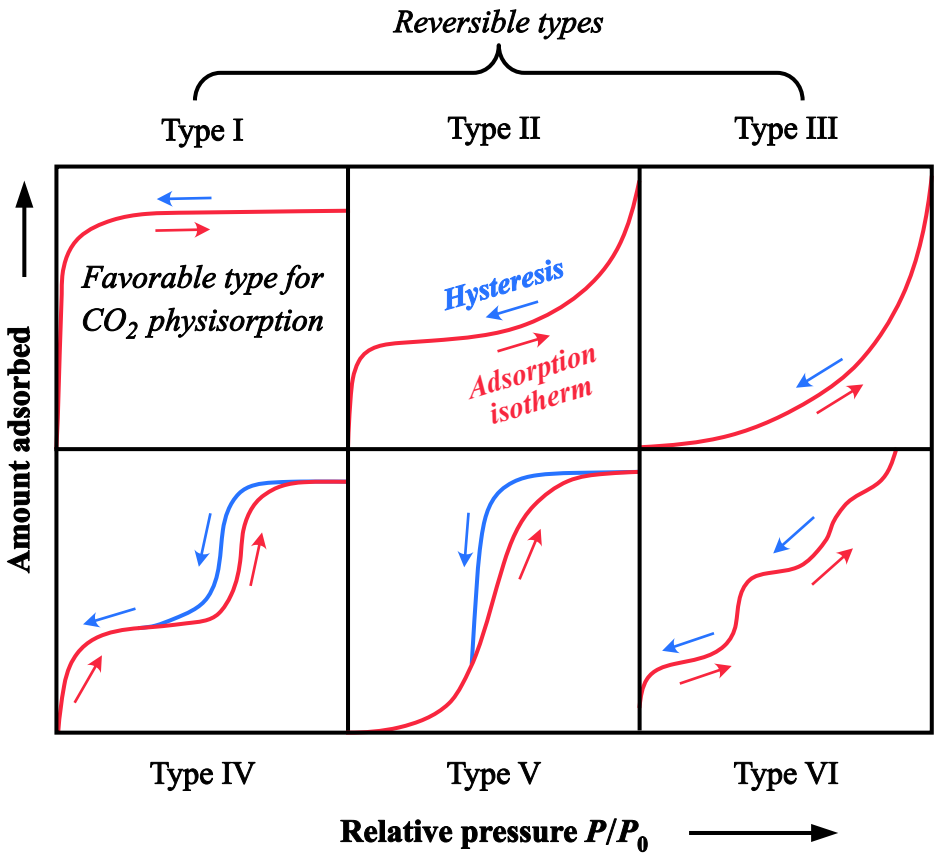

Figure 3. Classification of adsorption isotherms by *IUPAC* [36].

Adsorption isotherms related to CO_2 adsorption on conventional porous media in PCC are often Type I due to the preference to use highly microporous adsorbents, and mathematically described by the *Langmuir* isotherm and *Freundlich, Sips*, or *Tóth* adsorption isotherms derived from it in a single or dual-site forms depending on the competing adsorbate species with CO_2 [37]. Their mathematical formulation is presented in Table 1. Adsorption is accompanied by the release of adsorption heat (exothermic process), which is of the order of condensation heat. The reverse phenomenon of adsorption is desorption (endothermic process), also called "adsorbent regeneration", where the adsorbate is released from the adsorbent back to its original phase. In many cases, the course of desorption differs from adsorption, which is reflected in the appearance of hysteresis loops, usually unsuitable for CO_2 capture in the absence of water vapour [35, 36].

When separating CO_2 in the presence of other components, physical separation is usually performed by exploiting their different adsorption phase equilibria (*i.e.* equilibrium-controlled process), as the adsorbent selectively interacts with the gas components. Less frequently, separation relies on different kinetic rates, controlled by the velocity at which gas components transfer in and out of the adsorbent particle (*i.e.* kinetic-controlled process). To date, equilibrium-controlled processes are widely used for

most gases. As mentioned above, phase equilibrium is the dependence of the absorbed amount per adsorbent mass unit (q^*) on either total or partial pressure, or the concentration of the adsorbable components at a given temperature, for which the amount of separation of a particular component in a gaseous mixture depends on the selectivity toward other components that are present. Components with higher selectivity are more strongly adsorbed (*i.e.* strongly-adsorbed species) and are retained in the adsorbent, often packed in a column, when the off-gas flows through, while the exiting gas contains only weakly-adsorbed species.

Table 1. Common single-site adsorption isotherms used for CO_2 adsorption [38].

Adsorption isotherm	Mathematical formula	Note
Langmuir	$q_i^* = q_{s,i} \frac{b_i c_i}{1 + b_i c_i}$	Monolayer adsorbate formation on a homogeneous surface.
Freundlich	$q_i^* = k_i c_i^{\frac{1}{n_i}}$	Modification of Langmuir isotherm with a more linear trend and exponential decrease in adsorption heat.
Sips	$q_i^* = q_{s,i} \frac{(b_i c_i)^{\frac{1}{n_i}}}{1 + (b_i c_i)^{\frac{1}{n_i}}}$	Combination of Langmuir and Freundlich isotherms introducing a surface heterogeneity parameter *n*. For *n = 1*, this equation becomes Langmuir isotherm.
Tóth	$q_i^* = q_{s,i} \frac{b_i c_i}{[1 + (b_i c_i)^{t_i}]^{\frac{1}{t_i}}}$	Modification of Langmuir isotherm, which is best suited for heterogeneous adsorbents through the heterogeneity parameter *t*. For *t = 1*, this equation becomes Langmuir isotherm.

The equilibrium parameters are obtained from the adsorption isotherms. The mass transfer resistance plays a relatively minor role. In kinetically-controlled processes, the state of equilibrium never occurs. Therefore, the contact time between adsorbate and adsorbent plays a crucial role and must be short enough to prevent the system from approaching the equilibrium state, but long enough to preclude significant uptake of the adsorbate. Consequently, significantly higher sorption rates are enhanced by rapid pressure alteration, so the diffusion rate of the components into the adsorbent becomes the driving force and the faster-diffusing species are retained by the adsorbent, while the high-pressure species (product of the process) are concentrated in a more slowly-diffusing component [39]. Herein, the adsorption isotherm does not provide sufficient information, for example, on the kinetic parameters,

which must be determined from the barrier and diffusional resistances of mass transfer between the solid phase and the gas phase [40].

A wide range of experimental data on the adsorption equilibrium of pure gases and gas mixtures was collected by [41]. For CO_2 adsorption equilibrium data, online databases such as *NIST/ARPA-E* [42] (National Institute of Standards and Technology), *MOFX-DB* [43] (Northwestern University), or *CSD* [44] (Cambridge Structural database), or literature data are a good source of information, although comprehensive data on more adsorbents measuring gas mixtures are critically needed. The adsorption kinetics data have not been summarised, to the best of my knowledge, since the kinetics is usually studied for a specific gas component or mixture and adsorbent.

Combining adsorption and desorption into a single process forms an adsorption cycle capable of periodic operation. Adsorption cycles are classified according to the desorption principle because the physical background of adsorption remains unchanged. Desorption can be carried out by varying temperature, pressure, or by introducing an inert gas stream, as illustrated in Figure 4 except for the latter, which is will not be explained in detail here. To perform desorption by temperature, it must be increased without exceeding the thermal stability of the used adsorbent. Depending on the adsorption pressure, the pressure must be reduced to either atmospheric pressure using an inert gas or adsorbate gas to purge the column and remove desorbed adsorbate molecules, or to below atmospheric pressure using a vacuum pump, which often generates sufficient suction force to both desorb and remove these molecules. For the latter, a high-temperature inert gas stream is continuously introduced into the column, releasing (desorbing) the adsorbate, and purging the column. Different desorption methods have formed the basis for various cycles, which are traditionally based on alternating pressure (pressure swing adsorption (PSA) and VSA cycles), temperature (TSA cycle), or both (pressure-temperature swing adsorption (PTSA) cycle) alternating subsequently or simultaneously [35].

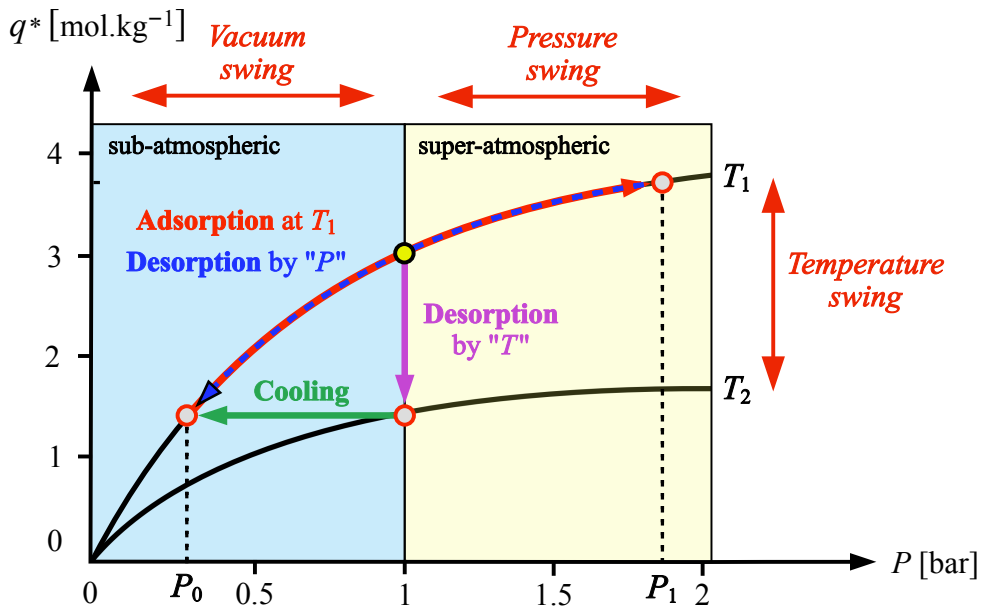

Figure 4. Operating principle of TSA, PSA, and VSA cycles, illustrated on two idealised Type I adsorption isotherms at temperatures T_1 (lower temperature) and T_2 (higher temperature). For clarity, pressure and temperature variations are neglected. The TSA cycle is displayed as isobaric, alternating between temperatures T_1 and T_2, while PSA and VSA are displayed as isothermal, alternating between 1 bar and P_1, and P_0 and 1 bar, respectively. The working capacities (*i.e.* the difference between the adsorbed and desorbed amounts at equilibrium per cycle, Section 2.2.2) for these simplified cycles can be seen along the *y*-axis: for ***TSA***: $q^*(T_1, 1\text{ bar}) - q^*(T_2, 1\text{ bar})$, for ***PSA***: $q^*(T_1, P_1) - q^*(T_1, 1\text{ bar})$, and for ***VSA***: $q^*(T_1, 1\text{ bar}) - q^*(T_1, P_0)$.

Adsorption processes are commonly found in fixed bed columns, although moving or fluidised beds have recently received increased attention [45]. Regardless of the bed configuration, this process is accompanied by concentration, momentum, and temperature waves (under non-isothermal conditions) dynamically moving from the inlet of the column to its outlet and vice versa for the reversed process steps, as explained in the following Section. These transfer phenomena form the fundamental basis of mathematical description of the process aiming to estimate the progression of these waves in time and space. The adsorbate concentration dependence measured at the column outlet is called the "breakthrough" curve. The adsorbate concentration at the outlet appears at breakthrough onset. In the processes that remove harmful pollutants, such as CO_2, the breakthrough onset typically does not occur, since the column switches to the desorption mode before reaching this point [35].

In practice, the separation of industrial off-gas, air separation to produce high-purity oxygen or high-purity hydrogen are typical examples of an equilibrium-controlled process. These processes also account for most of the CO_2 capture by adsorption at low-temperature using pressure or temperature-based

adsorption cycles. A kinetically controlled processes can be narrowed down to rapid-pressure swing adsorption (RPSA), which is historically associated with air separation and the *Bergbau Forschung* company [46]. The PSA and RPSA processes were commercialised for air separation on various scales, starting from portable PSA medical oxygen concentrators, while PSA is also used in hydrogen plants. However, a growing need to minimise energy consumption has hindered the greater development of RPSA. Although both processes can be used for CO_2 capture from point emission sources, the prevalence and benefits of the equilibrium-controlled process rule out the latter option [47].

2.2 Adsorption cycle principle and technology overview

Adsorption processes (equilibrium-controlled) are characterised by non-stationary behaviour and by almost instantaneously reaching a state of equilibrium, which distinguishes them from other separation techniques such as distillation, filtration, or membrane separation. These processes consist of several steps, operating at cyclic steady state (CSS), taking place between the always present adsorption and desorption steps (more details are provided in Section 2.2.1). As mentioned above, conventional technologies are classified according to the desorption method. PSA uses the effect of alternating pressure, whereas TSA alternates temperature changes.

The general principle of any adsorption cycle is to concentrate the target species, *i.e.* the product (or "heavy product" for strongly adsorbing target species), which is present in the feed stream at low concentrations. In the case of PCC, a stream of CO_2 dominated by N_2 is fed into the column, and while CO_2 retains in the adsorbent, a purified stream of N_2 ("light product") passes through. It is therefore imperative to use adsorbents highly selective towards CO_2 to minimise concurrent adsorption of species. Their choice is critically important as adsorption isotherm affects the cycle working capacity (the difference between the adsorbed amounts after desorption and after adsorption), scheduling (timing and choice of steps), and its shape determines the appropriate desorption method and cycle operating range (pressure and temperature). Simply put, the VSA cycles favour adsorbents with steep isotherms at sub-atmospheric region, while the PSA cycles adsorbents with linear isotherms or steep at super-atmospheric region; the TSA cycles are best suited for adsorbents with rectangular isotherms, although this cannot be taken as a rule. The target concentration for the CO_2, recovered during desorption, is generally greater than 90 %, allowing further processing as obtaining a purer product is very energy intensive [48, 49]. When the product is recovered, the cycle starts all over again in the same manner. High CO_2 feed concentration has the advantage of improving process efficiency and reducing the amount that must be processed, leading to lower operating costs and a smaller footprint of the auxiliary units [50].

The following sections explore the adsorption processes in more detail. First, various steps employed more or less in PCC adsorption processes are described, followed by a brief discussion of CO_2 adsorbent selection, their availability, and performance. Finally, an overview of the adsorption technologies formed from these steps using the discussed adsorbents is provided.

2.2.1 Adsorption cycle steps

Adsorption swing processes consist of various steps forming cycles, often named after their selection (*i.e.* number of steps) and arrangement. The step duration, direction of gas flow, column interconnection, initial and final process variables (*e.g.* concentration of gas species, temperature, and pressure) are characteristic features of each step. Historically, Skarstrom laid the foundation for adsorption cycles in 1960 by introducing a two-column 4-step PSA cycle consisting of pressurisation, adsorption, blowdown, and purge steps [51]. A few years later, his invention was modified by Guerin de Montgareuil & Domine with a VSA cycle regenerating adsorbent under sub-atmospheric pressure [52]. These processes quickly became the most frequently used techniques, providing a good solution for designing PCC adsorption technology nowadays. For various benefits, discussed in Section 2.2.3, VSA is used rather than PSA (or TSA, although here the benefits of VSA are case-specific). A typical PCC VSA cycle with two or more interconnected columns separating CO_2 from N_2 (in practice, O_2 and trace amounts of other gases are present) can operate in the following steps (indicatively described in Figure 5) [53]:

- **Pressurisation**: initial step of introducing the CO_2-rich flue gas into a column at sub-atmospheric pressure with CO_2-regenerated adsorbent. The flue gas serves as a pressuriser, since the column end remains closed until the atmospheric pressure, *i.e.* the adsorption operating pressure (P_A = the highest pressure (P_H) throughout the cycle), is reached. CO_2 is gradually absorbed with increasing pressure, displacing N_2 contained in the adsorbate.
- **Adsorption**: the column end opens while compressor-driven (W_C) inlet flue gas maintains a constant pressure. CO_2 is instantly adsorbed, and purified gas dominated by N_2 is discharged into the atmosphere.
- **Blowdown**: the column inlet closes and the remaining gas in the gas phase is withdrawn by a vacuum pump (W_{BD}) depressurising the column until the intermediate pressure P_I is reached.
- **Evacuation (regeneration)**: reverse step to blowdown, using a vacuum pump (W_{Ev}) to reach the lowest pressure P_L and counter-currently withdraw the adsorbed CO_2 at high purity (diluted by a small fraction of N_2) to be collected and processed, for example, compressed or liquefied for storage or pipeline transport. This step is responsible for the highest energy consumption.

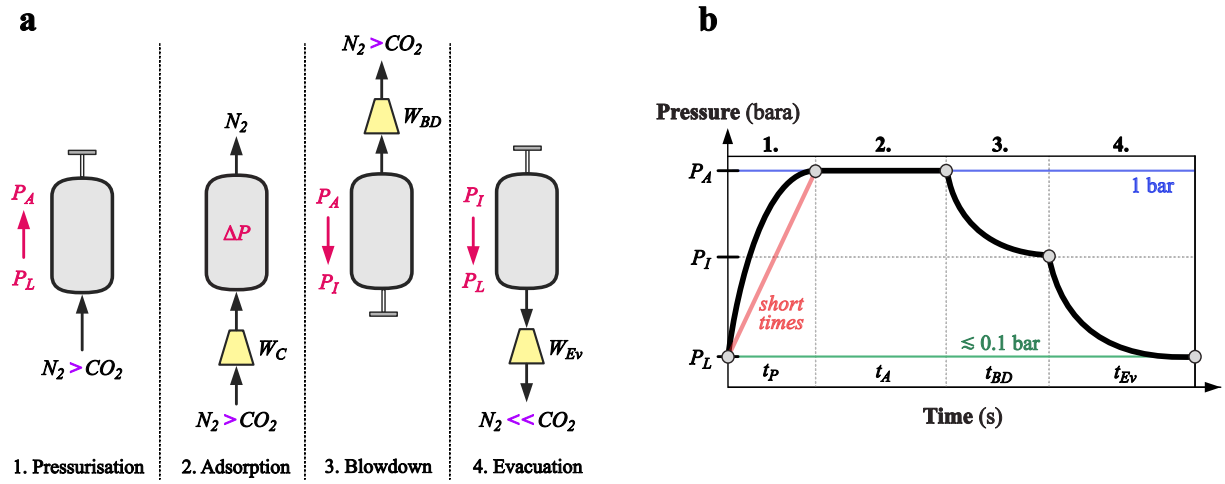

Figure 5. Illustrative representation of **(a)** the operating principle of a single PCC VSA column undergoing four subsequent steps; and **(b)** the corresponding pressure profile. In PCC processes using VSA, which operates up to 1 bar and processes a CO_2-rich stream, pressurisation is often the shortest step with nearly linear pressure growth, constrained by the compressor limitations. Evacuation pressures are about 0.1 bar or less to ensure high CO_2 purity [53]. ***Note**: W_C, W_{BD}, and W_{Ev} are the works of compressor, and blowdown and evacuation pumps, respectively.*

It is evident that steps represent a logical sequence, allowing continuous operation that intervenes between the main steps of adsorption and desorption. These steps must be carefully selected in relation to the process itself, *i.e.* the quality (purity) and the quantity (recovery and productivity) of the product as well as the overall energy consumption. Consequently, other steps are explored, and those relevant to PCC, including elementary TSA steps, are summarised in Table 2.

Table 2. Elementary steps of the pressure- and temperature-swing based cycles, described for the mixture of CO_2 and N_2 [45, 54, 55].

Cycle step	Mode of operation	Principal features
Pressure equalisation (PE) (*i.e.* Depressurisation and Pressurisation) (*PSA or VSA cycles*)	This step involves interconnecting two columns at different pressure levels. Before desorption, the column at higher pressure is depressurised by transferring some of its gas to the column at lower pressure, which was purged or desorbed and deprived of gas. This step can be repeated multiple times within the same cycle, typically, if more than two columns are interconnected.	Energy efficient step converging energy and separative work, potentially improving CO_2 purity.
Rinse or **Heavy reflux**	The column is purged with heavy product (CO_2), displacing light product (N_2) in the direction of the feed gas. This step takes place after adsorption before the withdrawal of adsorbed CO_2.	Improves CO_2 purity when the lighter species are co-adsorbed in large amount with a heavier component. Usually not combined with multiple PE steps.
Purge or **Light reflux**	The column is counter-currently purged with a light product (N_2) or inert gas (*e.g.* helium in laboratory experiments) withdrawing the desorbed CO_2 at high purity. A small portion of purging gas is preferred to avoid product dilution, not occurring in the Rinse (Heavy reflux) step.	Removal of the strongly adsorbed components (CO_2) from the gas phase. Usually not combined with multiple PE steps.
Idle *(all cycles)*	The column is inactive.	Usually used to maintain continuous operation.
Heating (desorption) *(TSA cycles)*	1. **Direct heating**: flux of hot air or steam stream is fed to the column during the regeneration step, satisfying the thermal duty required for desorption.	Diluted product. Steam cannot be used for water-sensitive adsorbents. Energy demanding and time-intensive process.
	2. **Indirect heating**: usually performed by letting a thermo-vector fluid flow on the external side of the column walls, *i.e.* a heat exchanger system. The most frequent method.	Non-diluted product with high purity, heat exchanger chamber allows rapid cooling. Energy demanding and time-intensive process, however, efficient for water desorption.
	3. **Electric heating**: low-voltage electric current is directly applied to the adsorbents for adsorbent regeneration.	Fast process overcoming the heat transfer limits of modes 1. and 2., while avoiding the unnecessary equipment heating. High purity of the desorbed component.
Cooling *(TSA cycles)*	Adsorption bed is cooled by cooling water or steam, while the pressure decreases.	Prepares the bed for the next cycle, *i.e.* it is a substitute for the pressurisation step in pressure-swing cycles.

2.2.2 Adsorbents for CO_2 capture: selection importance

Adsorbents are highly porous solids with pores of different sizes, which have been standardised by *IUPAC* into the aforementioned classes of micropores (up to 2 nm), mesopores (2 - 50 nm), and macropores (more than 50 nm). With the fast progress in adsorbent development, nanopores are sometimes included as a single class with an upper limit of about 100 nm. Each pore size plays a distinct role in the adsorption of gases and their transport mechanisms [36]. However, a detailed discussion of these roles is beyond the scope of this thesis. In the context of PCC, two types of adsorbents are typically used:

- ***Non-carbonaceous***: zeolite-based, silica-based, and metal-organic frameworks (MOFs);
- ***Carbonaceous***: activated carbon (ACs) and carbon molecular sieves,

with the former dominating the latter at both laboratory and pilot scales. Non-carbonaceous adsorbents degrade after exposure to moisture or reactive impurities (impurities affect all adsorbents), but they offer excellent CO_2 capture properties for dry CO_2/N_2 and $CO_2/N_2/O_2$ [56]. Advantages of carbonaceous adsorbents can be exploited for processing CO_2-rich humid gases [57]. Adsorbents can be further divided according to their structure; fine powders (non-structural adsorbents) are readily available, but their nature prevents handling without material losses and has disadvantages such as high pressure drop, low mass and heat transfer rates or difficulties during. Structural adsorbents are formed into various shapes; however, currently used shaping techniques are limited to the laboratory level [58]. The selection of adsorbent and its structure is related to the choices of the desorption method, cycle scheduling and timing, process parameters, the possibility of continuous operation without shutdown, process economics, and separation efficiency.

To make adsorbent selection easier, by analogy with adsorption processes (Section 2.2.3), adsorbents can be classified according to their CO_2 separation performance during adsorption and desorption processes. Five evaluation criteria addressing CO_2 capture from a binary mixture of CO_2/N_2 by pressure-swing cycles that can be obtained from the adsorption isotherm equilibrium data for a given adsorption pressure and temperature, were proposed by Bae & Snurr [59]:

- ***CO_2 uptake*** = the amount of CO_2 adsorbed per weight of adsorbent under adsorption conditions (*i.e.* pressure and temperature).

- ***Working CO_2 capacity*** = the difference between the amounts of adsorbed and desorbed CO_2 per weight of the adsorbent in one cycle. The working capacity may vary until the CSS has been reached.

- ***Adsorbent regenerability*** = the percentage of the adsorbent working CO_2 capacity that can be recovered per cycle and used in the following cycle.

- ***Selectivity*** = a preference for adsorbing one component over another under adsorption conditions. This criterion quickly assesses the influence of each component in the multicomponent mixture on the adsorption of target species.

- ***Sorbent selection parameter*** = an extended measure of *Selectivity*, taking into account the *Working CO_2 capacity*. It can be explained as finding a balance between highly selective adsorbents and adsorbents with high working capacities. Considering *Selectivity* and *Working CO_2 capacity* together provides more accurate information about adsorbent performance in PSA and VSA cycles.

Indeed, these criteria are desired to be high. A more general adsorbent properties that do not have explicit expression, although they are needed, can be summarised as follows [49, 56, 60]:

- ***Fast adsorption and desorption kinetics***: high kinetic rates yield sharp CO_2 breakthrough curves, while minimising the cycle time and, therefore, the column volume, which may lower capital costs.

- ***Low adsorption heat***: low adsorption heat allows for an energy-efficient regeneration process due to the less strongly-bonded CO_2 molecules, being easier to desorb.

- ***Long-term cyclic stability***: maintaining working CO_2 capacity at a constant kinetic rate as long as possible minimises the sorbent makeup rate and process shutdowns.

- ***Low adsorption hysteresis***: appearance of a hysteresis loop is associated with a higher energy consumption as higher pressure drop (PSA or VSA) or temperature increase (TSA) is needed to maintain the sorbent working capacity.

- ***Chemical stability and tolerance to impurities***: although flue gas pre-cleaning is performed, withstanding oxidizing environment and having resistance to common impurities to any level is always beneficial.

- ***Low cost***: the price-to-performance ratio is a key industrial objective. These data are difficult to obtain, but adsorbent can be considered economically feasible if the cost is less than $10 per kg of sorbent material.

From an industrial point of view, there are only few commercially available adsorbents in large quantities performing well among other potential materials. For example, a comprehensive work by Balashankar

et al. [61] evaluated more than 150 adsorbents for PCC via VSA, and ready-to-use industrial adsorbents, zeolites 13X and 5A, performed consistently across various performance indicators (defined in Section 2.2.3). Both achieved one of the lowest energy consumptions and a high CO_2 working capacity. Kim et al. [62] compared 75 adsorbents formed as thermally modulated fibre composites for PVSA cycle. Similar findings were observed for recovering 95 % pure CO_2 purity, with 13X being the most attractive commercially available adsorbent before MOF Cu-BTC. The development of new adsorbents and mass production techniques is of critical importance, with the greatest need to reduce overall costs, including the cost of transporting large adsorbent quantities to the emission source sand the cost of efficient conversion of captured CO_2, and improve material tolerance towards impurities and water vapour [63].

In numbers, more than 235 zeolites and 88000 MOFs have already been found or synthesised where the use of modular synthesis allows tuning and controlling various adsorbent properties [64]. Material databases already contain over 100000 experimental structures and over 500000 generated (hypothetical) structures of carbon capture adsorbents. Finally, technological advances in computing have made adsorbent screening (*i.e.* performance evaluation) a time-saving process [61, 65], and with the help of neural networks (*i.e.* machine-learning techniques), an adsorbent can be evaluated in less than a minute [66].

2.2.3 Adsorption cycle technologies and their performance

Pioneer work on CO_2 capture by adsorption for the energy industry appeared in the 1990s [67-71]. Since then, various pressure-swing based processes, from the "simple" Skarstrom [51] 4-step fixed-bed PSA concept to the processes having more than 10 steps alternating between sub- and super-atmospheric pressures [72, 73], have been tested. On the contrary, TSA development has focused more on different bed concepts (*e.g.* moving [74], rotating [75], or fluidised beds [76]) to increase the heat transfer rate and shorten the desorption time, and on alternative heating methods such as electrical heating using the Joule effect [77, 78], or faradaic electrochemical cell [79], or microwave heating [80] regenerating the bed even faster. Other categories were formed by combining PSA or VSA with TSA into a single process, often using fixed-beds, and by accelerating the reaction kinetics, *i.e.* rapid-pressure [81] and rapid-temperature (RTSA) [82] swing adsorptions. Both are uncommon for PCC. In this regard, an extensive survey of the theoretical and experimental literature consisting of more than 200 articles was conducted summarising these cycles with the aim of understanding the selection of low-temperature adsorption PCC technology for given process parameters and emission source size. A tabular overview is presented in Appendices A and B for pressure-swing and temperature-swing based technologies, respectively, sorted alphabetically by the first author. At the outset, it should be noted that technologies combining temperature and pressure swings have not been investigated due to their process control

complexity and design difficulties based on large number of design parameters that are available. Furthermore, it can be argued that their reliability is lower than that of simple single-method desorption processes.

The following part supports this summary by providing a brief insight into the principles of the most common technologies using single-method desorption, including their role in PCC. The second part defines process performance indicators (PIs) used to classify and compare PCC adsorption cycles, or as their design constraints.

- ***PSA***: adsorption is performed at elevated pressure, achieved in PCC by pressurising the flue gas using an auxiliary compressor, while desorption is performed at atmospheric pressure through a sudden pressure drop continuously releasing adsorbed species at about constant temperature. Released species are carried away from the column by a so-called carrier gas taken from the purified gas or the heavy product, depending on the product purity target. The level of pressurisation is non-linearly proportional to the maximum working capacity and responsible for most of the energy consumption. Pressure-swing cycles can run continuously at significantly shorter times than TSA cycles, which promotes high productivity (*i.e.* the amount of heavy product obtained per time and adsorbent mass) and minimises the adsorbent inventory, as well as the capital cost of the system. A typical PSA process takes place in a fixed-bed reactor and satisfies removing components at high concentrations or processes producing the weakly adsorbing components. In PCC, the PSA economy suffers from a high energy consumption of compressors, steeply increasing with emission flow rate usually supplied at atmospheric pressure, and low CO_2 concentrations. Both also contribute to a large footprint by increasing the number of continuously operating columns, having a limited size in the order of metres due to technical reasons and pressure drop. Desorption at 1 bar is not suitable to produce a high CO_2 purity stream, as intensive pressurisation is economically and technically challenging [47, 49].

- ***VSA***: adsorption takes place at about atmospheric pressure and at a near-room temperature, whereas desorption takes place in a vacuum achieved by a vacuum pump (usually a set of pumps) withdrawing the adsorbed species from the column. Basic VSA maintains a simple PSA design and good scalability, while the use of vacuum pumps eliminates the need to transfer gas between columns for purging, a step often required in PSA. It offers a potentially long adsorbent lifetime, low cost, and relatively low energy consumption, if the pump is operated under mild conditions. For PCC, VSA is more attractive for processing larger volumes of emissions than PSA in terms of separation efficiency, cost savings, and energy consumption, since only a fraction of gas is

evacuated compared to the compression of the entire gas, although vacuum puts more stress on the material, resulting in a thicker column walls [22]. The ease of unit maintenance, adsorbent regeneration, high CO_2 purity, and susceptibility to sieve dusting are also advantages. In addition, water vapour is less prone to condensation at low pressure, reducing the potential risk of corrosion; however, if trace amounts are adsorbed or humid gas is processed on a water-resistant sorbent, temperature-swing is the most powerful desorption technique. Despite multiple advantages over PSA for PCC, VSA does not solve problems of large area occupation and inefficient separation of CO_2-poor gases [47, 49].

- ***VPSA:*** combination of PSA and VSA working areas by switching between an adsorption step at above atmospheric pressure (PSA) and a desorption step under vacuum (VSA). Enhanced desorption provides an opportunity to pressurise the flue gas less, and therefore to save on the energy consumption of PSA and to increase the working capacity of VSA. The efficiency of a VPSA unit can be greatly improved by choosing the appropriate adsorbent [47]. Vacuum helps achieve higher purity of the product. In PCC, the VPSA process satisfies demands for high CO_2 purity and recovery. However, more complex operating conditions and additional auxiliary units must be set against more favourable capital and operating costs [83].

- ***TSA***: the oldest adsorption process using heat in desorption is usually atmospheric throughout the cycle. Adsorption proceeds similarly to PSA at low temperature. For PCC, the working temperature ranges from 40 °C to 120 °C, placing particular emphasis on adsorbent selection [47]. In desorption step, bed can be heated directly by a hot gas or steam, or indirectly by a heat exchanger. Direct heating using steam is often used and preferred because indirect heating requires more thermal energy. However, in PCC, direct heating can dilute desorbed CO_2 and reduce its purity and recovery, while indirect heating eliminates dilution and provides a higher heat transfer rate. The heat transfer rate is generally low in a fixed-bed, resulting in a long desorption time, whereas fluidised bed has very a high heat transfer coefficient. Desorption by temperature has a greater thermodynamic potential than pressure, making the separation of strongly adsorbing components (water vapor or even reactive components) more convenient [45]. On the contrary, cycling at high temperature reduces the lifetime of the adsorbent and consumes a large amount of energy, specifically, about 75 % of the process energy consumption. Improvements can be made by utilising waste heat for desorption, exploring different bed configurations (*e.g.* moving or fluidised beds), or combining temperature swing with vacuum swing. An advantage of TSA is in removing impurities at a high inlet temperature, simple maintenance, easy integration with an existing power plant, and lower operating costs compared to pressure swing cycles in some cases,

especially if the waste heat from power plants or CO_2 liquefaction (CCS power plants) can be utilised. There is currently a commercial application of TSA for gas drying in air separation units [84, 85], an aforementioned rotating TSA system by *Svante Inc.* [28] has the highest TRL among PCC adsorption technologies.

When commercialised, these technologies usually carry manufacturer-guaranteed values, such as recovery and purity of the product. For adsorption technologies, this typically involves oxygen production for medical applications [86] or hydrogen production [87]. For PCC technologies integrated in power plants with CCS burning carbonaceous fuels, ISO 27919-1:2018 [88] defines five process criteria: specific thermal energy consumption, specific electrical energy consumption, specific equivalent electrical energy consumption, specific reduction in CO_2 emissions, and specific absorbent consumption and specific chemical consumption. This currently applies, for example, to chemical absorption [89]. However, for non-commercialised PCC adsorption technologies, there exists no requirement guaranteeing, for example, constant CO_2 supply with purity constraint, or specific energy consumption for economic operation. Nevertheless, having a performance measure applicable to any PCC adsorption process for its evaluation, comparison, and integration within the appropriate process is critically important. PIs illustrate the separation efficiency, as well as the quality and quantity of recovered CO_2 and process energy consumption. They are based on pilot experiments and theoretical studies and considerably vary from system to system and from site to site, as shown in Appendices A and B. PIs are defined as follows [90]:

- ***CO_2 recovery:*** the total amount of CO_2 that can be separated from the feed gas and retained in the column, *i.e.* the ratio between the quantity of CO_2 obtained and the quantity of CO_2 in the feed gas:

$$\text{REC}\ (\%) = \frac{\text{Total moles of } CO_2 \text{ in the extract product}}{\text{Total moles of } CO_2 \text{ fed into the cycle}} \times 100 \quad (1)$$

- ***CO_2 purity:*** a measure of CO_2 dilution in the product stream, *i.e.* the ratio between the quantity of CO_2 in the product stream and the overall quantity of this stream:

$$\text{PUR}\ (\%) = \frac{\text{Total moles of the target species in the extract product}}{\text{Total moles of all species in the extracted product}} \times 100 \quad (2)$$

- ***Adsorbent** or **cycle productivity:*** the amount of CO_2 captured per adsorbent volume (or weight) and cycle time. Productivity per cycle is related to the working capacity and can be considered as an adsorption unit footprint indicator. The greater the productivity, the smaller the footprint [91]:

$$\text{PROD}\left(\frac{\text{mol}_{CO_2}}{\text{m}^3_{\text{adsorbent}} \times \text{s}}\right) = \frac{\text{Total moles of } CO_2 \text{ in the extract product}}{(\text{Total volume of adsorbent}) \times (\text{Cycle time})} \quad (3)$$

- ***Energy consumption:*** a measure of the energy consumed by the entire process, including the energy requirement of auxiliary units such as compressors, vacuum pumps, or heating equipment (the literature review revealed that the number of units considered is indefinite, as some literature considers only the energy consumption for separation or for energy intensive desorption, which differs from commercial units, *i.e.* from ISO standards):

$$\text{Energy consumption } (\text{MJ}.\text{t}_{CO_2}^{-1} \text{ or kWh}.\text{t}_{CO_2}^{-1}) = \frac{\text{Total cycle energy consumption}}{\text{Mass of } CO_2 \text{ in the extract product per cycle}} \quad (4)$$

The first two PIs, CO_2 purity and recovery, are often associated with the purpose of the application and must be respected or set as process constraints. The other PIs are optimised by other variables without being held accountable to any constraint [90].

The literature overview was based on these PIs; however, it turned out to be difficult to draw broad conclusions or compare technologies mutually differing in process and design parameters that use various adsorbents, and are subjected to a wide range of flue gases of specific temperature, pressure, CO_2 concentration (including species concentration), and volumetric flow. Although the PIs are highly dependent on each other, as expected, they also relate to other variables that cannot be seen. For instance, they do not reflect information about the technical implementation (footprint, columns, auxiliary equipment, etc.), scale-up considerations, long-term operation, equipment and adsorbent costs, process control, and study origin, *i.e.* experimental or theoretical.

Still, some statistically-based trends can be observed. Zeolite 13X is clearly the most widely used adsorbent in both laboratory and experimental studies, confirming its commercial availability and good separation efficiency, especially for VSA cycles, which dominate over PSA cycles that are also less frequent than VPSA cycles. In a TSA mode, the choice of adsorbents is wider, although zeolite 13X is still the material of choice, either as a solely-investigated adsorbent or as a benchmark for other adsorbents, being often limited to a laboratory-scale use. As expected, the occurrence of fixed-bed columns is sparse in TSA, unlike PSA, VSA, and VPSA cycles. Moreover, it is safe to say that theoretical

studies using mathematical models or simulation software dominate over experimental studies requiring space, time, and financial resources. According to reported comparisons of experimental and theoretical studies, mathematical models are able to simulate the ongoing adsorption process in terms of thermodynamic quantities, including the prediction of CO_2 purity and recovery, with high accuracy, with the largest deviation occurring in the prediction of overall energy consumption, which may be oversimplified. Further findings were less equivocal and not included.

To provide some concrete context, the PIs of CO_2 purity and energy consumption reported in experimental and theoretical studies of pressure- and temperature-swing processes using zeolite 13X are summarised in Figure 6. Their selection was based on data availability (not all PIs are reported, especially, cycle productivity) and on their relevance for large-scale use as a purity constraint is often set for CO_2 transport or utilisation, and energy consumption is of ultimate interest to the commercial sector or potential investors. A selection requirement was also applied for CO_2 content to reduce the range to less than 10 %. Except for a handful of studies considering CO_2 concentration corresponding to natural gas combustion (about 5 - 6 vol%), the concentrations are between 10 and 20 vol%, corresponding to coal-fired power plants. The temperature ranges from 276 to 323 K, with the highest occurrence of 293, 298, and 303 K. Although any conclusion is speculative and does not reveal all differences between processes, as explained above, the dominance of theoretical studies (red circles for pressure-swing processes and green circles for temperature-swing processes) is clearly evident, with TSA cycles tending to be more energy-intensive.

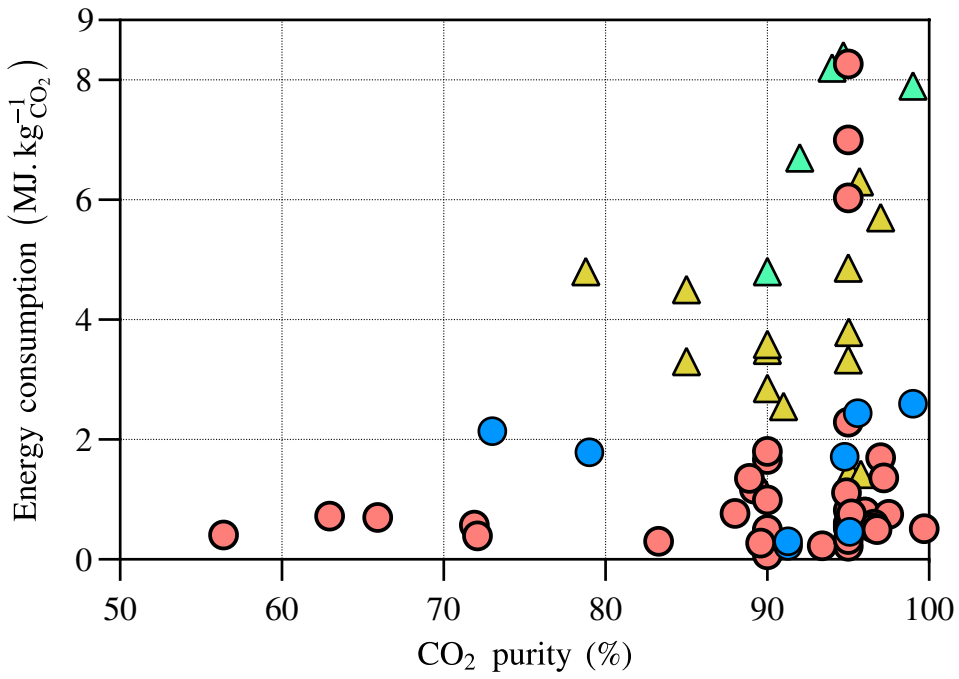

Figure 6. CO_2 purity and energy consumption reported for pressure-swing (PSA, VSA, VPSA) and temperature-swing based cycles, selected from Appendices A and B, using zeolite 13X. Red circles: theoretical studies of pressure-swing based cycles; blue circles: experimental studies of pressure-swing based cycles; red triangles: theoretical studies of temperature -swing based cycles; blue triangles: experimental studies of temperature-swing based cycles.

2.2.4 Adsorption cycle technologies in the context of PCC power plants

Adsorption for CO_2 capture has been studied for more than two decades. However, beyond laboratory-scale studies and those focusing only on the adsorption process, few have assessed the adsorption PCC in the context of fossil fuel power plants. Here, areas related to low-power district-scale emission sources producing CO_2-lean flue gases, where adsorption offers potential advantages over alternative PCC technologies [25-27], appeared to be poorly addressed. These sources require highly selective separation techniques, unlike CO_2-rich streams from the gradually declining coal power generation or large-scale industries such as cement and steel plants, which are better suited for competing technologies such as amine-based absorption.

This finding is supported by an overview in Table 3, an extension of the overview provided in [92], of studies taking power plants as a case study to assess adsorption PCC. These power plants emit flue gases at volumes 10 to 100 times higher than those identified as economically viable to incorporate adsorption processes [25-27], which is due to the substantial increase in the number of columns and auxiliary equipment, which are the most expensive parts of the flue gas cleaning process [92-95]. Table 3 also

reveals that scaling adsorption process for actual power plants, to meet their emission flow rates, is mainly approached theoretically, *i.e.* by process modelling. It also shows preference for designing "basic" 4-step cycles for similar scenarios (except for 8- to 9-step cycles in [96]), due to their straightforward process design, scalability, and established technological background, supported by successful implementation in various commercial applications, for example, air separation or hydrogen production. This is in line with the previous findings (Section 2.2.3; Figure 6) and summaries provided in Appendices A and B, where theoretical studies dominate and highly complex and experimentally unverified cycles are not scaled, as they necessitate expensive laboratory tests and rigorous optimisation. Furthermore, it can be observed that all cycles using zeolite 13X, the most common choice, achieve a CO_2 purity greater than 90 %. Studies [97-99] using activated carbon focus TSA cycles and are the only ones considering wet flue gas. Finally, clearly limited attention is paid to natural gas compared to less prospective coal, and large-capacity power plants for which the suitability of multi-column adsorption trains is questionable.

Table 3. Adsorption PCC studies considering an actual emission source for case study.

Ref.	Adsorption technology	Flue gas		Case study	CO_2 purity
		Composition	Parameters		
[92]	1-stage 4-step VSA zeolite 13X, UTSA-16 IISERP, MOF2	20 % CO_2 80 % N_2	1 bar(a), 25 °C, various: 23000 $m^3.h^{-1}$	450 TPD steam-methane reforming hydrogen plant	95.0 % (process constraint)
[97]	1-stage 4-step TSA activated carbon	9 % CO_2 79 % N_2 12 % O_2	1 bar(a), 30 °C, 13 $t.h^{-1}$	20 MW coal-fired power plant	99.1 %
[98]	1-stage 4-step TSA activated carbon	3.72 % CO_2 75.29 % N_2 12.57 % O_2 8.41 % H_2O	1 bar(a), 20 °C, 2380 $t.h^{-1}$	411 MW natural gas combined cycle power plant	-
[100]	2-stage 5-step VPSA zeolite 5A activated carbon	14.3 % CO_2 77.8 % N_2 4.6 % O_2 0.94 % Ar 0.002 % SO_2 2.3 % H_2O	1 bar(a), 20 °C, 304.3 $mol.s^{-1}$ (2 bara at 360 $mol.s^{-1}$ before the 2nd stage)	1666 MW advanced super-critical pulverised coal-fired plant	95.1 %
[99]	Moving-bed TSA (1-stage with circulating adsorbent) zeolite 13X	5–15 % CO_2 94.85 % N_2	1.05 bar(a), 30 °C, 3298 $t.h^{-1}$	802 MW natural gas combined cycle power plant	95.1 - 95.8 %
[101, 102]	4-stage[1] TSA with fluidised bed (steam regeneration) amine-grafted ion-exchange resin	15.0% CO_2 76.5% N_2 8.5% O_2 < 1 ppm_v SO_2	0.5-0.53 bar(a), 40 °C, 612 - 2718 $m^3.h^{-1}$ (plant study: 3060 $m^3.h^{-1}$)	1 MW_e sub-bituminous coal-fired power plant	93.0% (process constraint: 90.0%)
[103]	1-stage 3-step VSA zeolite 13X	11.4 % CO_2 88.6 % N_2	1 bar(a), 30 - 50 °C, 1670 $t.h^{-1}$	20 MW coal-fired power plant	99.1 %
[104]	1-stage 4-step PTSA (solar-assisted) zeolite 13X	14.98 % CO_2 85.02 % N_2	1.5 bar(a), 30 °C, 590 $t.h^{-1}$ of CO_2	800 MW_e coal-fired power plant	99.9 %
[103]	1-stage 8-step VPSA–2-stage 4-bed 9-step DR-VPSA activated carbon	13.4 - 13.8 % CO_2 86.2 - 86.6 % N_2	1.6 bar(a), 18 °C, 60 - 100 $m^3.h^{-1}$(bypass)	460 MW pilot plant	75.2 % (VPSA), 87.5 % (DR-VPSA)
[103][2]	1-stage–rotary TSA activated carbon AP4-50 synthetic zeolite Calsit 5A	2.5 - 4.5 % CO_2 89.0 - 91.0 % N_2 0.05 - 0.16 ppm_v SO_2 0.02 ppm_v NO_X	1.5 bar(a), 60 °C, 211 $t.h^{-1}$ of CO_2	250 MW_e brown coal power plant (Prunéřov II)	95.0 %
[105][3]	4-bed 10-step–VTSA Zeolite 13X-APG	12.3% CO_2 81.3% N_2 6.2% O_2 0.2% H_2O 19 ppm NO_2 42 ppm NO	1.13 bar(a), 28.5 °C, ~ 1 - 1.1 $m^3.h^{-1}$ (exp.)	4000 MW ultra-supercritical coal-fired power plant.	93.5%

[1]Three-stages were used for adsorption, one-stage was used for desorption.
[2]Before a theoretical scale-up, 140 $m^3.h^{-1}$ of flue-gas was used for pilot study of the TSA rotary system.
[3]During the experiments (exp.), 1 ~ 1.1 $m^3.h^{-1}$ of extracted stack flue-gas was processed via VTSA.

2.3 Adsorption process modelling

As evidenced by the literature review, a majority of studies are theoretically-based, using mathematical models to study PCC via adsorption, where options such as process configuration, step scheduling, feed gas composition, and flow rate can be simulated. Subsequently, one can better understand their influence on process performance, efficiency and energy intensity, and strength of their interactions. Furthermore, one can also intervene in an already existing process and explore its behaviour in scenarios that are either technically impossible or expensive and time-consuming to conduct experimentally. Another application is to qualify potential adsorbents (hypothetical or real), which are often unavailable in large quantities, are expensive to purchase or difficult to synthesise, or to scale-up laboratory experiments to an industrial-scale. One of the biggest challenges is the lack of model input data, for example, for new technologies [106].

A mathematical model of the adsorption process is based on the thermodynamic behaviour, *i.e.* the mass, energy, and momentum transport mechanisms, between the gas and the solid (adsorbent) phases. When the gas enters the column, it is transported by a combination of convection and diffusion fluxes, with a change in momentum occurring when the gas velocity is non-zero. The mass transfer of gas components into the solid phase depends on their convection and diffusion rates to the surface and into the particle pores, respectively. Adsorption takes place at the gas-solid interphase and, in the context of overall mass balance, acts as a source term causing the difference between the mass entering and leaving the column (desorption acts in an opposite way). Its magnitude is proportional to the rate of diffusion transport into the adsorbent particle, releasing heat that is accounted for in the energy balance. This heat is the main source of increasing internal column temperature [107, 108].

The course of diffusion transport is given by the morphology of the adsorbent and the flow regime inside the adsorbent pores. The primary transport mechanisms of diffusion are surface, Knudsen, molecular, and transient diffusions. Adsorbate molecules typically do not diffuse perpendicularly to the pore axis; instead, they move freely between the pore walls, reducing the diffusion rate. Consequently, the diffusion path is greater than the physical length of the pore, which is given by the coefficient of pore geometry, the so-called "tortuosity", taking into account pore structure, size, and shape. This coefficient is difficult to measure experimentally; however, for most of the adsorbents, the diffusional path is two or three times longer that the physical length of the pore. The number of pores (*i.e.* adsorbent particle voidage) as well as the number of free spaces between adsorbent particles (*i.e.* adsorbent bed voidage) occupied by the gas are equally important in the overall mass transfer rate. Other parameters influencing the adsorption rate are the gas velocity, the adsorption isotherm, the physical and sorption properties of the

adsorbent relative to the separated gas, the intensive variables: pressure and temperature, and the composition of the flue gas.

All together, these parameters formulate a system of governing (transport) equations describing the unsteady behaviour of adsorption before equilibrium is reached. Mathematically, the unsteady state leads to a system of coupled non-linear partial differential equations (PDEs) with boundary conditions in the form of ordinary differential equations (ODEs). These boundary conditions are specified for each cycle step, based on the actual change of state (intensive) variables and the gas flow regime. Solving this system of PDEs necessitates a numerical approach. When formulating the governing equations, additional thermodynamic assumptions are made to simplify the ongoing process as well as the mathematics [107, 108].

The following is an example of a one-dimensional mathematical model for diffusion-dispersion plug flow column consisting of mass, energy, and momentum balances with often applied thermodynamic assumptions. This model has been successfully applied and experimentally validated for PSA, VSA, and VPSA PCC processes removing CO_2 from a binary mixture with N_2 on zeolite-based adsorbents in a fixed-bed column [109].

The thermodynamic assumptions can be defined as follows:

1. The ideal gas model considers a binary mixture of two species without impurities.
2. The gas flow model is represented by an axially-dispersed plug flow model for one dimensional flow (axial axis z) without radial concentration, pressure, and thermal gradients.
3. The mass transfer rate between the gas and solid phases is approximated by the linear driving force (LDF) model [110].
4. The main LDF rate-controlling mechanism is defined by the mass transfer resistance in macro and mesopores and the corresponding adsorption kinetic rates of both species, assuming instant adsorption in micropores.
5. The physical properties and geometry of the adsorption bed and the adsorbent particles are assumed constant.
6. The change in internal energy in the gas and solid phases is expressed by a single non-isothermal pseudo phase, where the thermal properties (thermal conductivity and specific heat capacity) do not change throughout the process.

7. The local changes in gas velocity and pressure in the axial direction are bound by a pressure drop equation.

8. The change in momentum (kinetic and potential energies) is negligible and represented by the Darcy's pressure drop equation (*i.e.* Assumption 7).

These simplifications are valid for the following system of governing equations defined in space and time by the axial coordinate z (Assumption 2), and time t:

Mass balance of component *i* in the gas phase:

$$\frac{\partial c_i}{\partial t} = \frac{\partial}{\partial z}\left(cD_{ax}\frac{\partial y_i}{\partial z}\right) - \frac{\partial (vc_i)}{\partial z} - \rho_b\left(\frac{1-\varepsilon_b}{\varepsilon_b}\right)\frac{\partial q_i}{\partial t} \tag{5}$$

where c_i and y_i represent concentration and molar fraction of component i (CO_2 and N_2 per Assumption 1) in the gas phase, c is the total concentration of gas in the gas phase, D_{ax} is the axial dispersion coefficient, v is the gas interstitial velocity, ρ_b is the adsorbent bed density, ε_b is the bed voidage, and q_i the concentration in the solid phase, *i.e.* the amount adsorbed at equilibrium. By applying Assumption 1, state variables are related to each other by the ideal gas law:

$$c_i = \frac{Py_i}{R_gT}, \qquad c = \frac{P}{R_gT} \tag{6}$$

where $R_g = 8.314\,\mathrm{J.mol^{-1}.K^{-1}}$ is the universal gas constant, P and T stand for pressure and temperature, respectively. Introducing Equation (6) into Equation (5) yields the following:

$$\frac{\partial y_i}{\partial t} + \frac{y_i}{P}\frac{\partial P}{\partial t} - \frac{y_i}{T}\frac{\partial T}{\partial t} = \frac{T}{P}D_{ax}\frac{\partial}{\partial z}\left(\frac{P}{T}\frac{\partial y_i}{\partial z}\right) - \frac{T}{P}\frac{\partial}{\partial z}\left(\frac{vPy_i}{T}\right) - \frac{R_gT\rho_b}{P}\left(\frac{1-\varepsilon_b}{\varepsilon_b}\right)\frac{\partial q_i}{\partial t} \tag{7}$$

Total mass balance in the gas phase:

$$\frac{\partial c}{\partial t} = -\frac{\partial (vc)}{\partial z} - \rho_b\left(\frac{1-\varepsilon_b}{\varepsilon_b}\right)\sum_{i=1}^{n_{comp}}\frac{\partial q_i}{\partial t} \tag{8}$$

where n_{comp} expresses the number of gas components considered within the system. The total mass balance is akin to the previous equation, except for treating the gas mixture as a whole, and thus neglecting the axial dispersion of the individual components in the mixture. By analogy, substituting the gas concentration c using Equation (6) gives the final form:

$$\frac{\partial P}{\partial t} - \frac{P}{T}\frac{\partial T}{\partial t} = -T\frac{\partial}{\partial z}\left(\frac{vP}{T}\right) - R_g T \rho_b \left(\frac{1-\varepsilon_b}{\varepsilon_b}\right) \sum_{i=1}^{n_{comp}} \frac{\partial q_i}{\partial t} \quad (9)$$

Mass balance of component *i* in the solid phase:

$$\frac{\partial q_i}{\partial t} = k_i(q_i^* - q_i) \quad (10)$$

where k_i is the mass transfer coefficient of component i into the particle is represented by the LDF model (Assumption 3). The mass transfer coefficient incorporates several mass transfer resistances (*e.g.* surface, or micropore resistances); however, using Assumption 4, it includes only the mass transfer resistance in macropores, which prevails:

$$k_i = f(c_i, q_i^*) = \frac{c_i}{q_i^* \rho_p} \frac{15\varepsilon_p D_{p,i}}{\tau_p r_p^2} \quad (11)$$

where $q_i^* = f(c_i, T)$ is the concentration in the solid phase at equilibrium represented by an appropriate adsorption isotherm model, ρ_p is the particle density, ε_p is the adsorbent particle voidage, τ_p is the particle tortuosity, r_p is the particle radius, and $D_{p,i}$ is the diffusion coefficient into the particle macropores (Assumption 4). An effective diffusion accounting for particle voidage and pore geometry is contained in the fraction of ε_p/τ_p. For low-temperature adsorption columns with fixed-bed processing CO_2-rich gas stream, this coefficient often consists of Knudsen and molecular diffusion coefficients representing the transient phenomena in the region between laminar and turbulent flows [111].

Momentum balance:

$$-\frac{\partial P}{\partial z} = \frac{150}{4r_p^2}\left(\frac{1-\varepsilon_b}{\varepsilon_b}\right)^2 \mu_g v \quad (12)$$

where μ_g is the dynamic viscosity, couples the local changes in pressure and interstitial gas velocity in space. This equation is represented by the Darcy's law (Assumptions 7 and 8); another frequently used equation for bead-type or pelletised adsorbents is described by Ergun [112].

Enthalpy (energy) balance of pseudo-phase:

$$\left[\rho_p\left(\frac{1-\varepsilon_b}{\varepsilon_b}\right)\cdot\left(C_{p,s}+C_{p,a}\sum_{i=1}^{n_{comp}}q_i\right)\right]\frac{\partial T}{\partial t} = \frac{K_{ax}}{\varepsilon_b}\frac{\partial^2 T}{\partial z^2} - \frac{C_{p,g}}{R_g}\frac{\partial P}{\partial t} - \frac{C_{p,g}}{R_g}\frac{\partial}{\partial z}(vP)$$

$$+\rho_p\left(\frac{1-\varepsilon_b}{\varepsilon_b}\right)\sum_{i=1}^{n_{comp}}\left[\left(-\Delta H_i - C_{p,a}T\right)\left(\frac{\partial q_i}{\partial t}\right)\right] - \frac{2h_{in}}{\varepsilon_b r_{in}}(T-T_w) \quad (13)$$

where $C_{p,s}$, $C_{p,a}$, and $C_{p,g}$ are the heat capacities of solid, adsorbed, and gas phases (sometimes they are all assumed to be equal), K_{ax} is the axial thermal conductivity, ΔH is the i heat of adsorption, h_{in} is the heat transfer coefficient between the pseudo-phase and column wall (inside heat transfer coefficient), r_{in} is the inner column radius, and T_w is the column wall temperature. By combining gas and solid energy balances, a thermal equilibrium between both phases is assumed at all times and a single temperature profile of T is used for the internal column space (Assumption 6).

Adsorption column wall balance:

$$\rho_w C_{p,w}\frac{\partial T_w}{\partial t} = K_{ax}\frac{\partial^2 T_w}{\partial z^2} + \frac{2r_{in}h_{in}}{r_{out}^2 - r_{in}^2}(T-T_w) - \frac{2r_{out}h_{out}}{r_{out}^2 - r_{in}^2}(T_w - T_a) \quad (14)$$

where ρ_w, and $C_{p,w}$, are the wall density, and heat capacity, K_{ax} is the axial thermal conductivity, r_{out} is the outer column radius, h_{out} is the heat transfer coefficient between the column wall and ambient surroundings (outside heat transfer coefficient), and T_a ambient temperature. The wall temperature depends mostly on the difference between internal and ambient temperatures; its change is usually negligible for large columns made from steel.

To be solved, all PDEs must be discretised into the set of ODEs and bound by boundary conditions defined for each step. The following is an example of boundary conditions coupling each step of 4-step VSA cycle (based on the review, provided in Appendices A and B, an often choice for processing large gas emissions or for theoretical process scale-up) consisting of columns of length L. The four steps involved in the cycle are pressurisation, adsorption, blowdown, and counter-current evacuation steps. This cycle works on the same principle as described in Section 2.2.1 and illustrated in Figure 5. The column inlet, $z = 0$, refers to the direction of gas flow during pressurisation, adsorption, and blowdown steps; therefore, the column outlet is $z = L$; evacuation is performed in the opposite direction (the left

cells contain the names of cycle steps and the state of column ends by the direction of gas to be deprived of CO_2) [109]:

	Column inlet: $z = 0$	**Column outlet:** $z = L$
PRESSURISATION (co-current) **Column state:** OPEN-CLOSE	$P\|_{z=0} = P_H - (P_H - P_L)\mathrm{e}^{-\alpha t}$	$v\|_{z=L} = 0$
	$D_{ax}\left.\frac{\partial y_i}{\partial z}\right\|_{z=0} = -v\|_{z=0}\left(y_{i,feed} - y_i\|_{z=0}\right)$	$\left.\frac{\partial y_i}{\partial z}\right\|_{z=L} = 0$
	$K_{ax}\left.\frac{\partial T}{\partial z}\right\|_{z=0} = -\varepsilon_b v\|_{z=0}\rho_g C_{p,g}\left(T_{feed} - T\|_{z=0}\right)$	$\left.\frac{\partial T}{\partial z}\right\|_{z=L} = 0$
	$T_w\|_{z=0} = T_a = 293\ \mathrm{K}$	$T_w\|_{z=L} = T_a = 293\ \mathrm{K}$

	Column inlet: $z = 0$	**Column outlet:** $z = L$
ADSORPTION (co-current) **Column state:** OPEN-OPEN	$v\|_{z=0} = v_{feed}$	$P\|_{z=L} = P_{feed} = P_H = 1\ \mathrm{bar}$
	$D_{ax}\left.\frac{\partial y_i}{\partial z}\right\|_{z=0} = -v\|_{z=0}\left(y_{i,feed} - y_i\|_{z=0}\right)$	$\left.\frac{\partial y_i}{\partial z}\right\|_{z=L} = 0$
	$K_{ax}\left.\frac{\partial T}{\partial z}\right\|_{z=0} = -\varepsilon_b v\|_{z=0}\rho_g C_{p,g}\left(T_{feed} - T\|_{z=0}\right)$	$\left.\frac{\partial T}{\partial z}\right\|_{z=L} = 0$
	$T_w\|_{z=0} = T_a = 293\ \mathrm{K}$	$T_w\|_{z=L} = T_{amb} = 293\ \mathrm{K}$

	Column inlet: $z = 0$	**Column outlet:** $z = L$
BLOWDOWN (co-current) **Column state:** CLOSE-OPEN	$\left.\frac{\partial y_i}{\partial z}\right\|_{z=0} = 0$	$\left.\frac{\partial y_i}{\partial z}\right\|_{z=L} = 0$
	$\left.\frac{\partial T}{\partial z}\right\|_{z=0} = 0$	$\left.\frac{\partial T}{\partial z}\right\|_{z=L} = 0$
	$T_w\|_{z=0} = T_a = 293\ \mathrm{K}$	$T_w\|_{z=L} = T_a = 293\ \mathrm{K}$
	$v\|_{z=0} = 0$	$P\|_{z=L} = P_I + (P_H - P_I)\mathrm{e}^{-\alpha t}$

	Column inlet: $z = 0$	**Column outlet:** $z = L$
EVACUATION (counter-current) **Column state:** OPEN-CLOSE	$\left.\frac{\partial y_i}{\partial z}\right\|_{z=0} = 0$	$\left.\frac{\partial y_i}{\partial z}\right\|_{z=L} = 0$
	$\left.\frac{\partial T}{\partial z}\right\|_{z=0} = 0$	$\left.\frac{\partial T}{\partial z}\right\|_{z=L} = 0$
	$T_w\|_{z=0} = T_a = 293\ \mathrm{K}$	$T_w\|_{z=L} = T_a = 293\ \mathrm{K}$
	$P\|_{z=0} = P_L + (P_I - P_L)\mathrm{e}^{-\alpha t}$	$v\|_{z=L} = 0$

In the boundary conditions, the subscript "feed" refers to a stream of gas that is deprived of CO_2 introduced into the column during pressurisation and adsorption steps, ρ_g is the gas density. Pressures

P_A, P_I, and P_L, define the ceiling value at the end pressurisation and during adsorption steps (the highest pressure), and the floor values at the end of blowdown (intermediate pressure), and evacuation (the lowest pressure) steps, respectively. The dimensionless parameter α expresses a rate of pressure change (the suction gas velocity) in time, which is non-linear, provided by the vacuum pumps or compressors. Its choice must respect the power of the installed pumps (and valves) and affects the cycle dynamics by changing the time of steps involving the use of compressor or vacuum pump as well as the bed dynamics, *i.e.* the magnitude of gas velocity and column pressure changes. High α provides an almost instant change to the targeted pressure allowing faster cycling and higher productivity; however, this case requires large capacity vacuum pump increasing with the column dimensions [112].

2.4 Adsorption process economy

The economic aspect is crucial from the point of view of the energy sector, the potential for commercialisation, and the investors themselves. However, for non-commercial processes such as PCC by adsorption, there is currently no well-defined procedure of techno-economic analysis (TEA). The procedures recommended in the literature are, thus, based on experience with small-scale operation. Simply put, TEA can be carried out on two levels having the same cost measure, either per mass unit (often tonne) of CO_2 captured ($€.\,t_{CO_2,captured}^{-1}$), or per annual operating cost ($€.\,year^{-1}$). Both can be further extended by including the capital cost (CAPEX) payback (*i.e.* capital recovery factor (CRF)), which is influenced by actual market interest rates. For fossil fuel plants above 20 MW, the consideration of emission allowances, as described by the EU Emissions Trading System [113], is adequate. Alternatively, the economy can be expressed as the net present value, *i.e.* CO_2 avoided cost ($€.\,t_{CO_2,avoided}^{-1}$), which is not suitable without having a revenue source, such as CO_2 utilisation in carbon, capture, utilisation, and storage systems. The first level consists of the economic calculation for a PCC adsorption plant; the second subsequent level includes optimization of the first level through the most sensitive parameters used in its calculation to reduce the original cost measure [114]. This Section is limited to the first level; a detailed description of TEA in the context of VSA/VPSA adsorption unit scale-up to power plant level, including optimisation, can be found elsewhere [27, 92, 94].

A priori TEA, it is necessary to establish the concept of a PCC adsorption plant through, for example, the P&ID diagram, and consider the type, size, and number of components for which Danaci et al. [114] recommend several things to consider:

- ***Emissions flow rate*** to size equipment.
- ***Cycle time*** to optimise cycle productivity, CO_2 purity, and recovery.
- ***Cycle scheduling*** to determine the number of beds and their interconnections.

- ***Vacuum pump curves*** to set limits for maximum volumetric flow rate, respecting the valve's limitations.
- ***Mechanical design*** to propose appropriate material, size, and wall thickness of the column withstanding strains during pressurisation, and evacuation (or temperature elevation for TSA cycles).
- ***"Heat and work"*** to quantify the quality of an energy source (electrical, chemical, and kinetic energies can be converted to work, while thermal energy is proportional to its temperature).
- ***Adsorbent evaluation*** to demonstrate their efficiency and long-term stability.

They also recommended various economic considerations, which the aforementioned VSA/VPSA studies approached by conducting TEA for the total annualised costs (TAC) consisting of CAPEX, extended by CRF, and operating costs (OPEX):

$$\mathrm{TAC} = \mathrm{CRF} \times \mathrm{CAPEX} + \mathrm{OPEX} \tag{15}$$

expressed per CO_2 captured [27, 94], and CO_2 avoided [92] costs.

To give a perspective, CAPEX typically consists of total direct costs of all components and other expenditures ensuring continuous operation, planning and management, and a financial buffer against potential costs [27]:

- ***Direct costs (equipment installed costs)***: equipment purchase cost, installation costs, instrumentation and control costs, painting, insulation, electrical, piping costs, buildings, service facilities costs, spare parts, taxes, insurance, and freight charges. The following equipment may be considered:
    - ♦ Fans and blowers
    - ♦ Columns
    - ♦ Compressors
    - ♦ Heat exchangers (*e.g.* drying units)
    - ♦ Initial adsorbent cost (before replacement)
    - ♦ Switching valves
    - ♦ Vacuum pumps
- ***Indirect costs***: engineering and supervision, construction expenses, contractor fees (owner fee), process contingency, project contingency, and start-up expenses.
- ***Balance of plant costs***: auxiliary buildings, service facilities, site development, and yard improvements.

The number of equipment corresponds to the total number of columns capable of continuous operation. Multiple columns form a column train that is placed in parallel with other trains when a single train cannot process the emission flow rate [94]. Generally, constructing columns larger than about 4.3 m in diameter poses transport difficulties [114].

OPEX typically includes [27, 92]:

- ***Fixed costs***: maintenance, labour, insurance, and administrative costs.
- ***Utilities costs***: energy supplies (typically electrical or thermal), cold and hot utilities.
- ***Technologies specific costs***: replacement, transport, and supply of materials, chemical agents (*e.g.* reducing agents or catalysts).

When the TAC is determined, optimisation can be performed for multiple scenarios. These scenarios are established by varying 5 [92] or 6 operating parameters for 4-step VSA systems (Figure 5), specifically, the adsorption, blowdown, and evacuation step times (pressurisation step time is often kept constant since this step practically ends once the highest pressure is reached), the intermediate and low pressures, and the feed velocity of emissions entering the column. For VPSA, an additional parameter of highest pressure (1 bar(a) for VSA) is added. By setting upper and lower bounds for these parameters, multi-objective optimisation can be performed, if the computational power demand is met [94, 109].

2.5 Aims of the thesis

The overall aim of this thesis is to find and investigate the potential of a suitable method for PCC from industrial flue gases. A physical adsorption with a zeolite-based adsorbent was chosen based on the literature review. This review followed a necessary theoretical study of adsorption phenomena and process fundamentals, and assessed more than 200 PCC adsorption processes to find the appropriate configuration. For the case of PCC using commercially available zeolites, VSA emerged as a preferred choice among various adsorption methods when high CO_2 purity, simple design, and process scalability are required. The aspect of scalability was investigated in a subsequent literature review, identifying a research gap in evaluating the design and performance of PCC by adsorption within small-scale power plants producing CO_2-lean emissions. To address this gap, there is no adsorption design tool available and starting the experiment from scratch is an expensive, time-consuming, and complex task, requiring experience. Therefore, mathematical modelling offers the best and frequently used alternative, providing valuable insight into the process.

The resulting objective was to explore the low-temperature adsorption and 4-step VSA process for PCC in the context of a small-scale power plant, because of the advantages of adsorption over other processes

at this scale. The development of mathematical modelling as an adsorption process design tool ultimately aims at simulating continuous process operation and analysing the feasibility of VSA PCC integration into a power plant, including basic economics.

The main contribution of this thesis is the development of mathematical model and its application for the prediction of breakthrough experiments at elevated pressure with zeolite 13X, and for design and economy assessment of the PCC natural-gas CHP, which is an attractive solution for urban-scale systems, capable of providing an immediate energy supply. To achieve these objectives, the following steps had to be carried out:

1. Development of a simplified non-linear dynamic mathematical model of adsorption phenomena. The reliability of the model will be verified using high-pressure breakthrough experimental data, and its robustness assessed through analysis of the numerical approach and balance equations, and application for process design.
2. Development of a complex non-linear dynamic mathematical model of 4-step VSA process, enabling simulation of various scenarios for different process parameters and configurations, and its application to experimental and theoretical studies.
3. Design of adsorption PCC system integrated into an urban-scale energy system, including general economic assessment.

Chapter 3

3 Adsorption experiments and modelling

This chapter combines theoretical modelling with practical application, demonstrated by experimental breakthrough measurements using zeolite 13X, which were carried out in collaboration with the University of Chemistry and Technology (UCT) in Prague, with results published in [MN3]. First, a simplified mathematical model (isothermal and isobaric) is developed to predict the breakthrough response (onset time) and the slope of the breakthrough curve. The results of CO_2 equilibrium capacities measured at 2 and 5 bar are presented to examine the use of high-pressure sorption on zeolite 13X. Then, the results and analysis of mathematical modelling, including the results of sensitivity analysis affecting the prediction accuracy, are discussed. The last Section demonstrates the use of a mathematical model to design a PCC process using the so-called "empirical approach".

The main motivation of this approach was to analyse the fundamentals and capabilities of mathematical modelling, to study the sensitivity of process parameters, and to verify its usability for the prediction of adsorption phenomena based on experimentally measured data. An additional aim was to assess the initial phase of adsorption process design. The breakthrough measurements are an effective method for obtaining equilibria (*e.g.* equilibrium adsorption isotherm parameters) and kinetic (*e.g.* mass transfer rate constants) parameters and gas transport characteristics (*e.g.* axial dispersion, or heat transfer characteristics), taking place in a fixed-bed column packed with adsorbent particles. The course of the measurement is akin to the adsorption step in equilibrium-controlled adsorption processes (PSA, VSA, or TSA), indicating a time when CO_2 begins to enter the atmosphere. The breakthrough curve is obtained by monitoring the concentration of adsorbing components (in this case CO_2) at the outlet of the column and plotting this value as a function of time. In addition, gas flow rate, pressure, and temperature are often also monitored. For single-component equilibrium measurements, a carrier inert gas (*e.g.* helium) is used; otherwise a multicomponent mixture of adsorbing gases is introduced into the column. When the concentration at the outlet of the adsorbing gases is equal to the inlet concentration, it can be assumed that the adsorbent is fully saturated. These experiments are an easy way to test and validate a mathematical model compared to conducting experiments with PSA or VSA units requiring complex process control and a more detailed mathematical model [116].

3.1 Materials

The zeolite molecular sieve 13X (*Merck - Sigma-Aldrich*, Germany) was used, as synthesised by the manufacturer, for the CO_2 breakthrough experiments. The adsorbent particles had a compact structure

and a smooth surface and were assumed to be homogeneous spheres (Figure 7). Their diameter ranged from 1.9 to 2.1 mm with a volume of 2.84 - 3.46 mm^3. More detailed characteristics in the context of column packing are summarised in Table 3, together with the column dimensions.

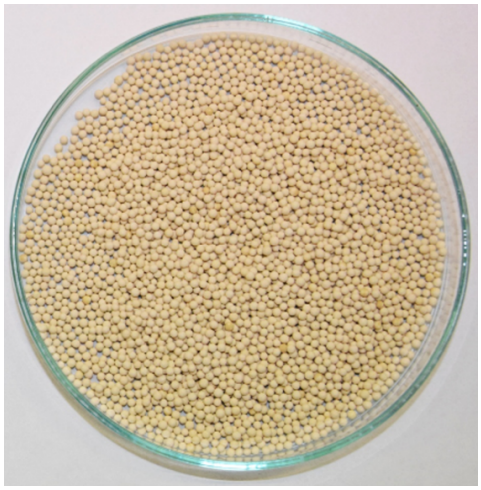

Figure 7. Zeolite molecular sieve 13X particles (*Sigma-Aldrich, Germany*).

3.2 Experimental breakthrough apparatus

The breakthrough apparatus is composed of the gas distribution and flow control systems, the adsorption column and humidifier, the climate chamber with programmable temperature controller, and the analytical terminal. Figure 4 shows the outside view of the entire apparatus (a), the front and top views of the breakthrough system with a humidifier placed inside the climate chamber for the outside temperature constant (b), and the adsorption column detail (c), which is a cylindrical stainless-steel column packed with about 0.143 kg of zeolite 13X.

3.2.1 Main components

The gas mixture consisting of 13 vol% CO_2 balanced by synthetic air is supplied from a pair of gas cylinders and simulates a pre-purified flue gas (*i.e.* undergoing a denitrification, desulphurisation, and eventual drying). After passing through the flow controller, this gas can be directed into the adsorber or spectrometer by using a manual ball valve switch. This principle is used to evaluate the adsorption capacity. The gas stream can be pre-humidified before entering the adsorber. The humidification path leads to humidifiers capable of achieving a relative humidity (RH) of 70 - 85 % at a given temperature and pressure. Here, these humidifiers were bypassed to maintain dry conditions. The gas then flows through the adsorber column from top to bottom, passing through the glass beads controlling the flow distribution, and absorbs the released adsorption heat, which is removed outside the climate chamber by cooling in a liquid bath.

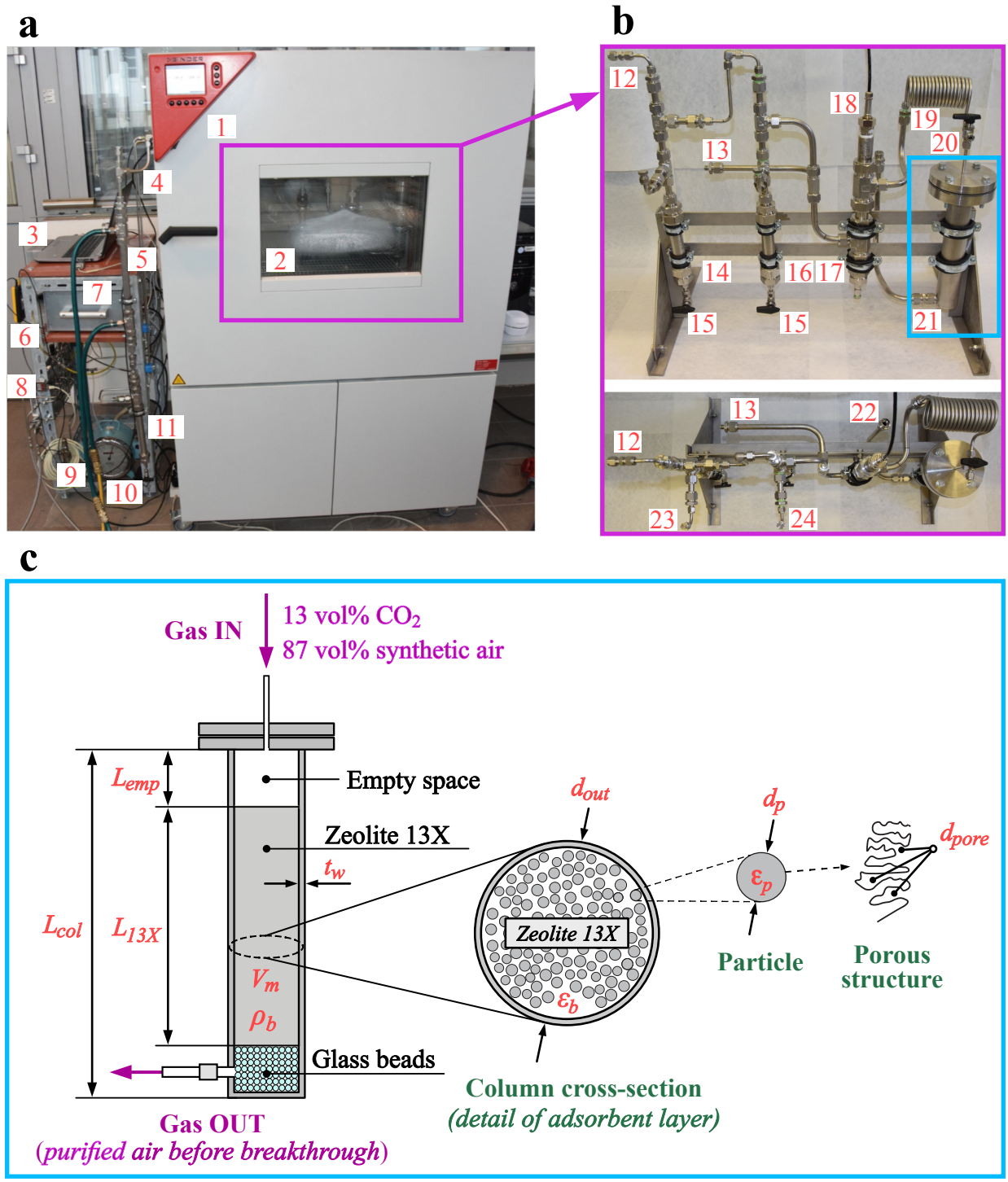

Figure 8. The breakthrough apparatus: **(a)** Outside view: 1 - glazed chamber, 2 - climate chamber, 3 - PC (data collection and process control), 4 - side chamber passage of pipes and cables, 5 - liquid cooler, 6 - thermometer with data-logger, 7 - IR spectrometer, 8 - mass flow meter, 9 - safety valve, 10 drum-type gas meter, 11 - condensate sump**; (b)** Climate chamber: 12 – humidifier gas inlet, 13 - dry gas path inlet, 14 - first humidifier chamber, 15 - water discharge, 16 - second humidifier chamber, 17 - hygrometer pressure sump, 18 - hygrometer probe, 19 - heat exchanger, 20 - three-way valve (adsorber column bypass), 21 - adsorber column, 22 - adsorber column outlet, 23 and 24 - water inlet regulators (humidifier wetting); **(c)** Adsorption column detail: no. 21 in (b).

Table 4. Adsorption column geometry, physical properties of the adsorbent packing, and of the adsorbent particles (zeolite 13X).

Adsorption column: geometry	
Bed type, material	*Fixed-bed, stainless steel*
Inner column length, L_{col}	0.26 m
Empty space length, L_{emp}	0.08 m
Inert bed length	$0.019 - 0.025$ m (glass beads layer)
Adsorbent bed length, L_{13X}	$0.155 - 0.161$ m
Inner diameter, D_{in}	0.04 m
Wall thickness, t_w	0.002 m
Adsorption column: packing (zeolite 13X)	
Material, manufacturer	*Molecular sieve 13X, Sigma Aldrich*
Total material volume[1], V_m	$195 - 202$ cm^3
Material weight[1], m_m	$0.1425 - 0.1435$ kg
Bulk density, ρ_b	$710 - 730$ kg.m^{-3}
Mean bed voidage, ε_b	0.373[1]
Particles shape	*Homogenous spheres*
Particle diameter, d_p	$1.90 - 2.10$ mm
Particle volume, V_p	$2.84 - 3.46$ mm^3

[1]Material volume and weight correspond to the entire packing, including interparticle and intraparticle spaces.
[2]Estimated using Equation (16).

For humid gas measurements, excess moisture is condensed in a condensate sump. The gas pressure is then reduced to the atmospheric level using a back pressure regulator before entering the IR spectrometer *Ultramat 23 IR* and subsequently a drum-type gas metre. Monitoring of adsorption and desorption is carried out by an online analysis of the gas flowing through the apparatus. The sorption rate evaluation is based on a comparison of the adsorptive content in the gas at the adsorption column inlet and outlet.

3.2.2 Measurement protocol

To ensure validity and reproducibility of measurements, the same procedure must be followed in each experiment. Before all of them, a blank volume correction (Figure 9) was performed using inert material (glass beads) of the same total volume as the real sample. All experiments were carried out with a constant gas flow rate for two pressures (2 and 5 bar) and four temperatures (283, 293, 303, and 313 K) with a gas mixture of known composition.

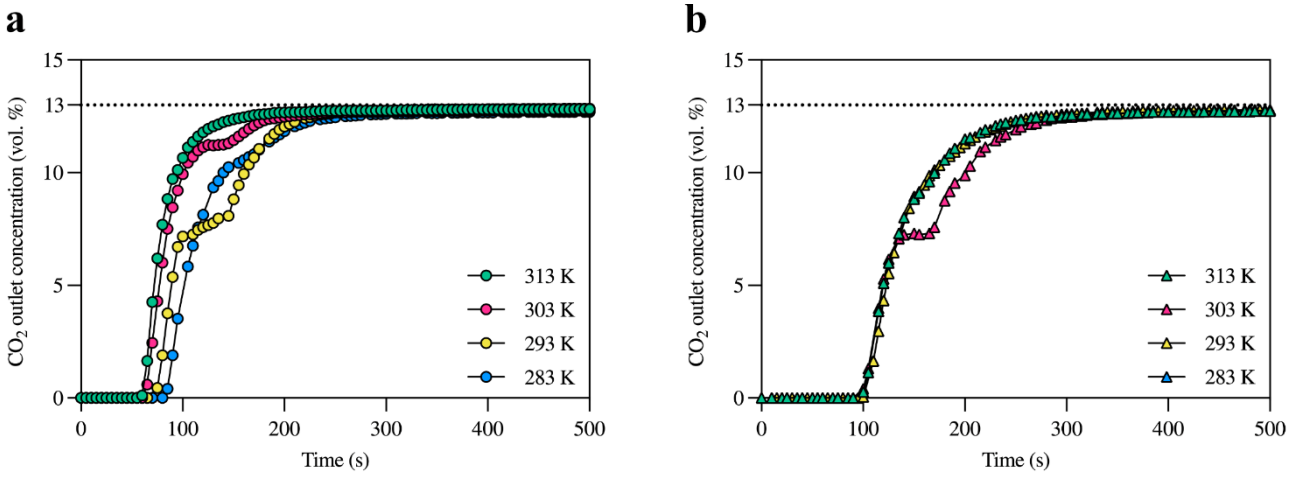

Figure 9. Blank curves at 283, 293, 303, and 313 K and **(a)** 2 bar, and **(b)** 5 bar. *The time interval is shortened from about 1800 s to 500 s, when the CO_2 concentrations at the outlet have almost stabilised.*

The procedure was as follows:

1. **Regeneration (adsorbent and column)**: the adsorbent is dried to a constant weight and placed into the adsorption column. Nitrogen at a flow rate of 2 $cm^3.min^{-1}$ is introduced into the adsorber, which is heated to 393 K. After a complete regeneration, indicated by the IC spectrometer, a breakthrough experiment begins.

2. **Breakthrough experiment (adsorption)**: initially, N_2 stream passes through the adsorption column, which is set to the working pressure (2 or 5 bar). The chamber temperature is reduced to the working temperature (283, 293, 303 or 313 K), and after stabilising, the inert gas is changed to the simulated flue gas (13 vol% CO_2 balanced by synthetic air). The adsorption phase ends when the CO_2 concentrations at the inlet and outlet of the adsorber are equal, indicating adsorption equilibrium and maximum saturation of adsorbent.

3. **Desorption**: the desorption was carried out at atmospheric pressure and elevated temperature (*i.e.* PTSA cycle). Once CO_2 is released from the adsorbent, the column is purified by N_2 or any other non-reactive gas (as opposed to adsorption cycles, CO_2 cannot be used due to the limitations of the IR spectrometer).

3.3 Constitution of simplified mathematical model

A mathematical model was developed taking into account the experimental nature of adsorption phenomena and the adsorption column design (*i.e.* packed fixed-bed). This column was modelled for idealised one-dimensional plug-flow, while the adsorption phenomenon was simplified with the following assumptions:

1. The gas is a binary mixture of CO_2 and N_2 and behaves according to the ideal gas law (O_2, contained in the synthetic air, has similar adsorption characteristics as N_2, which is relevant for zeolite 13X [117]; in addition, the prediction of diffusion in ternary gas mixture is inaccurate [118].).
2. The system is isothermal and adiabatic (adsorption heat and heat loss to the outside environment are neglected).
3. The system is radially homogeneous without the occurrence of concentration, diffusion, and temperature radial gradients.
4. The change in kinetic and potential energies is negligible.
5. The physical properties of the gas mixture, such as adsorption enthalpy, density, diffusion coefficients, specific heat capacity, and dynamic viscosity, are constant.
6. The physical properties of the adsorbent as well as the bed voidage are uniform.
7. The mass transfer rate between the solid and gas phases is described by the LDF model.
8. The adsorbent is fully regenerated at the beginning, as described in the measurement protocol (Section 3.2.2).
9. The pressure drop is negligible, and thus the interstitial gas velocity does not vary.

The ongoing adsorption process in the breakthrough column differs from real adsorption systems in its placement and configuration. Normally, the temperature continuously varies with respect to the generated adsorption heat and the volumetric flow, affecting the behaviour of both phases. However, the

thermally insulated chamber enables isothermal conditions to be reached after a few minutes from the start of the process. Assuming isothermal conditions (Assumption 2) may still compromise the prediction accuracy, but significantly reduces the computational effort and complexity of the model, leaving room for in-depth sensitivity analysis. Assumptions 1, 3, and 5-7 also simplify the phenomenon, although their application was shown to be relevant [108]. Assumption 8 is typical for breakthrough experiments [116], or for the first cycle in adsorption systems, as subsequent cycles do not achieve full adsorbent regeneration and lose some of their working capacities. The adsorption of gases causes a different volumetric flow at the column inlet and outlet, depending on the amount of strongly adsorbed species, which equalises after the full adsorbent saturation. However, during the adsorption step in the breakthrough experiment, this effect is insignificant unless the amount of strongly adsorbed species exceeds 20 %, as reflected in Assumption 9 [119].

Based on these assumptions, the adsorption phenomenon is described by two governing equations, Equations (5) and (10), retrieved from a VSA model detailed in Section 2.3. The former balance equation describes the mass flow of component *i* in the gas phase, and the latter the mass transfer of the adsorbate in the solid phase, simplified by the LDF model [110].

In the model, the mean bed voidage was calculated using a correlation proposed by [120] due to its calculation difficulties and unequal distribution within the bed, which incorporates the ratio of column and adsorbent particle diameters (d_{in}/d_p):

$$\overline{\varepsilon}_b = 0.373 + 0.917 \exp\left(-0.824 \frac{d_{in}}{d_p}\right) \tag{16}$$

This value was used to determine the interstitial velocity from a known inlet superficial velocity: $v = v_0/\overline{\varepsilon}_b$. The axial dispersion coefficient was calculated using a correlation of Edwards and Richardson (1970), incorporating Wicke (1973) approximation of coefficient γ, and Bischoff (1969) expression of coefficient β. This coefficient dominates over pure convection flux at higher Reynolds numbers ($Re_p >$ 10) [121], which was maintained within a range of about 3 - 8 across all measurements, as strong dispersion affects adsorption efficiency. A detailed calculation can be found in [116] for adsorption of CO_2 from CO_2/N_2 mixture in a packed fixed-bed:

$$D_{ax} = \gamma D_{m,CO_2-N_2} + \frac{Pe_\infty^{-1}\, v d_p}{1 + \frac{\beta\gamma D_{m,CO_2-N_2}}{v d_p}} \tag{17}$$

where Pe_∞ is the limiting value of Péclet number calculated by [122] as $Pe_\infty = 6.7d_p$ for particle size lesser than 2.5 mm.

The mass transfer coefficient k_i of component *i*, found in Equation (10), was simplified to the resistance of mass transport by diffusion in macropores, prevailing the commercial zeolites that are purposely made to minimise micropore diffusion. The resistance to gas permeation through the adsorbent film layer is usually insignificant [123]:

$$k_i = \frac{15 D_{p,eff}}{r_p^2} \frac{c_i}{\rho_p q_i^*} \tag{18}$$

where r_p is the adsorbent particle diameter, $D_{p,eff}$ is the effective value of the diffusion coefficient in the particle pores (macropores in this case), and $c_i/(\rho_p q_i^*)$ is the dimensionless slope of the adsorption isotherm valid for adsorbent particles with homogeneous structure. The adsorption isotherm (q_i^*) was represented by single-site Langmuir (SSL) model, which will be discussed later in the text due to the specifics of its determination. Effective diffusion depends on the flow regime in the macropores, which is determined by the Knudsen number [124]. The diffusion transport in macropores in zeolites takes place in the transition area, where both mechanisms, Knudsen and molecular diffusions, play an equal role:

$$D_{p,eff} = \frac{\varepsilon_p}{\tau_p} \left(\frac{1}{D_{m,CO_2-N_2}} + \frac{1}{D_K} \right)^{-1} \tag{19}$$

where the tortuosity τ_p ranges from about 2 to 3 in packed beds filled with a non-structured zeolite adsorbent [125], however, a more often used value of 3 was assumed [116]. The adsorbent particle voidage ε_p was calculated combining estimated (ε_b) and experimentally (ρ_b, V_{pore}) obtained values:

$$\varepsilon_p = \rho_p V_{pore} = \frac{\rho_b}{1 - \varepsilon_b} V_{pore} \tag{20}$$

where ρ_p is the particle density and V_{pore} is the volume of pores expressed in $\mathrm{m^3.kg^{-1}}$.

There are many correlations that can be applied to estimate the molecular diffusivity. An approximation of Fuller et al. (1969) was used, which, according to [118], provides high accuracy for the binary mixture of CO_2/N_2:

$$D_{m,CO_2-N_2} = \frac{0.00143 T^{1.75}}{P M_{CO_2-N_2} \left[\left(\sum v_{CO_2} \right)^{1/3} + \left(\sum v_{N_2} \right)^{1/3} \right]^2} \tag{21}$$

where P is the gas pressure (in bar), T is the temperature, and ν is the molar volume of the gas phase. The Knudsen diffusion coefficient D_k was approximated for both components using the Derjaguin correlation having higher precision for zeolites [125]:

$$D_{K,i} = \frac{9}{13}\left(\frac{d_{pore}}{3}\sqrt{\frac{8R_gT}{\pi M_i}}\right) \tag{22}$$

where d_{pore} is the pore diameter, and M_i is the molar weight of component *i*. The Knudsen diffusion of binary gas mixture was calculated as resistances connected in parallel.

Adsorption isotherm assessment

Adsorption isotherms are essential components of any mathematical model; their parameters are often provided explicitly as input. Here, they were not measured, and the manufacturer does not provide them. Although zeolite 13X is a frequently used adsorbent, limited experimental data are available at higher pressures in the existing literature. Adsorption isotherms at high pressure on zeolite 13X can be found in [126] and their summary, or in the *NIST ARPA-E* [42] database, which contains about 25 experimental studies with competitive CO_2 adsorption isotherms up to 6 bar on zeolite 13X. However, these isotherms differ by the 13X manufacturer, its Si/Al ratio, particle size and geometry, and packing structure, which excluded their use. Therefore, the approach used by [127] was applied. It involved fitting of the SSL isotherm (Equation (23)) model parameters, within the typical range for zeolite 13X.

$$q_i^* = \frac{q_s b_i c_i}{\rho_p(1 + b_{CO_2}c_{CO_2} + b_{N_2}c_{N_2})} \tag{23}$$

where q_s is the maximum saturation capacity, b_i and c_i is the Langmuir equilibrium constant and concentration of component *i*, respectively, and ρ_p is the particle density to correspond with the balance equations dimensions. The use of the SSL model may seem like a simplification because more complex models can better approximate the nonlinearity of CO_2 adsorption. However, the idea was to start with a simple isotherm model, which proved to be sufficient even for higher pressures, as discussed in Section 3.5. Furthermore, using another model may raise questions about the number of fitting parameters and, consequently, uncertainty.

The methodology was based on changing the $b_{0,i}$, the internal energy ΔU_i (both are functions of b_i), and the maximum saturation capacity of the monolayer q_s, within the constrained range [127]. The goal was to predict the breakthrough onset time by one-time adjustment of the adsorption isotherm within the

range of five experimentally measured isotherms at each of four cycles at 2 bar because using the data measured at 5 bar may question the validity (*i.e.* the model assumption) of ideal gas behaviour.

Numerical solution

The PDE system with fixed initial and boundary conditions was differentiated into N control volumes with respect to the axial (spatial) axis z and the time t to obtain the concentration profile of CO_2 and N_2 in the gas phase and the adsorption rate in the solid phase. Adsorption is a dynamic process accompanied by a step change in concentration caused by the decomposition of the transport mechanism from purely convective to convection and diffusion once the gas enters the unsaturated empty bed; therefore, the Danckwerts' boundary condition for the column inlet was applied: $D_{ax}[\partial c_i(t,0^+)/\partial z] = v[c_i(t,0^+) - c_0(t,0^+)]$, where the subscript "0" refers to the initial value and the superscript "+" to the axial position just beyond the column inlet. A better approximation was achieved by using a higher-scheme with flux limiters recommended by [109, 128, 129] for a lumped kinetic model to ensure stability of the solution. Consequently, a second-order TVD (total variation diminishing) explicit finite volume (FVM) scheme was used. This scheme converts the conserved values f (Equations (5) and (10)) in the centre of N control volumes with a volume of ΔV into algebraic expressions by integrating spatial derivatives over each of these volumes:

$$f_j(t) = \frac{1}{\Delta V}\int_{V_j}^{0} f(t)\mathrm{d}V \tag{24}$$

where $j \in \mathbb{Z} = (0, N)$ is the index of each control volume centre. The FVM scheme was combined with flux (slope) limiters, putting control volume centre and wall values ($j = j + 0.5$) in relation. The initially incorporated van Leer flux limiter is defined as:

$$\phi(r_{j+0.5}) = \frac{r_{j+0.5} + |r_{j+0.5}|}{1 + |r_{j+0.5}|} \tag{25}$$

where r is the successive slope ratio, a determinant of the numerical solution smoothness:

$$r_{j+0.5} = \frac{f_j - f_{j-1} + \delta}{f_{j+1} - f_j + \delta} \tag{26}$$

where $\delta = 10^{-10}$ is a small number, preventing a division by zero. Further details can be found in [109]; van Leer limiter provides a good match in approximating steep changes associated with adsorption phenomena, as shown by [109, 128, 129], and was therefore chosen for this model.

The differentiated equations were solved in MATLAB using the *ode23s* solver for the length step $\Delta z = 0.003$ m and time step $\Delta t = 0.003$ s.

3.4 Evaluation of experimental data

Textural properties of zeolite 13X

Zeolite 13X characteristics had to be obtained prior to running a mathematical model.

The BET surface area (S_{BET}) and pore size distribution (Figure 10) were analysed by a *Coulter SA 3100* particle size analyser using N_2 physisorption at 77 K. BET analysis was also used to estimate the average size of the pores:

$$d_{pore} = \frac{4V_{pore}}{S_{BET}} \tag{27}$$

The BET surface area of 511.65 $m^2.g^{-1}$ and pore volume of 3.317×10^{-4} $m^3.kg^{-1}$ were measured, while average pore size of 3.33×10^{-8} m was estimated. The pore size distribution, limited by partial pressure $P/P_0 \approx 1$ owing to the nature N_2 physisorption, indicated a mesoporous nature of adsorbent particles (pore size classification by *IUPAC* [36]). As a result, diffusional resistance in micropores was excluded from consideration.

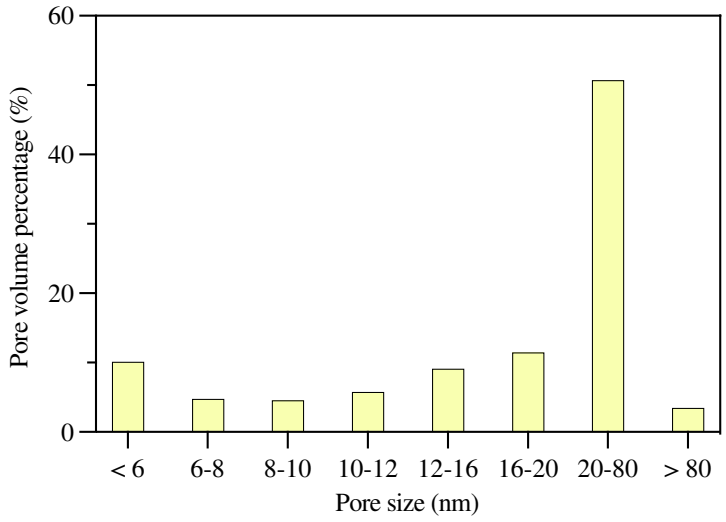

Figure 10. Pore size distribution obtained by N_2 physisorption at 77 K at $P/P_0 \approx 1$.

CO_2 sorption properties of zeolite 13X: breakthrough experiments

The breakthrough experiments were carried out in 5 cycles of adsorption and desorption after 24 h of degassing at 423 K, as described in Section 3.3.2. The measured equilibrium adsorption capacities were averaged over all cycles and can be seen in Figure 11 with the summary presented in Table 4.

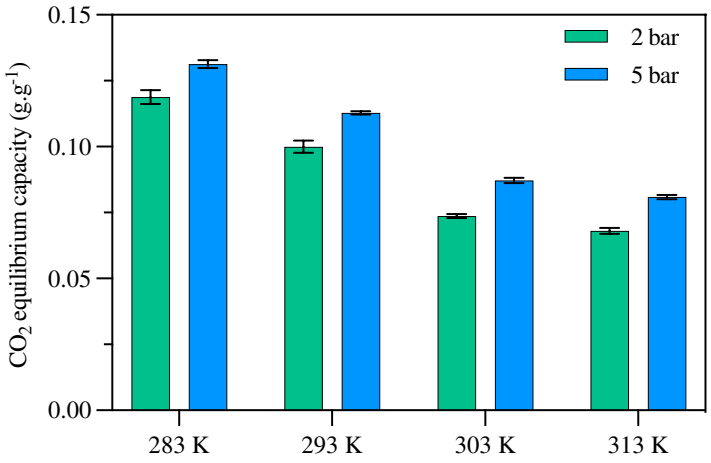

Figure 11. CO_2 equilibrium capacities at 283, 293, 303, and 313 K obtained from the breakthrough experiments.

A maximum variation for each adsorption pressure ranged from 0.97 % to 2.32 % at 2 bar and 0.49 % to 1.20 % at 5 bar. The dependence of the magnitude of the error on the measurement conditions did not show a clear trend for adsorption temperature, but the average adsorption capacity varied more between cycles at the lower adsorption pressure (2 bar). A possible explanation could be that higher pressures cause faster adsorption, as evidenced by the breakthrough curves measured at 5 bar (Figure 12).

As expected, zeolite 13X showed the highest CO_2 adsorption capacities at high pressure and low temperature, that is, 0.1188 $g_{CO_2}.g_{13X}^{-1}$ at 283 K and 2 bar, and 0.1313 $g_{CO_2}.g_{13X}^{-1}$ at 283 K and 5 bar. These conditions can be reached only under dry conditions, which is a typical demand for zeolite-based adsorbents. If the water vapour content is negligible or a water-resistant adsorbent is used, it can be argued that reducing the flue gas temperature from 303 K to 293 K would enhance CO_2 adsorption capacity the most. Although this is true for both pressures, a higher pressure significantly reduces the influence of adsorption temperature on the CO_2 adsorption kinetic rate, as evidenced by about a 30 % time difference between breakthrough onsets at 283 K and 313 K at 5 bar (Figure 12b), compared to more than a 300 % difference for the same temperatures at 2 bar (Figure 12a). This prominent feature could provide a solution for processing wet gas streams or at least eliminate the energy consumption of dehydration by adsorbing CO_2 at elevated pressure and temperature, above the dew point of the flue gas,

without substantially lowering the amount adsorbed. However, further research would have to be conducted in this manner.

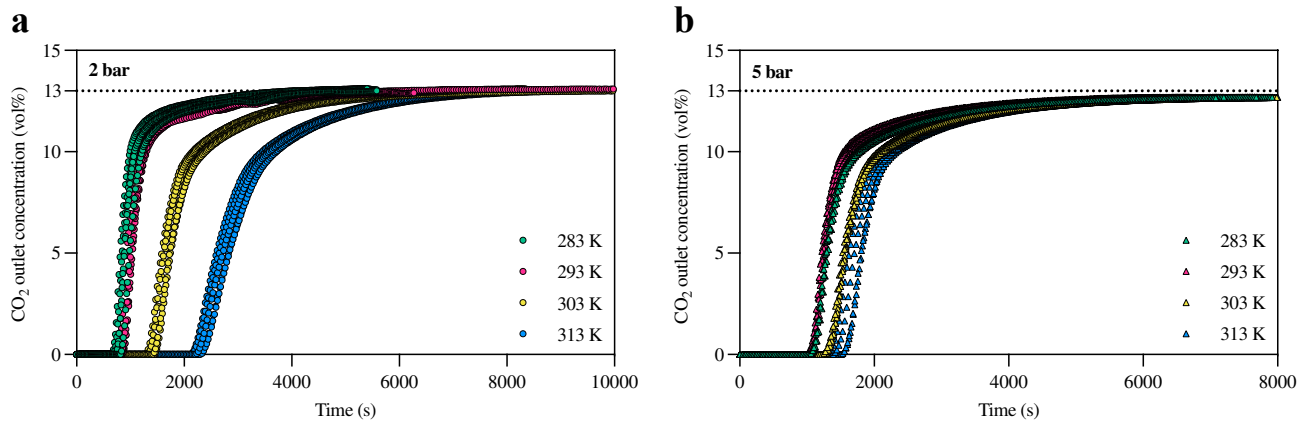

Figure 12. Experimentally measured breakthrough curves at 283 K (green), 293 K (red), 303 K (yellow), and 313 K (blue) at **(a)** 2 bar and **(b)** 5 bar.

Observing an almost linear dependency between the outlet volumetric flow and the CO_2 outlet concentration after the breakthrough onset (Figure 13), which is not surprising, is worth practical consideration. Given the difficulty of measuring CO_2 concentration using an IR sensor, sensing mass-flow rate may provide an alternative or control means. For example, mass flow meters could serve as indicators of CO_2 concentration at each column outlet in multicolumn systems, detecting the permissible amount of CO_2 in the effluent that can be released into the atmosphere, because the increase in volumetric flow rate between the breakthrough onset and the adsorbent saturation is almost proportional to the CO_2 outlet concentration. Their difference is about 4 % when averaged over five measurements at 5 bar and 283 K and declines below the curve plateaus. Specifically, it is about 0.2 % when 15 % CO_2, relative to its inlet concentration, exits the adsorber, which is a standard limit in commercial PCC technologies [88]. Clearly, such a comparison is valid for a controlled laboratory conditions and would not replace direct concentration measurements; however, it may offer additional measure for CO_2 emissions monitoring. Inversely, from a process modelling perspective, one can use CO_2 outlet concentration to estimate the effluent volumetric flow rate and, therefore, its velocity, column pressure drop, and axial dispersion. It should be noted that this hypothesis requires a proper verification.

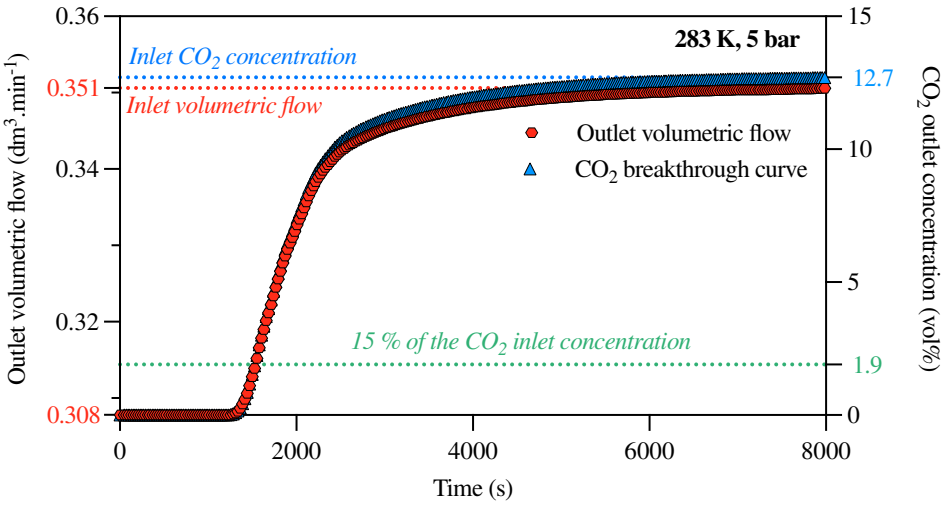

Figure 13. Experimentally measured curves: volumetric flow (red) and CO_2 outlet concentration (blue) averaged over five measurements at 283 K and 5 bar.

Table 5. Experimental results of zeolites 13X obtained from N_2 physisorption at 77 K and CO_2 equilibrium capacities derived from breakthrough experiments.

Adsorption / desorption pressure	2, 5 bar / 1 bara
Adsorption / desorption temperature	283, 293, 303, and 313 K / 393 K
Volumetric flow	*2 bar*: 0.024 - 0.045 $m^3.h^{-1}$
	5 bar: 0.021 - 0.023 $m^3.h^{-1}$
CO_2 molar fraction, y_{CO_2}	0.13 (0.87 of synthetic air)
CO_2 adsorption capacities, $q^*_{CO_2}$	
2 bar (283, 293, 303, and 313 K)	0.119, 0.100, 0.074, and 0.068 $g_{CO_2}.g^{-1}_{sorbent}$
5 bara (283, 293, 303, and 313 K)	0.131, 0.113, 0.087, and 0.081 $g_{CO_2}.g^{-1}_{sorbent}$

3.5 Evaluation of breakthrough curve modelling

The breakthrough curve modelling had to deal with a missing adsorption isotherm. Consequently, the experimental breakthrough data were reduced to the CO_2 adsorption capacities, the time of the breakthrough onsets, and the shape (slope) of the breakthrough curves. Paradoxically, this challenge allowed to further examination of the possibilities of mathematical modelling and understanding its suitability and limits. Other model parameters were obtained from the measured textural properties of zeolite 13X (Section 3.4) and from the estimated parameters (Table 4).

The fitting of SSL model parameters was performed in *MATLAB 2021b* for 283 K. The best possible shape of the breakthrough curve was achieved by changing q_s , and b_{0,CO_2} (the internal energy remained constant after few tests, because of high sensitivity to the stability of the numerical solution in the region before the breakthrough occurred), and the flux limiter, which showed a high influence on the breakthrough curve slope. The following parameters were used:

$$\textbf{Fitting constraints}\begin{cases} q_s = 3.6 - 4.6\ \text{mol.kg}_{13X}^{-1} \\ b_{0,CO_2} = 2 - 2.5 \times 10^{-6}\ \text{m}^3.\text{mol}^{-1} \\ \Delta U_{CO_2} = -35\,000\ \text{J.mol}^{-1} \\ \Delta U_{N_2} = -10\,000\ \text{J.mol}^{-1} \\ \textbf{Flux limiter}: \text{van Leer (1974)} \end{cases} \tag{28}$$

The "optimum solution" was obtained for $q_s = 3.7\ \text{mol.kg}_{13X}^{-1}$ and $b_{0,CO_2} = 2.1 \times 10^{-6}\ \text{m}^3.\text{mol}^{-1}$; for the nitrogen site: $b_{0,N_2} = 1.0 \times 10^{-6}\ \text{m}^3.\text{mol}^{-1}$ as shown in Figure 14.

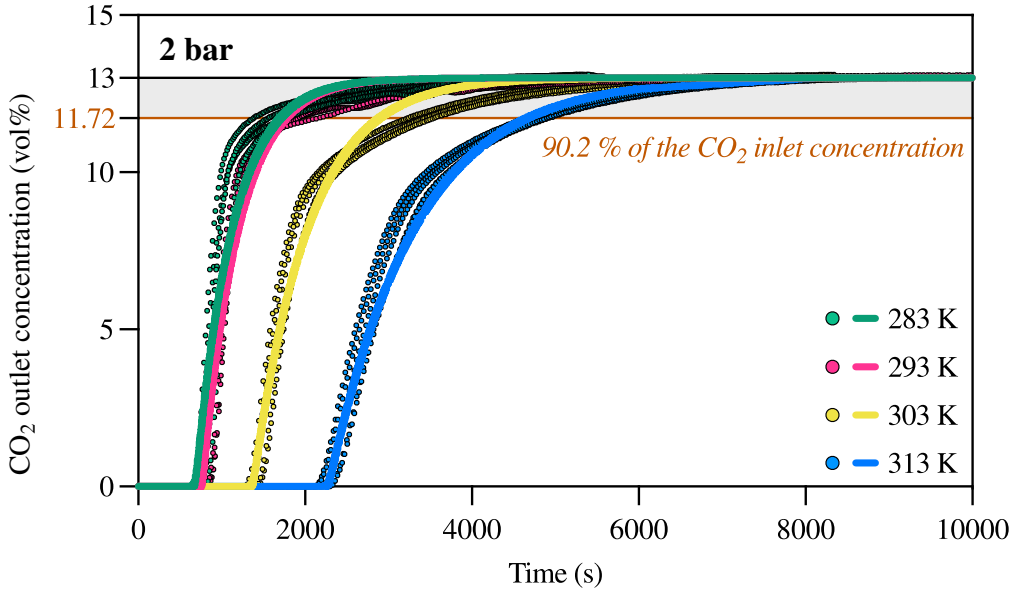

Figure 14. Comparison between the experimentally measured breakthrough curves (dotted lines) and simulation results (solid lines) at 283 (green), 293 (red), 303 (yellow), and 313 K (blue) and 2 bar. The grey-shaded area represents the largest deviation between simulation and experimental data, which exceeded 10 % when the total amount of 90.2 % of CO_2 in the simulated gas (about 11.72 vol% CO_2 relative to synthetic air) appeared at the column outlet.

The breakthrough onset time correlated with a high degree of accuracy for other adsorption temperatures, 293, 303 and 313 K, while the fitting parameters remained constant. The region where the adsorption rate slows down as a result of high saturation of the adsorbent (the upper end of the curve reaching a plateau) was accompanied by the highest deviation across the adsorption temperatures. An improvement

was achieved by adapting the flux limiters used in the non-linear schemes [129], namely, van Leer limiter instead of using the QUICK scheme.

Applying this approach, the results can be generalised as follows:

- The prediction of the breakthrough onset time can be made with a satisfying accuracy having a 2 % maximum deviation from the experimental values (averaged over five cycles that were tested) across the range of adsorption temperatures. This also includes the area where the amount of 5 to 15 % of the CO_2 inlet concentration appears at the outlet, which, in an application scaled for PCC, would likely be an indication to terminate the adsorption step and transfer the CO_2-rich stream into the regenerated column. The highest deviation was found for 283 K, where the predicted time for the occurrence of 15 % CO_2 from the inlet CO_2 concentration was 4.3 % (in contrast, the deviation for 293 K was 0.2 %).

- Accurate prediction of the adsorbent utilisation efficiency (indicated by the slope of the breakthrough curve along its length) requires a deeper analysis of the parameter estimation and of the chosen numerical scheme. There is a relatively long-time interval before the breakthrough curve reaches its peak point (*i.e.* the plateau) because the change in the CO_2 outlet concentration decreases after about 75 % of the CO_2 inlet concentration. In simulation, the deviation exceeded 10 % when the total amount of 90.2 % of CO_2 in the simulated gas (about 11.72 vol. % CO_2 relative to synthetic air) appeared at the outlet and continued to grow moderately until reaching the plateau. One of the possible explanations may be the negligence of the non-uniform generation of adsorption heat, *i.e.* exclusion of energy balance by assuming isothermal conditions, or by performing experiments in a small column (L_{col}/d_{in} ratio of 6.5), for which any temperature change is more significant relative to the breakthrough curve shape. A potentially higher correlation for the experimental data obtained if the energy balance is included can be found in the literature [130, 131], pointing out that using temperature as a variable affects both the adsorption rate and the equilibrium capacity, so it can result in a flattened curve plateau, *i.e.* the long tail, until the inlet and outlet CO_2 concentrations equalises. On the contrary, the isothermal model seems to be relevant for low flue gas velocities (higher velocities increase temperature) if the LDF mass transfer coefficient is selected properly, which was in the model estimated using Equation (18) [132]. Looking at the results from the real operational perspective of PCC, it is unlikely that a similar amount of CO_2, at which the breakthrough curve model showed the highest deviation, would be permitted to enter the atmosphere due to significant decreases in CO_2 capture efficiency (for coal-fired and natural gas combined cycle power plants, *ISO 27919-1-2018* [88] recommends

90 and 85 %, respectively) and CO_2 produced, and additional expenses for CO_2 allowances. In this context, the inaccuracy of the isothermal model is significantly less important. This is especially true, when the design of pressure-swing based cycles aims to shorten step times to increase productivity, ruling out the breakthrough occurrence. Furthermore, using a simple empirical approach [133] may be useful and ensure the process-required breakthrough curve steepness (discussed in Section 3.6). Nevertheless, for a rigorous study of process efficiency (for example, the efficiency of adsorbent utilisation), the entire breakthrough curve should be known, and only the high CO_2 outlet concentrations could be neglected because they do not bring any significant improvement in estimation while, for a less sharp breakthrough curves, this period of CO_2 concentration slowly reaching its plateau is difficult to predict accurately with any mathematical models.

Sensitivity analysis

The sensitivity analysis was performed by changing the model input parameters, which are difficult to measure experimentally by nature. Their initial estimate was based on the literature (Section 3.3), providing a variety of empirical correlations derived from experimental data. The range of change in parameters was dictated by these correlations. This approach was chosen for its experimental basis; selecting a random confidence interval range could not be sustained by any relevant criteria. This analysis also incorporated varying flux (slope) limiters, which affect the convergence of a numerical solution and may compromise its accuracy. The goal was to identify the most sensitive parameters and their overall impact on the predicted results. For this analysis, a single breakthrough curve with the highest deviation (about 4 % before any parameter changes, referred to as the "original prediction") at 2 bar and 293 K was selected. The rationale was twofold: it exhibited the highest deviation; and its temperature fell within typical PCC, as supported by the literature review in Appendices A and B.

It is noteworthy that among the constant model inputs, column dimensions, dictating the adsorbent amount, have a substantial impact on the breakthrough onset time. For example, in the breakthrough experiments, no adsorption occurs within the empty spaces and glass beads (non-porous spheres) sections. However, when these sections are occupied with zeolite 13X, the breakthrough onset is predicted to be delayed by about 51.6 % (2 bar and 293 K). As expected, the breakthrough onset time also shifts with volumetric flow rate due to the limited adsorbed amount in a sense that it decreases with increasing velocity, while the ramp-up phase between the curve onset and plateau widens. Moreover, as demonstrated experimentally, lower temperatures and higher pressures result in increased adsorbed amount and delayed breakthrough onset, although this relationship is non-linear.

The sensitivity analysis was performed for four estimated parameters, yielding the following findings:

- ***Axial dispersion coefficient***: if the axial dispersion increases, the mixing of the gas molecules becomes more intensive, resulting in an uneven adsorption and widening of the breakthrough curve. Several correlations, chosen from [134], for the gas flow through the fixed bed packed with solid spherical particles were investigated. The values obtained were within the range of $3 \times 10^{-5}\ \mathrm{m.s^{-1}}$, and the breakthrough curve showed a negligible slope change. The highest difference was found between the correlations proposed by Edwards and Richardson (1968) and Wen-Fan (1975) with a total difference of 1.62 % in the onset time.
- ***Bed voidage***: it is proportional to the increase of the interstitial velocity, and therefore influences the axial dispersion. The estimate proposed by Ribeiro et al. [120] was at the limit of its validity. Therefore, the calculation suggested by Dixon [135] for packed beds with regular spherical particles and a small ratio of the diameters of the column and the particles was analysed. The increase in the estimate of the bed voidage by approximately 14 % moved the results towards the experimentally obtained onset time by about 3.2 % and achieved the highest accuracy of 0.8 % for the breakthrough curve studied. When considering the averaged onset time for 2 bar, this change would also provide the best fit.
- ***Mass transfer coefficient***: the mass transfer coefficient used in the model accounted for the mass transport resistance in macropores. As mentioned previously, commercial zeolites are purportedly made with a porous structure with reduced micropore diffusion. Therefore, it was investigated whether the residual mass transfer, which occurs on the adsorbent surface, slows the penetration of gas to a noticeable degree or whether this effect is negligible as suggested by [123]. An external mass transfer coefficient: $k_f = ShD_{m,CO_2-N_2}/d_p$ is contained in the Sherwood number definition. As both were unknown, an approximation of the Sherwood number [136] was included in the calculation of the overall mass transfer resistance. The deviation of about 0.3 % confirmed the insignificance of this parameter.
- ***Molecular diffusion coefficient***: a less sensitive parameter. Any of the well-known empirical formulas tested, for example, Fuller et al. (1965), Wilke & Lee (1955), or Chapman-Enskog (1967), all described in [118], including their suitability for various gas mixtures, provided results laying within the range of 1.5 %.
- ***Flux limiters***: for this particular case, superbee and Koren flux limiters achieved almost the same accuracy of 4 % (the highest accuracy of 3.8 % was achieved by the superbee flux limiter), slightly better than van Leer limited used in the original numerical scheme. An error of about 5 % was observed similarly for van Albada and minmod flux limiters. A lower-order smart flux limiter

performed the worst among these limiters, highlighting the importance of using second-order numerical schemes. Although superbee and Koren flux limiters appeared to be better suited for predicting breakthrough curves of this nature than van Leer, further analysis revealed that van Leer limiter provides the best fit for the upper end of the curve, although the prediction error exceeded 10 % at very high CO_2 outlet concentrations (Figure 13). This suggests that the limiter function, which determines the course of solution converging the limiting value, avoiding oscillations, is crucial for the simulated phenomenon in terms of adsorption kinetics and dynamics of the process (flue gas velocity, axial dispersion, *etc.*), and a single limiter cannot satisfy all cases. As a side note, slight variations in the computational time were observed, which could also be ascribed to the definition of flux limiter functions such that if it requires decision making on every iteration (for example, superbee, Koren, and minmod flux limiters use "min" and "max" functions), this time increases. These variations are more evident for finer numerical grids, increasing the number of decision-making operations.

The results of the sensitivity analysis for the selected parameters are shown in Figure 15 as breakthrough curve prediction error. These prediction errors associated with each parameter reflect the impact of changing that parameter, while keeping all other inputs consistent with the "original prediction" (Figure 14), incorporating the van Leer flux limiter. For the analysis of different flux limiters, all model input parameters corresponded to those of the "original prediction".

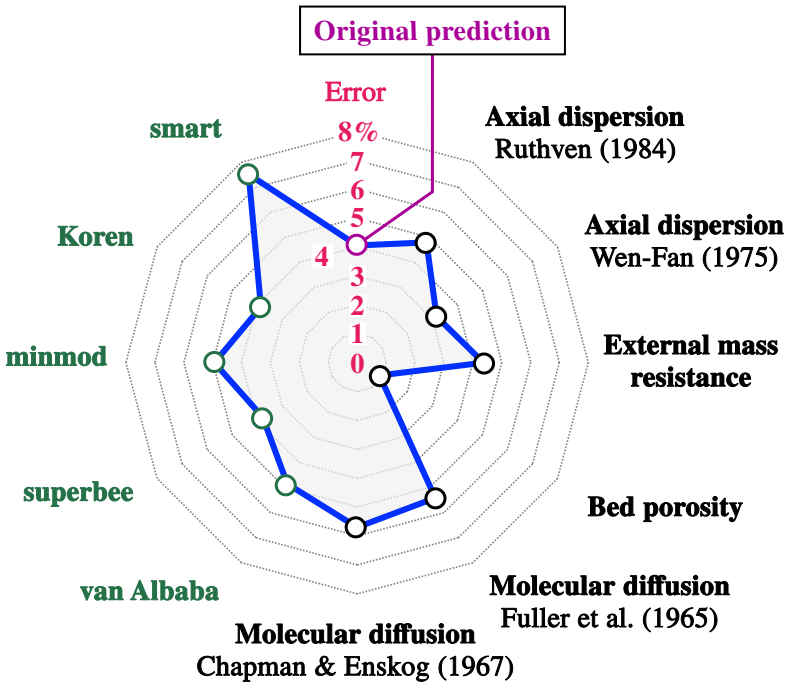

Figure 15. Deviation from the breakthrough curve onset time at 293 K and 2 bar performed for four estimated parameters (black circles) and five flux limiters (green circles). The purple circle indicates

the deviation of about 4 % from the breakthrough curve obtained by the "original prediction". The formulas were retrieved from various literature sources [107, 122, 123, 128, 134-137].

3.6 Numerical model-based adsorption process design

This Section builds on a previous idea (Section 3.5) of using an empirical approach to propose an initial adsorption process design for a small-scale natural gas CHP facility, which aligns with the previously identified research gap of low-power emission sources with CO_2-lean emissions. A natural gas-fired *TEDOM Quanto D2000* with total power output of 4.3 MW was selected for analysis. An abbreviated summary of its emission protocol is presented in Table 6.

Table 6. Emission protocol summary for *CHP TEDOM Quanto D2000.*

Parameter	**Value**
Dimensions (height × width × length) (m)	3 × 3 × 15
Average fuel consumption (natural gas) ($m^3.h^{-1}$)	553
Nominal electric power, nominal heat power (kW)	2000 / 2238
Electric efficiency, thermal efficiency (%)	43.7 / 43.2
Average annual operating hours ($h.year^{-1}$)	7900
Measurement conditions	
Atmospheric pressure (Pa), ambient temperature (K)	98310 / 295.2
Sampling time (h), gas concentration analyser	6 / *Horiba VA 3000*
Flue gas	
Wet / dry flue gas flow rates ($m_N^3.h^{-1}$)[1]	9850 / 8740 ± 520
Pressure (Pa), average temperature (K), fictitious humidity ($kg.m^{-3}$)	98310 / 355.2 / 0.086
Mean O_2 (%), NO_X ($mg.m_N^{-3}$), CO ($mg.m_N^{-3}$) concentrations	9.4 / 326 ± 36 / 34 ± 5
NO_X mass flow ($kg.h^{-1}$)[2]	2.851 ± 0.358
CO mass flow ($kg.h^{-1}$)[2]	0.294 ± 0.047
CO_2 concentration (vol%)[3]	6.4

[1]STP: 101325 Pa, 273.15 K. Calculated using burned gas balances.

[2]Dry gas assumed.

[3]Calculated from the balanced equation of natural gas burning under dry gas conditions.

***Note**: if provided, the range represents the maximum deviation from the mean value.*

To develop an initial design for the 4-step VSA process, several assumptions were made: trace pollutants (NO_X and CO) are neglected; a dehydration process is placed prior to VSA (*i.e.* H_2O is neglected); and a flue gas at the VSA inlet has a temperature of 303 K and a pressure of 1 bara. Subsequently, these assumptions were reflected by recalculating the normalised conditions (Table 6). To account for the potential presence of other gases when a complete PCC chain is proposed, a lower CO_2 concentration was assumed than determined for a completely dry gas without impurities. This allowed to tackle the complex problem of designing a complete PCC process chain, necessitating auxiliary sub-systems, and to concentrate primarily on the VSA and assess the mathematical model application for process design.

The methodology of the empirical approach combined three tasks: (1) simulation of the adsorption step with a mathematical model similar to that of breakthrough experiments; (2) application of empirical dimensionless criteria proposed for swift evaluations of swing adsorption processes [133]; and (3) use of literature-based recommendations for adsorption process design [92, 94, 138], as identified within the literature review. As a result, the following was possible: (1) determine a theoretical saturation time of the adsorbent bed; (2) ensure efficient use of the adsorbent bed by maintaining a steep CO_2 concentration profile; and (3) define initial process setting, including the length-to-diameter column ratio (I incorporated a ratio of 2) and column dimensions, keeping the interstitial gas velocity in close proximity to the fluidisation threshold to maximise cycle productivity and minimise the total number of columns, and prevent dusting, collapse of adsorbent layer, or flue gas channelling. The pelletised form of zeolite 13X considered was also based on the literature as a practical choice in commercial processes. Additional notable differences from the previously constituted mathematical model (Section 3.3) included modification of its assumptions, adherence to the desired empirical criteria range, and consideration of the dual-site Langmuir (DSL) adsorption isotherm model for the N_2/CO_2 mixture on pelletised zeolite 13X. The latter was retrieved from the existing literature [109], excluding the need to fit the adsorption isotherm parameters.

Model assumptions

The following assumptions were formulated:

1. The ideal gas model considers a binary mixture of CO_2 and N_2, without trace pollutants, water vapour, and oxygen. Exclusion of water vapour is due to the zeolite hydrophobicity and its significant impact on the CO_2 adsorption capacity, which decreases substantially even in the presence of trace amounts of water vapour [139]. Oxygen has a negligible influence on the CO_2 adsorption rate, similar to N_2 [117].
2. The equilibrium adsorption isotherm of the CO_2/N_2 binary mixture on zeolite 13X is expressed by the DSL model [109].

3. The mass transfer rate between the gas and solid phases is approximated by the LDF model.
4. The adsorption step is considered isothermal (thermal effects due to adsorption heat are neglected) and adiabatic.
5. There are no radial concentration or thermal gradients.
6. The gas phase parameters: viscosity, density, enthalpy, molar heat capacity, and thermal conductivity are constant.
7. The axial gas velocity and the axial dispersion coefficient are constant along the column.
8. The pressure drop of the packed bed is obtained by the Ergun equation.
9. The change in momentum (kinetic and potential energy) is negligible.

These assumptions formed a set of PDEs similar to that of the breakthrough curve model (Section 3.3). In this model, the DSL adsorption isotherm model for the CO_2/N_2 mixture (Assumption 2) substituted the previously fitted SSL model (Equation (23)) and has the following definition:

$$q_i^* = \frac{q_{sb,i} b_i c_i}{1 + \sum_{i=1}^{n_{comp}} b_i c_i} + \frac{q_{sd,i} d_i c_i}{1 + \sum_{i=1}^{n_{comp}} d_i c_i} \tag{29}$$

$$b_i = b_{0,i}\, e^{\left(-\frac{\Delta U_{d,i}}{RgT}\right)},\ d_i = d_{0,i}\, e^{\left(-\frac{\Delta U_{d,i}}{RgT}\right)},\ i = CO_2, N_2 \tag{30}$$

where $b_{0,i}$, $d_{0,i}$ and d_i are the Langmuir equilibrium constants that are summarised in Table 7, as reported in the literature [109]:

Table 7. DSL parameters for competitive adsorption of CO_2 and N_2 on zeolite 13X [109].

Parameter	$\boldsymbol{i = CO_2}$	$\boldsymbol{i = N_2}$
$q_{sb,i}, q_{sd,i} (\mathrm{mol.\,kg^{-1}})$	3.09 / 2.54	5.84 / 0
$b_{0,i}, d_{0,i}$ $(\mathrm{m^3.\,mol^{-1}})$	8.65×10^{-7} / 2.63×10^{-6}	2.50×10^{-6} / 0
$-\Delta U_{b,i}$, $-\Delta U_{d,i}$ $(\mathrm{J.\,mol^{-1}})$	36600 / 35700	15800 / 0

Figure 16 shows this isotherm for four temperatures in the range of expected inlet temperature to the VSA system in the PCC scenario and illustrates the preferential affinity of zeolite 13X for CO_2 by the reverse courses of CO_2 and N_2 curves with increasing CO_2 partial pressure, *i.e.* CO_2 content.

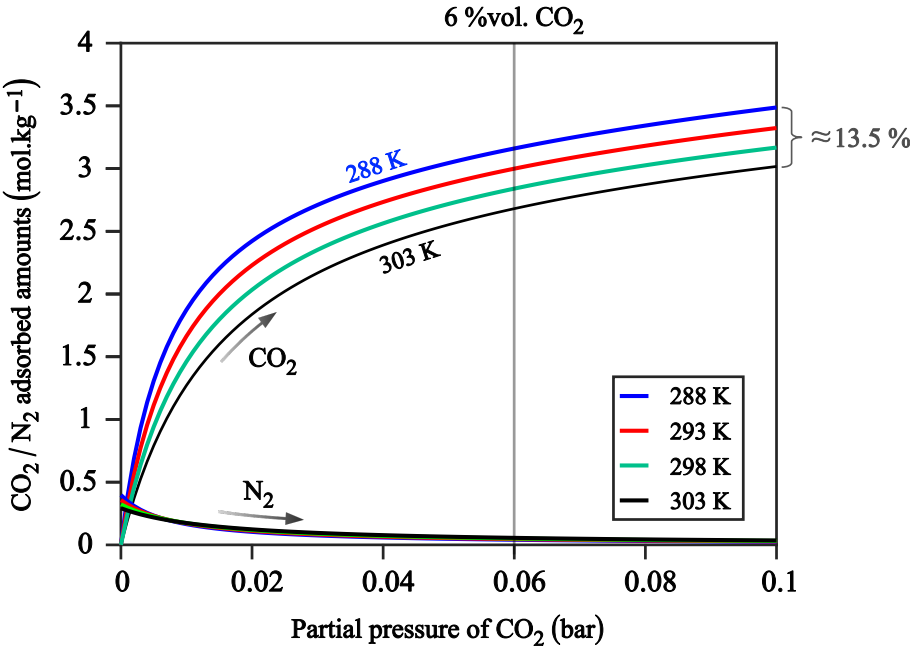

Figure 16. Competitive adsorption isotherms of CO_2 and N_2 on zeolite 13X as a function of CO_2 partial pressure. The vertical grey line indicates the adsorption capacity of zeolite 13X at CO_2 concentration of 6 vol% in the flue gas, corresponding to the considered dehydrated flue gas.

The DSL model was obtained for a commercial-grade zeolite 13X in a pelletised form (physical properties detailed in Table 8 [109]). The preference towards selecting pelletised adsorbent resulted from its favourable handling properties compared to powder materials, reduced material losses during transportation and packing, and lower pressure drop during VSA operation.

Table 8. Physical properties of commercial-grade zeolite 13X [109].

Parameter	**Value**
Adsorbent	*Zeolite 13X*
Particle density (kg. m^{-3}), diameter (m), tortuosity (−)[1], voidage (−)	1130 / 2×10^{-3} / 3 / 0.35
Adsorbent bed density (kg. m^{-3})[2], voidage (−)	712 / 0.37
Specific heat capacity (J. kg^{-1}. K^{-1})	1070
Mass (kg per column)[2]	1118

[1]An upper value for zeolite 13X posing higher mass transfer resistance [125].

[2]Bed density and adsorbent mass can be calculated using $\rho_b = (1-\varepsilon_b)\rho_p$ and $m_{ads} = L\, S_b\, \rho_b$, respectively.

Due to the scaling of the column sizes, the axial dispersion coefficient was estimated according to [136]:

$$D_{ax} = \frac{D_m}{\varepsilon_b}\left(20 + 0.5\, ScRe_p\right) \tag{31}$$

where $Sc = \mu_g/\rho_g D_m$ is the Schmidt number. This correlation does not account for wall-channelling, which becomes significant when the ratio of pellet diameter to inner diameter of the bed is small [140], which correlated with the considered adsorbent geometry (Table 9) and the column size, which will be described later in the text. The threshold for fluidisation interstitial gas velocity was obtained from [35], who recommend keeping its value at about 80 % of the minimum fluidisation velocity in packed beds to prevent adsorbent particle attrition:

$$v_{max} = 0.8\, v_f \approx\ 6 \times 10^{-4} g \frac{d_p^2}{\mu_g}\left(\rho_p - \rho_g\right) \approx\ 6 \times 10^{-4} g \frac{d_p^2}{\mu_g}\rho_p \tag{32}$$

where v_f is the fluidisation velocity and g is the acceleration due to gravity. Although the interstitial velocity threshold was calculated to be about 1.8 m.s^{-1}, in practice, higher velocities up to 180 % of the fluidisation velocity threshold are allowed [35]. The initial design considered a slightly increased value of 1.9 m.s^{-1}, about 85 %, as higher velocities may entail risks, including wall-channelling.

Empirical criteria

Three dimensionless criteria were considered in designing VSA: Biot number (Bi), and factors π_1 and π_2. These criteria contribute to a favourable steep slope of the breakthrough curve, which, in turn, reduces the amount of unused adsorbent near the column outlet once the CO_2 outlet concentration reaches the maximum allowed value. At this point, the adsorption step is terminated, and flue gas is transferred to the second column in a pair packed with regenerated adsorbent. The maximum allowed CO_2 outlet concentration was set to 15 vol%, relative to the CO_2 inlet concentration, corresponding to about 1 vol% of CO_2 relative to its concentration in unprocessed flue gas (further denoted as "raw").

These criteria were proposed through an empirical approach as follows:

$$Bi = \frac{\beta_{mass} d_p}{2D_{p,eff}} = \frac{\text{Transfer to the particle surface}}{\text{Difussion into the particle}} \tag{33}$$

$$\pi_1 = \frac{v d_p^2 \varepsilon_b}{L D_{p,eff}(1-\varepsilon_b)} = \frac{\text{Convection through the column}}{\text{Difussion into the particle}} \tag{34}$$

$$\pi_2 = \frac{D_{ax}}{v_0 L} = \frac{\beta_{mass} d_p}{2L} = \frac{\text{Axial dispersion}}{\text{Convection in the column}} \tag{35}$$

where β_{mass} is a dimensionless parameter. This definition originates from conventional mass transport through the column (column length L is a reference dimension), affected by dispersion in the case of multicomponent gas mixtures, and diffusional adsorbate transition into the adsorbent particle (adsorbent particle diameter d_p is a reference dimension).

Detailed discussions of these criteria can be found in [133]; in a nutshell, respecting values of

$$Bi > 10, \quad \pi_1 < 0.1, \quad \text{and} \quad \pi_2 < 0.001 \tag{36}$$

provides a sufficiently steep adsorption isotherm slope and a narrow concentration front (*i.e.* smaller active mass transfer zone), which increases adsorbent utilisation per cycle. When the Biot number is greater than 10, mass transport by diffusion becomes significant, and the internal resistance of mass transfer prevails over the external mass resistance. Both π-criteria reflect the adsorption isotherm slope, with π_1 accounting for the intraparticle diffusion effect on the breakthrough curve. At low π_2 values, convection flux dominates over axial dispersion and can often be neglected [124].

Evaluation of empirically-designed VSA process

The ultimate focus of the empirical approach to establish the initial 4-step VSA design led to the following findings:

- ***VSA column sizing***: to meet the desired range of empirical criteria, keep the interstitial velocity below fluidisation threshold, and propose columns that potentially reduce cost, dimensions of 2 × 1 m (0.003 m wall thickness) per column were obtained. Then, a single column would be packed with about 1.1 t of zeolite 13X processing flue gas with interstitial gas velocity of 1.9 $m.s^{-1}$ (superficial velocity of 0.7 $m.s^{-1}$). Under these conditions, Biot number and π_1-factor criteria were satisfied, indicating diffusion dominance and providing steep breakthrough curve, respectively. Although the velocity was close to the fluidisation threshold, the columns appeared to be sufficiently long to reduce axial dispersion effects, as the π_2-factor of 0.028 was obtained. Due to the various simplifications and the fact that the axial dispersion is often included, its effect was accounted for the breakthrough curve prediction. Finally, a theoretical boundary of 0.13 bar(a) was proposed for the evacuation step, as industrial vacuum pumps cannot typically provide lower pressures.

- ***VSA train sizing***: using the proposed values and the adopted adsorption isotherm, along with the geometry of pelletised zeolite 13X, the mathematical model estimated that the maximum allowed CO_2 outlet concentration of 15 % from its inlet concentration will be reached after 274 s, as demonstrated by the blue curve in Figure 17 (the red and green curves show a linearly proportional

development of the breakthrough curve in time at 1/2 and 3/4 of bed length, respectively, *i.e.* the duration of adsorption step in shorter columns). This maximum duration of adsorption step is above the range often considered in process optimisation, however, with more than twice the CO_2 concentration in the flue gas corresponding to coal emissions [53, 92, 94, 109], corresponding to shorter adsorption times. These times can be longer when adsorbents with lower working capacities are evaluated under VSA conditions, such as MOFs [50]. For the optimistic assumption that the adsorption step time is on par with the residual steps, distributing flue gas among 8 columns (placed vertically to decrease the deployment area) would satisfy the continuous processing of 9000 $m_N^3.h^{-1}$ of dry flue gas, diluted by 6 vol% of CO_2.

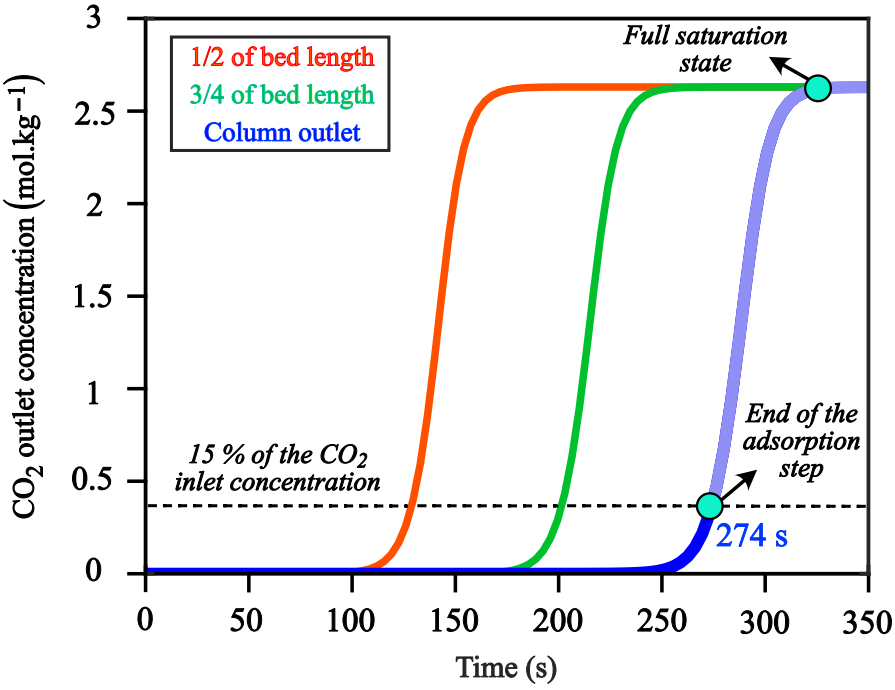

Figure 17. Theoretical CO_2 breakthrough curves at different positions in the column obtained by the mathematical model with an estimate of adsorption step length of 274 s, highlighted by a turquoise circle. The black dashed line corresponds to 15 % of the CO_2 outlet concentration relative to its inlet concentration.

In this part, published in [MN1], the design of the process using a simplified model established an initial configuration of VSA, adhering to the suggested ranges of empirical criteria and incorporating recommendations from the review of the literature. Although adsorption is a fundamental step and determines the column sizing to a high extent, simulating one step of a 4-step cycle does not allow for a complete evaluation of the entire cycle (*e.g.* cycle scheduling or CO_2 purity). Furthermore, neglecting temperature and momentum variations introduces inaccuracies. To circumvent these issues, the mathematical model must be refined in three aspects:

1. Simulation of all cycle steps in continuous operation (*i.e.* continuously-updated model).
2. Discretisation and implementation of solid-gas and wall energy balances along with the momentum balance.
3. Determination of process performance (*e.g.* CO_2 purity).

Detailed modelling would also help confirm the reliability of the approach used here. From a practical point of view, integration of VSA as a tail-end CO_2 capture unit requires to design a complete flue gas cleaning process to verify whether the simplified flue gas composition is achievable (*i.e.* removing impurities, water, and reactive components such as NO_X) prior to the VSA unit. Both the pollutants and the water vapour would damage the adsorbent and hamper the VSA operation. Consequently, the viability of VSA within the PCC system can be assessed in a context of other auxiliary sub-systems, and basic process economics can be estimated.

3.7 Summary of results

In this chapter, mathematical modelling was examined for the prediction of adsorption phenomena via breakthrough response and fitting of various parameters using experimentally measured data. Good agreement with the experimental data and rapid assessment of the parameter fitting and optimisation made the simulation a powerful tool that can save time, space, and financial funds once properly tuned with respect to the experimental condition.

High prediction accuracy was shown for the prediction of breakthrough onset time, where the deviation did not exceed 2 % from the averaged experimental values, although the prediction of breakthrough curve tail, where the CO_2 outlet concentration reaches its plateau, yielded lower accuracy. The flexibility of theoretical models was highlighted by performing sensitivity analysis, showing high tunability, which can satisfy application for various experimental apparatuses that have a wide range of dimensions, gas compositions, and adsorbent materials. This proved the suitability of mathematical modelling to investigate adsorption processes.

Subsequently, the adsorption process design was demonstrated on a small-scale CHP (4.3 MW, natural gas), taken as a representative of an industrial application. For this purpose, the same breakthrough curve model, but with implemented process-design empirical criteria control was used; VSA configuration and sizing were partly based on a well-established findings from the literature review. As a result, column dimensions and configuration, operating parameters, adsorbent packing, and interstitial gas velocity were proposed. Furthermore, several key implications for revising model were identified to enable a rigorous VSA simulation and assessing its performance, and evaluation of VSA PCC within the retrofitted CHP plant.

Chapter 4

4 Simulation, design, and evaluation of a 4-step VSA process for CO_2 capture in urban-scale CHP

This chapter explores the application of mathematical modelling for process design of a 4-step VSA cycle, incorporating pressurisation, adsorption, blowdown, and evacuation steps. The VSA is evaluated in the context of a small CHP facility, as specified in Section 3.6. The ultimate goal is to refine the mathematical model and use its capabilities to assess a variety of input conditions through rigorous VSA simulation. Then, to integrate this VSA within the PCC system of the aforementioned CHP to investigate the potential of scaling up adsorption technology, its efficiency, and basic economy when using zeolite 13X. This adsorbent has been identified in the literature overview as a high-performing material among commercially available alternatives (Section 2.2.2) and was further explored (Chapter 3) through modelling of experimental breakthrough experiments. The fundamentals of VSA process were laid in Section 3.6. Except for the process economy assessment (Section 4.3), the results of this chapter were submitted for publication [MN4].

4.1 CO_2 capture plant design

The first step toward assessing the VSA was to propose a complete flue gas cleaning process within the CHP, to obtain realistic VSA inlet flue gas parameters. These parameters are an essential input for the mathematical model. The main goal was to propose a ready-to-operate process by considering real operating conditions of the CHP system without any previous simplifications (Table 6), including the climate of the Czech Republic to search for cost-efficient solutions. Conditioning of the VSA-recovered CO_2, either by storage or pipeline transport, was added to illustrate the CCS process. However, these areas were not examined in detail for case-specific requirements.

Subsequent discussion focuses on the design and calculation of all necessary auxiliary sub-systems in the PCC chain. These include treatment processes for NO_X and water vapour and gas conditioning components such as fans or heat-exchangers, which were determined from the overall process flow balances, as dictated by requirements of each sub-system. Particulate matter is removed within the CHP, the NO_X removal (deNOx) is solved using a selective catalytic reduction (SCR) system, and the dehydration of the flue gas stream is carried out by combining a condenser with TSA; the CO_2 removal is performed via VSA. The designing procedure of the core systems sought to (1) identify the key operating parameters; and (2) propose a conceptual design with appropriate dimensions and construction

materials. The design of VSA, specifically, the number of steps, column size, adsorbent, low pressure boundary, and interstitial velocity were adopted from the empirical approach (Section 3.6).

4.1.1 Process flow diagram

The creation of the process flow diagram followed the development and validation of the revised mathematical model (Appendix D), which was used for VSA simulation and evaluation (Section 4.1.4) after the flue gas inlet parameters were determined. The process flow diagram constitution consisted of eight successive steps:

1. Definition of purified gas composition for PCC and quality of CO_2 for storage or transport.
2. Selection of flue gas cleaning processes capable of achieving the targets defined in Step "1".
3. Definition of technical and operational constraints for individual processes.
4. Design of process flow diagram.
5. Calculation of heat exchangers, heat duties, and bypassed flue gas exiting the CHP.
6. Iteration of steps 3-5 to comply with the process constraints defined in Step "3".
7. Placement of fans to compensate for pressure losses.
8. Correlation for annual temperature fluctuations relevant to the Czech Republic climate.

For this part, the number of simplifications was minimised by adopting the entire emission protocol provided, which described the CHP parameters and flue gas properties (Section 3.6), into the calculation and design procedures.

The proposed block flow diagram before determination of flow balances is shown in Figure 18. The operation of this process, including all key sub-systems and auxiliary components, can be explained as follows: after combustion, the flue gas temperature rises to 677 K and subsequently drops to 355 K, following heat exchange in the economiser, an integral part of the CHP system. Still within the CHP system, particulate matter is removed by an integrated filter. When leaving the CHP unit, the flue gas (a mixture of N_2, O_2, Ar, H_2O, CO_2, and NO_X) is heated and fed to the SCR system (Section 4.1.2). Here, reactive and toxic NO_X are removed by vanadium-based catalysts. Consequently, two heat exchangers were placed prior to the SCR to heat the incoming flue gas stream. The first one uses the SCR outlet stream to do so ("SCR-HE circuit" in Figure 18). The second one serves three purposes: (1) heating the stream to the SCR operating temperature; (2) providing extra heat during start-up; and (3) balancing the temperature losses in the previous heat exchange ("CHP-HE circuit" in Figure 18). Next, the two-step dehydration process (Section 4.1.3) removes moisture. It consists of a water-cooled condenser and a 3-step TSA with zeolite 5A. A dry flue gas (N_2 and CO_2 mixture assumed) then enters the 4-step VSA system with fixed-bed columns packed with zeolite 13X (Section 4.1.4). The flue gas is deprived of CO_2,

which is recovered with a purity of 90 % to comply with storage or utilisation requirements, which is illustratively added. The flue gas fans are used to compensate for pressure losses. The bypassed "Raw flue gas" serves for additional heating and is subsequently recirculated back to the CHP to utilise residual heat within the economiser section.

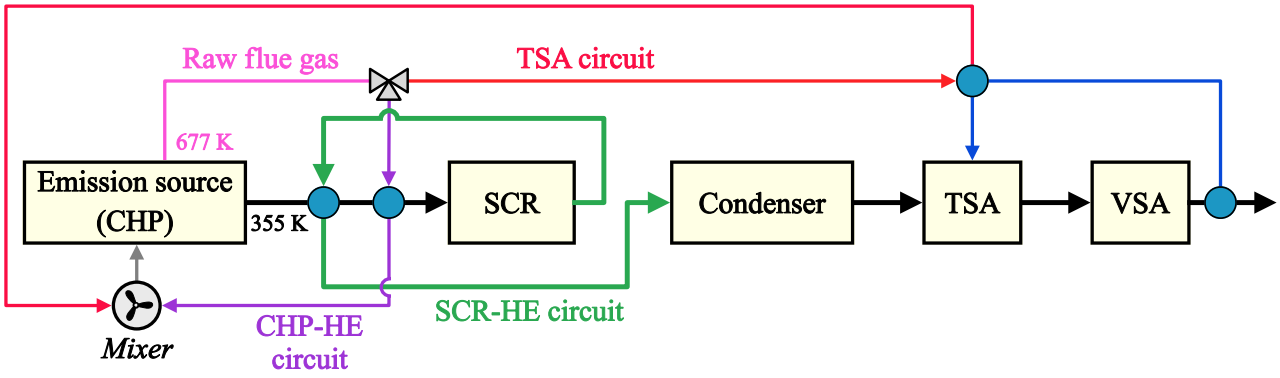

Figure 18. Process block flow diagram of individual sub-systems for CHP flue gas cleaning.

The following is the description of core sub-systems.

4.1.2 NO_X reduction - SCR

Sub-system designing procedure

SCR is employed to reduce the concentration of NO_X in the flue gas from the CHP upstream of the VSA. For systems like internal combustion engines in the CHP, SCR is the only viable option, as selective non-catalytic reduction systems are unsuitable for low flue gas temperature, which cannot be efficiently increased to the required 1173 - 1273 K range. The SCR system is placed first, as it still requires the highest operating temperature among the involved sub-systems and to protect the equipment and both zeolite adsorbents used for drying and CO_2 separation, respectively, due to the high toxicity of nitric oxides. A similar SCR process as described by Jeníková et al. [141] was used for favourable operating conditions and high efficiency at temperatures as low as 533 K. Choosing a low-temperature process benefits the economy by reducing the heat demand.

Sub-system evaluation

The SCR components were scaled up according to the inlet flue gas flow rate of 9634 $m_N^3.h^{-1}$ at a temperature of 533 K and a pressure of 1 bara, as well as the type and size of the catalyst. The choice of vanadium pentoxide (V_2O_5) catalyst in titanium dioxide (TiO_2) had a background in positive experiences from scaling experimental fluidised bed boiler with SCR-deNOx technology at *Juliska laboratory* [142]. This technology integrates a 0.16 × 0.16 × 1.26 m V_2O_5 catalyst to process a flow rate of 150 $m_N^3.h^{-1}$. Assuming a constant flue gas residence time, the SCR dimensions can be linearly scaled, with the results

summarised in Table 9. These dimensions correspond to the standard size of commercially available SCR modules of 0.97 × 0.97 × 1.00 m and 1.94 × 0.97 × 1.00 m, both with 0.46 × 0.46 × 0.46 m catalyst blocks. The preference for the module with larger cross-sectional area is due to the lower flue gas velocity and, consequently, a lower pressure drop.

Table 9. SCR design and operating parameters.

SCR Parameter	Value
Module geometry[1]	*Carbon steel*
Width × height × length (m)	1.94 × 0.97 × 1.00
Number of modules	1
Catalyst block[1]	*V_2O_5 (TiO_2 carrier)*
Width × height × length (m)	0.46 × 0.46 × 0.46
Minimum / installed number of blocks	5 / 8
Process parameters	
Feed temperature (K)	533[1]
Feed flow rate ($m^3_N . h^{-1}, m^3 . h^{-1}$)	8740[2] / 9634
NO_X amount ($kg . h^{-1}$)	2.85[2] (326[2] $mg . m_N^{-3}$)
Normalised stoichiometric ratio ($mol_{NH_3} . mol_{NO_X}^{-1}$)	0.8[1]
Reducing agent, consumption ($kg . h^{-1}$), NO_X removal efficiency (%)	NH_3 / 1.2 / 90[2]

[1]Selected based on practical experiences at *Juliska laboratory*.

[2]Calculated for a dry gas.

4.1.3 Dehydration - Condenser and TSA

Sub-system designing procedure

Dehydration consists of a water-cooled condenser and a TSA system. A two-step concept turned out to be necessary because of the high moisture content in the flue gas and the need to remove even the last bits of water. In both designs, the main emphasis was placed on economically efficient operation, although the condenser must reduce the water content to a level where the TSA system, consisting of only two columns, can continuously process it. To minimise the TSA column size, that is, capital expenditures, adsorbent material with high H_2O capacity had to be found.

Sub-system evaluation

Condenser

The main design assumption is that the cooling water is freely available (river or lake), which substantially reduces both operating and capital costs by eliminating the need for a chiller. This water is filtered before entering the condenser, and should be recycled after use or utilised within the facility premises; the risk of water contamination is minimal. The annual average ground water temperature in the Czech Republic was estimated to be 284 K, using the correlation between annual water and air temperatures [143, 144]. The use of a natural water reservoir was found sufficient to remove most of the water vapour from the incoming flue gas at 365 K when a baffled shell-and-tube heat exchanger is used. Specifically, it allowed to remove 87 vol% of water vapour from the denitrified flue gas. The drying efficiency strongly depends on the attainable dew point temperature, given by the water temperature and heat transfer rate. The seasonal variations of water temperature were addressed by considering a "worst-case scenario" of extremely hot summer, for which the average water temperature was estimated to be 300 K. The condenser design does not reflect these variations; instead, they were addressed by proposing a larger TSA system.

The design and calculation of the condenser were performed in *Aspen Plus v12.2*. A conventional shell-type *BEM* condenser geometry, following the *TEMA* standards, was found to be most suitable for this application. Under nominal conditions, the water pump supplies 75 $\mathrm{kg.\,s^{-1}}$ of natural water through the condenser tubes while 0.22 $\mathrm{kg.\,s^{-1}}$ of gas-condensate is separated from the flue gas. Condenser operating parameters are specified in Table 10, with technical details provided in Appendix C.

Table 10. Condenser design and operating parameters.

Condenser parameter	**Value**	
Heat duty (kW_{th})	860	
Heat transfer rate ($W.m^{-2}.K^{-1}$)	512 (clean)	
Heat transfer area (m^2)	98.9	
Dimensions: L × H × W (m)	4.29 × 1.44 × 0.73	
Tubes: count, material, length (m), pitch (mm), inner/outside diameter (mm)	634, *Carbon steel*, 2.7, 19, 15/19	
Fluid parameter	Tube side	Shell side
	Water	*Flue gas*
Inlet, outlet temperature (K)	284 / 287	365 / 286
Inlet, outlet water content (vol%)	100 / 100	11.5 / 1.5
Fouling resistance factor ($m^2.K.W^{-1}$)[1]	0.0004 (*filtered river water*)	0.0009 (*natural gas emissions*)
Mass flow rate ($kg.s^{-1}$)	75	3.37
Mean velocity ($m.s^{-1}$)[1], flow regime	0.68, turbulent	24.5, turbulent
Pressure drop (bar)	0.04	0.09

[1]Values taken from [145].

[2]The velocity changes only for flue gas, as a result of condensation.

TSA

TSA is a second dehydration step removing all of the remaining water vapour for successive VSA. It operates in a three-step sequence: adsorption, desorption (heating to 390 K), and cooling (to the adsorption temperature of 286 K). During this sequence, the regenerated bed reaches the adsorption temperature before the humid flue gas (about 2 vol% H_2O) is redirected from the second column. TSA comprises paired fixed-bed columns packed with a commercial-grade zeolite 5A. This adsorbent was chosen over cheaper silica gels for a higher adsorption capacity at low partial pressures of H_2O, allowing for a smaller column at the same inlet gas flow rate (*i.e.* a prolonged adsorption step can be utilised), and reduced sensitivity to variations in adsorption temperature. In addition, 5A would likely have a longer lifespan as a result of higher cyclic stability [146], decreasing operating costs. A commercial-grade zeolite 5A has adsorption capacity of 0.35 grams per gram of adsorbent for temperatures below 300 K [147]. The desorption temperature must exceed 373 K; consequently, direct heating with purified gas exiting the VSA was proposed. This gas is heated to 390 K in a gas-gas heat exchanger of a plate-

fin type by the unprocessed flue gas ("Raw flue gas" in Figure 16) exiting the CHP. Another purpose of heating gas is to purge the desorbed column. External water cooling of the column shell provides nearly constant outlet temperature of the dehydrated flue gas and sufficient cooling to the adsorption temperatures. Both are crucial for maintaining the efficiency of the subsequent VSA process.

The TSA scaling benefits from low flue gas temperature (up to 286 K) and reduced water content obtained in the condenser. Both depend on the cooling water (*i.e.* ambient) temperature, which peaks during summer up to estimated 300 K, affecting condenser performance. Under these conditions, a significantly higher bypassed "Raw flue gas" flow rate and a larger column dimensions are required. The condenser would remove 67 vol% of water vapour (by 20 vol% less), and the TSA columns would more than double their height for the same diameter while consuming almost twice as much energy. At the same time, "Raw flue gas" would have to be supplied to the heat exchanger in the amount of 20 vol% of total CHP emissions, compared to about 4 vol%, determined for annually averaged water temperature. The influence of cooling water temperature on condenser performance, TSA energy consumption and amount of adsorbent needed, is displayed in Figure 19. TSA calculations were performed with *MS Excel* using an empirical approach [148-150]; the results for various cooling water temperature are summarised in Table 11.

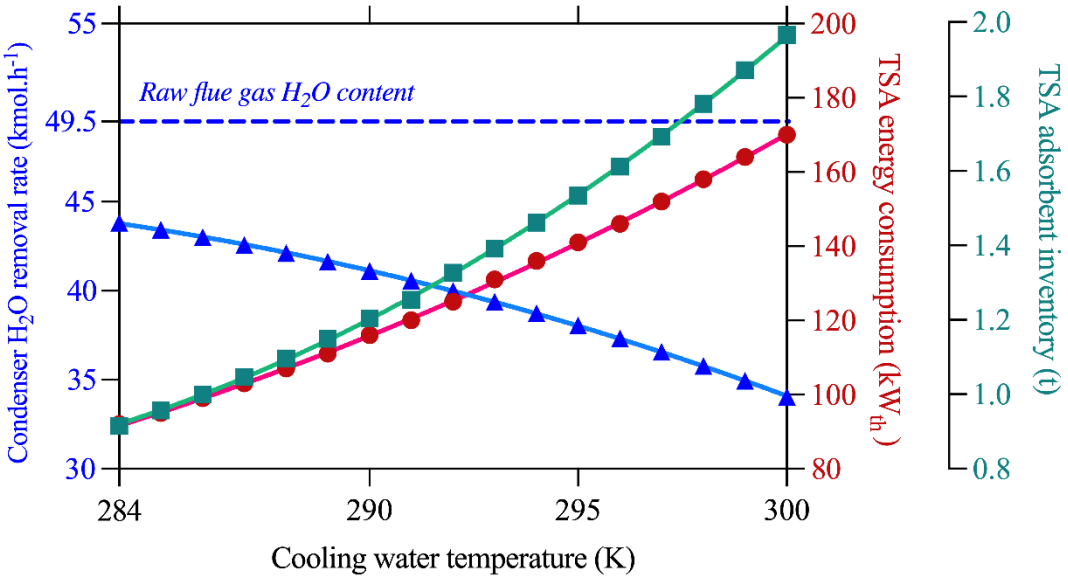

Figure 19. The influence of cooling water temperature on condenser performance expressed as H_2O removal rate (blue triangle curve), TSA energy consumption (red circle curve), and amount of adsorbent needed to fill both columns (green square curve). The blue dashed line at 49.5 kmol.h^{-1} indicates the H_2O content in the unprocessed (*i.e.* raw) flue gas.

Table 11. TSA design and operating parameters.

TSA parameter		
Case	Annually averaged temperature	Summer temperature extreme
Column geometry and packing	*Carbon steel*	
Diameter × height × wall thickness (m)[1]	2.08 × 1.15 × 0.01	2.08 × 2.50 × 0.01
Adsorbent inventory - zeolite 5A (kg)[2]	916	1969
Process parameter		
Feed (adsorption), regeneration temperature (K)	286 / 390	302 / 390
Feed, regeneration gas flow rate ($m^3_N.h^{-1}$)	8524 / 2000	8524 / 4416
Regeneration time (h)	1.5	1.5
Bypassed raw flue gas for heating ($m^3_N.h^{-1}$)	655	1927
Energy consumption (kW_{th})[3]	92	170

[1]The pressure vessel geometry respects the *ASME BPV Code, Sec. VIII D.1 Part UG-27* standard [151].
[2]A bulk density of zeolite 5A of 715 kg.m^{-3} was assumed.
[3]Heat requirement for adsorbent regeneration including heat transfer resistance of the construction material.

4.1.4 CO_2 removal - VSA

Sub-system designing procedure

The primary objective was to verify and scale up the previous VSA design, obtained using an empirical approach (Section 3.6), by simulating continuous operation of a 4-step cycle. The following model inputs from the previous design were maintained: (1) individual column sizes (2 × 1 m) and arrangement (paired columns arranged in vertical trains); (2) low- and high-pressure boundaries ($P_L = 0.13$ and $P_A =$ 1 bara), gas interstitial velocity (1.9 m.s^{-1}), and (3) review-based selection and sequence of cycle steps (pressurisation, adsorption, blowdown, and evacuation). The flue gas properties at the VSA inlet were updated, with respect to the prior TSA dehydration process. In nominal mode, VSA receives dry flue gas at adsorption temperature of 286 K and pressure of 1 bara. Here, a binary mixture of 6.4 vol% CO_2 and 93.6 vol% N_2 (practically involving O_2 and Ar) was assumed, as determined from the emission protocol for dry gas conditions (Table 6). Commercial-grade zeolite 13X is used as an adsorbent (Table 8). Except for the evacuation pressure (P_L), further optimisation of constant inputs was not carried out due to the scope thesis scope, problem complexity, and requirement of high computing power.

Evaluation of VSA performance and scheduling, along with the quantification of columns and trains, was obtained using a newly developed a mathematical model in *MATLAB R2022a*. This model is based

on mass, enthalpy, and momentum balances (Section 2.3), and implements one-dimensional axially dispersed plug-flow reactor model. It enables prediction of 4-step PCC VSA cycle (as described in Section 2.2.1) by simulating one continuously operating column with bulk separation of the N_2 and CO_2 mixture. The balance equations, forming a set of second-order PDEs, along with the boundary and initial conditions, are based on an experimentally validated model in a non-dimensionless form from the literature [109]. To control the stability of convection fluxes gradients and exponential pressure decay, another factor of non-converging solution, FVM with a weighted essentially non-oscillatory scheme was used for discretisation. For the sake of clarity, a detailed description of the PDEs, including model assumptions, calculation of all incorporated variables, CSS, system sizing and performance, and the validation procedure, is provided in Appendix D. Further details on transformation of PDEs, selected variables, and boundary conditions into non-dimensionless form can be found in [109]. The input parameters of the mathematical model are summarised in Table 12.

Table 12. Summary of VSA model input parameters.

VSA model input parameter name (constant values)	Parameter value
Adsorption column	*Stainless steel*
Length × inner diameter × wall thickness (m)[1]	2 × 1 × 0.007
Column wall density ($\mathrm{kg.m^{-3}}$)[2]	7800
Heat capacity of column wall ($\mathrm{J.kg^{-1}.K^{-1}}$)[2]	502
Thermal conductivity of column wall ($\mathrm{W.m^{-1}.K^{-1}}$)[2]	16
Outside heat transfer coefficient ($\mathrm{W.m^{-2}.K^{-1}}$)[2]	2.5
Process conditions	*Stainless steel*
Feed temperature (K), pressure (bar)[3]	286 / 1
Feed flow rate, CO_2 flow rate ($\mathrm{m_N^3.h^{-1}}$)[4]	8524 / 553
Elemental composition: CO_2, N_2, H_2O (vol%)[4]	6.4 / 93.6 / ∼0
Gas interstitial velocity ($\mathrm{m.s^{-1}}$)[1]	1.9
Characteristic pressures: high[1] (adsorption), low[1] (evacuation) (bara)	1 / 0.1
Vacuum pump pressure change rate ($\mathrm{s^{-1}}$)	0.2
Physical gas properties	
Molecular diffusion coefficient ($\mathrm{m^2.s^{-1}}$)[5]	1.54×10^{-5}
Dynamic viscosity (Pa. s)[5]	1.75×10^{-5}
Specific heat capacity of gas and solid phases ($\mathrm{J.kg^{-1}.K^{-1}}$)[5]	1026
Effective axial thermal conductivity ($\mathrm{W.m^{-1}.K^{-1}}$)[2]	0.09
Inside heat transfer coefficient ($\mathrm{W.m^{-2}.K^{-1}}$)[2]	8.6
Adsorbent physical properties	*Zeolite 13X (pelletised)*
Particle density ($\mathrm{kg.m^{-3}}$), diameter (m), tortuosity (−)[6], voidage (−)	1130 / 2×10^{-3} / 3 / 0.35
Adsorbent bed density ($\mathrm{kg.m^{-3}}$)[7], voidage (−)	712 / 0.37
Specific heat capacity ($\mathrm{J.kg^{-1}.K^{-1}}$)	1070
Mass (kg per column)[7]	1118

[1]Parameters obtained by a heuristic approach, except for the wall thickness, which was corrected to be in accordance with *ASME BPV Code, Sec. VIII D.1 Part UG-27* standard [151].
[2]Typically assumed values for stainless steel columns packed with 13X in VSA cycles [109].
[3]Assumed values or values calculated from the mass flow balances derived from the process flow diagram.
[4]Emission protocol data that were recalculated based on the process flow balances.
[5]Calculated values with further specifications provided in Appendix D.
[6]An upper value for zeolite 13X posing higher mass transfer resistance [125].
[7]Bed density and adsorbent mass can be calculated using $\rho_b = (1 - \varepsilon_b)\rho_p$ and $m_{ads} = LS_b\rho_b$, respectively.

Sub-system evaluation

The final results were subtracted from the mathematical model in CSS. CSS is reached once the simulation converges towards a single solution, which, in reality, never happens, as evidenced in all simulation runs. Instead, considerable errors in prediction persist throughout the initial cycles, with a gradual decline over time. These errors arise from variations in mass fluxes into (pressurisation and adsorption) and out of (adsorption, blowdown, and evacuation) the adsorption column, as a result of the ongoing adsorption phenomena. The so-called "total mass balance error" (TMBE), defined as the difference between the mass of gas entering and leaving the simulated adsorption column per cycle (expressed in percentage), and its decay time were found to depend mostly on process parameters and the type of adsorbent, *i.e.* adsorption isotherm. The adsorption isotherm describes the change in adsorbate mass retained in the adsorbent during each step (in all simulated cases, the partial saturation of the adsorbent along the entire column is not immediate), which depends on variables such as CO_2 concentration (CO_2 partial pressure), gas temperature and pressure, and cycle step times. CSS was recognised when TMBE dropped below 1 % for five consecutive cycles, as suggested in the literature [90, 92], and the simulation was terminated for the VSA evaluation. This evaluation included predicting CO_2 purity, often required for CO_2 storage and pipeline transportation, and CO_2 recovery.

In term of sizing, 15 columns arranged in 5 parallel trains were determined to continuously process 8524 $m_N^3.h^{-1}$ of dry flue gas containing 6.4 vol% of CO_2 at 286 K and 1 bara. Each cycle takes 360 s with an active operation time of 335 s (Table 13). To ensure continuous operation, a timing controls of individual steps, particularly the ratio between cycle time and time of steps receiving inlet flue gas (detailed in Appendix D), were implemented. Unsatisfactory timing control was compensated by introducing idle step after evacuation, where the column remains in a non-operating mode. Although the idle step inclusion seemed unavoidable, its duration should be minimised through optimisation, which was not examined. The step timing range adhered to the optimisation process in [109], maintaining a fixed pressurisation step duration (20 s), while a minimum gap of 0.02 bar was kept between the intermediate and low pressures [94].

Furthermore, the model results showed that the low-pressure boundary P_L (proposed in the empirical approach) does not meet the required CO_2 purity of 90 %.To achieve this purity, it is necessary to: (1) decrease the evacuation pressure to 0.061 bar(a), assuming that a 0.02 bar gap is maintained; and (2) keep the inlet flue gas temperature as low as technically possible. Then, the highest purity can be achieved for this setting when P_I and P_L are in close proximity and when adsorption and blowdown times are roughly equal (Figure 20d).

Table 13 summarises the mathematical model results, including VSA system sizing, and the predicted values upon reaching CSS. To reach CSS, a total of 103 cycles had to be simulated (Figure 20d). Figures 20a-d graphically illustrate these results, excluding the idle step. The concentration profiles of CO_2 and N_2 in the gas phase are shown in Figure 20a. The internal temperature profiles at 1/3 and 2/3 of the column length, and at the column outlet, until the point (after CSS) where the outlet flue gas temperature stabilises, are presented in Figure 20b. The pressure profile is presented in Figure 20c, and the progression of TMBE (*i.e.* the difference between the mass of gas entering and leaving the simulated adsorption column, expressed in percentage) along with CO_2 purity and recovery until CSS are shown in Figure 19d. It is worth noting that the evacuation was performed counter-currently, and that the state variables change dynamically at the opposite end of the column, which is not reflected in the figure.

Table 13. Summary of VSA model output parameters (*i.e.* results).

VSA model output parameter name (simulation results)	**Parameter value**
Adsorption system	*4-step VSA*
Number of columns per train, column trains, total number of columns (-)[1]	3 / 5 / 15
Adsorbent inventory – zeolite 13X (t)[1]	16.8
Total number of vacuum pumps (for blowdown and evacuation steps) (-)[1]	10
Process parameters, scheduling, and performance	
Cycle time: column operation time, total time (s)[1]	335 / 360
Step duration: pressurisation, adsorption, blowdown, evacuation, idle (s)[1]	20 / 100 / 95 / 120 / 25
Characteristic pressures: high[2] (adsorption), intermediate[1], low[1] (bar)	1 / 0.081 / 0.061
CO_2 purity / recovery (%)[1]	90.4 / 15.6

[1]Predicted values (under CSS) using mathematical modelling of a 4-step VSA cycles
[2]Parameters obtained by a heuristic approach.

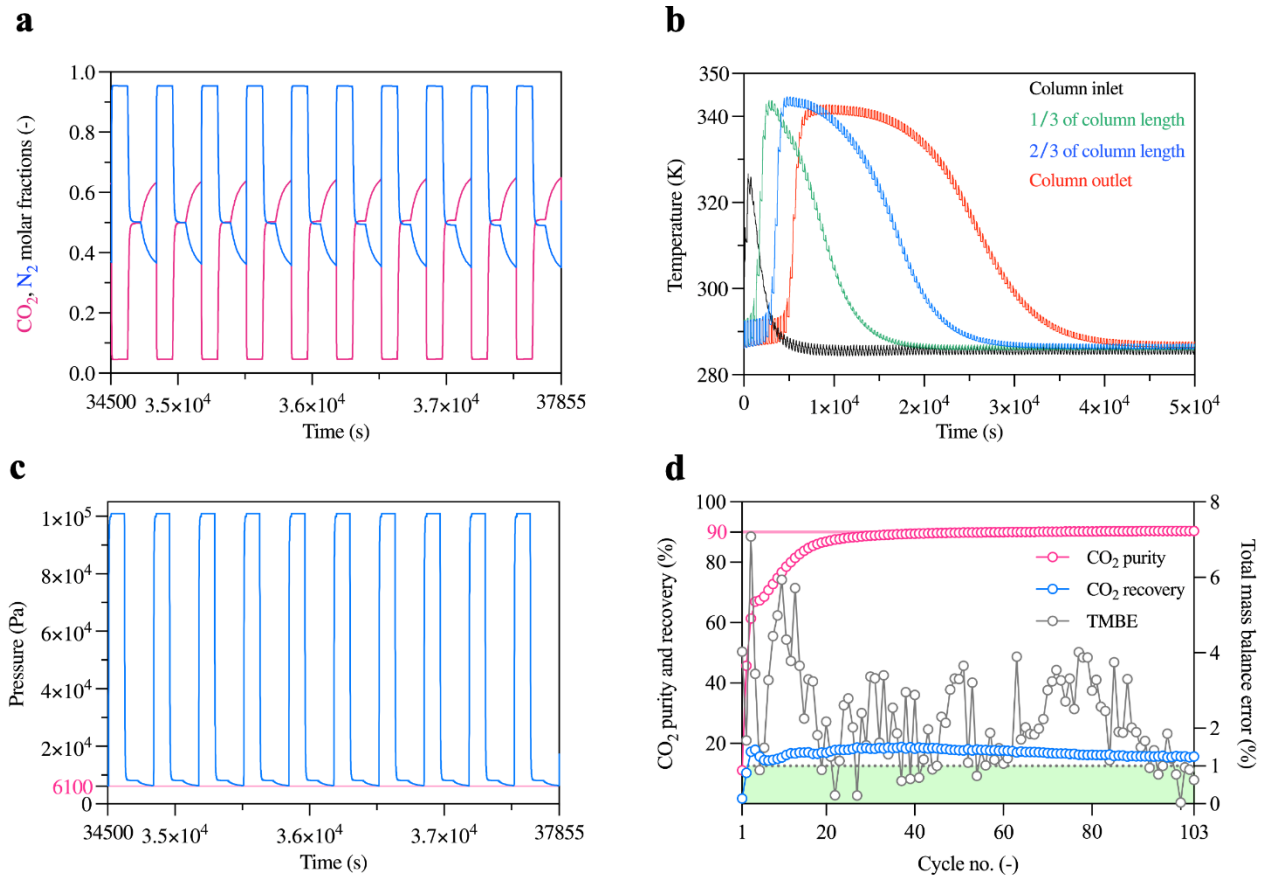

Figure 20. Results of 4-step VSA cycle simulation: **(a)** concentration profiles of CO_2 (red) and N_2 (blue) in the gas phase under CSS for 10 consecutive cycles; **(b)** temperature profiles at the column inlet (black), and the column outlet (red), along with internal temperature profiles at 1/3 (green) and 2/3 (blue) of the column length. The red line indicates the cessation of flue gas outlet temperature fluctuations after about 50000 s of VSA operation; **(c)** pressure profile of 10 consecutive cycles under CSS with adjusted evacuation pressure (red) highlighted at 0.061 bara; **(d)** progression of TMBE (grey), along with the CO_2 purity (red) and recovery (blue) values. The green-shaded area indicates the desirable TMBE below 1 %, and the solid red line represents the target CO_2 purity of 90 %. The total of 103 cycles were required to reach CSS, where CO_2 recovery and purity values are 90.4 % and 15.6 %, respectively.

4.2 Summary of CO_2 capture plant design

In this chapter, a comprehensive mathematical model using validation against literature data was developed (details in Appendix D). This model addressed the shortcomings of the "simplified" mathematical model (defined in Section 3.3), identified during the empirical VSA process design (Section 3.6). This new model enabled the simulation of a continuously operating 4-step VSA cycle (defined in Section 2.3), and therefore a rigorous evaluation. Additionally, it provided essential inputs for a basic VSA economic analysis (Section 4.5); basic" in terms of lacking optimisation, which may reduce the initial cost estimate.

Before VSA design and simulation, all necessary sub-systems required for retrofitting a district-scale natural gas-fired CHP system (4.3 MW) with PCC by low-temperature adsorption technology were selected, determined, and proposed. These sub-systems, forming a complete flue gas cleaning process, determined the practically achievable flue gas parameters and composition that will undergo CO_2 removal via VSA. Their potential operability was ensured by incorporating actual CHP emission data and using well-established design principles and standard operating parameters for their deployment. Figure 21 illustrates the process flow diagram of this process. It consists of: (1) core sub-systems: SCR-deNOx for NO_X removal, two-step dehydration for water vapour removal, and 4-step VSA for CO_2 removal; and (2) auxiliary components: fans, heat-exchangers, and pumps. Moreover, it includes CO_2 storage and transport to illustrate the complete CCS chain. However, this part was not analysed in detail, as the final purpose of CO_2 utilisation was unspecified and difficult to implement within the Czech Republic infrastructure.

The results showed that the SCR for flue gas denitrification upstream of the adsorption system can operate efficiently without an external heat source when utilising 7 vol% of the "Raw flue gas" emitted by the CHP. Dealing with a considerable amount of water vapour in natural gas emissions proved to be likely the most complex process, requiring more than one technology. However, using free natural cooling water to supply a gas-water heat exchanger reduced moisture by 87 vol% when considering the annually averaged cooling water temperature. The remaining moisture in the flue gas is then removed via TSA using zeolite 5A, consuming about 7 vol% of the "Raw flue gas" for adsorbent regeneration. This consumption can increase up to 20 vol% during extreme weather conditions. Complete dehydration was essential due to the water-sensitivity of zeolite 13X, selected for CO_2 capture via VSA. It can be argued that the CO_2 sorption performance of zeolite 13X can compensate for the energy-intensive dehydration with highly efficient CO_2 capture at 286 K and 1 bar(a).

The redesigned mathematical model revealed that 4-step VSA, consisting of 3 columns (2 × 1 m) placed in 5 parallel trains, can achieve CO_2 purity of 90.4 % and CO_2 recovery of 15.6 %. Furthermore, very low vacuum levels are required in a simple VSA process to reach the CO_2 purity target of 90 %, especially for low CO_2 concentrations. Consequently, both evacuation and intermediate pressures were reduced to 0.061 bar(a) and 0.081 bar(a), respectively. In practice, this pushes the technical limit of vacuum pumps, which was set at 0.13 bar(a) in Section 3.6 (*i.e.* the empirical approach). It can be postulated that pre-pressuring the CO_2-rich flue gas would allow a milder evacuation pressure to meet the 90 % CO_2 purity target, but could potentially increase the energy consumption as the entire flue gas volume of 8524 $m_N^3.h^{-1}$ would be compressed. Qualitatively, the CO_2 produced complied with the requirements for the storage or transportation of CO_2 onshore after conditioning. Although VSA optimisation is beyond the scope of this thesis, addressing the low predicted value of CO_2 recovery should be to improve the cost per mass of CO_2 captured.

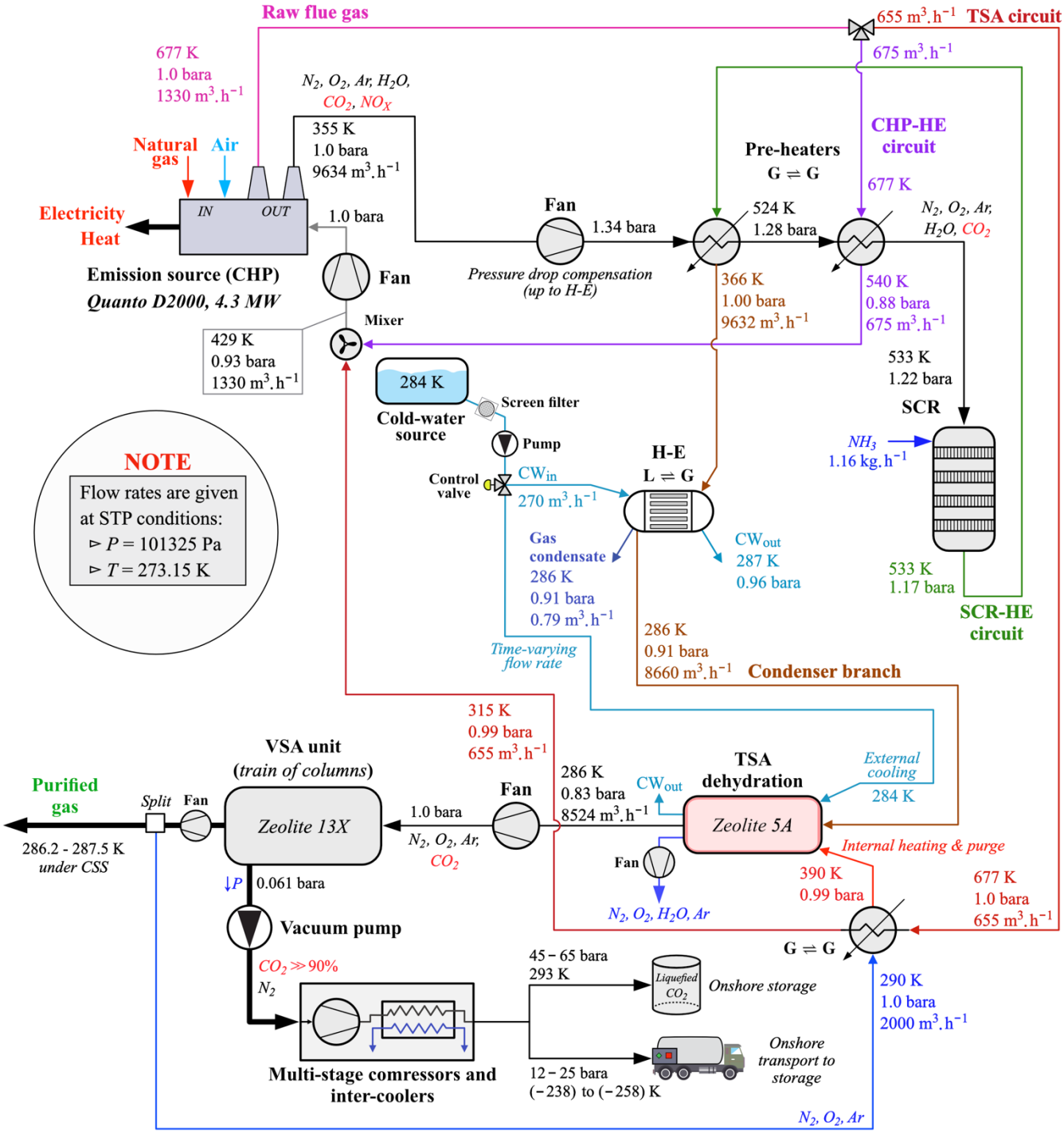

Figure 21. Process flow diagram for CHP flue gas cleaning with CO_2 capture operating in nominal mode.

4.3 CO_2 capture plant economy assessment

Basic economy assessment aims to compare the cost of deploying a recently commercially unavailable PCC using a 4-step VSA against the financial requirements associated with other technologies found in the proposed process. Their technical solutions as well as their applications have been in practice for decades. This assessment provides a broad view of each treatment process, which may offer valuable insight for those in the industrial and commercial sectors looking to draw a general conclusion.

The economic assessment is limited to the configuration of the previously proposed PCC chain and to the estimation of total direct cost (TDC) of all sub-systems, including the cost of adsorbents (zeolite 5A and zeolite 13X for TSA and VSA, respectively), the V_2O_5 catalyst, and NH_3 (both for SCR), assuming that the cooling water supply is free of charge. The cost of electricity is excluded due to difficult quantification, along with operating cost or cash flow models (Section 2.4), which would likely increase the uncertainty of the cost estimate obtained.

The cost estimation methodology is based on determining the TDC of dehydration, PCC by 4-step adsorption, pipeline transport, and NO_X removal by SCR as a sum of direct costs of all individual components related to these sub-systems for a plant lifetime. Their direct costs were obtained through cost functions reported in the existing literature. Whenever possible, the cost function was selected in accordance with the component type, material, operating parameters (*e.g.* power, volumetric flow rate, heat transfer area, pressure and temperature, or efficiency), and purpose of application. The cost of the aforementioned utilities was also retrieved from the literature. All costs (cost functions and utilities) are provided in Euros converted to prices in 2021 ($€_{2021}$). This conversion is made using the Chemical Engineering Plant Cost Index (CEPCI) ratios:

$$\text{Cost in } (€_{2021}) = \text{Cost in } \left(€_{year-X}\right) \times \frac{708.8}{\text{CEPCI}_{year-X}} \tag{37}$$

where "year-X" is the year of cost function or utility cost validity, and 708.8 is the annual CEPCI for 2021 [152]. If costs were not expressed in Euros, their currency was converted using an average annual conversion rate for the year of their validity (*i.e.* "year-X") and then adjusted to 2021 using Equation (37).

Additionally, the following assumptions were made:

- The CHP operation and deployment costs, pipeline network, stream splitters, electric network, gas mixer, three-way valve, and components with negligible cost (*i.e.* components of low-power or small size without construction difficulties) were excluded.

- The economic assessment ends, as well as the theoretical design analysis, before the CO_2 conditioning process.

- A 25-year plant lifetime was estimated and shared among most components, except for those described otherwise in Table 14.

- All cost functions selected are within the components and sub-systems actual operating range, avoiding cost extrapolation.

- The cooling and make-up waters are freely-available, while its treatment to prevent fouling of condenser tubes is not considered in the total cost. In addition, there is no water storage tank. To give the reader an idea, cost estimate of water tank is also provided.

- The water pump was determined to have 1.4 kW to supply 270 $m^3.h^{-1}$ of water (*Aspen Plus v 12.1*). This pump also supplies cooling water to regulate the temperatures in both TSA columns. Due to variable flow rates (a higher cooling rate is required after desorption compared to maintaining temperature during adsorption), which are difficult to determine, the water pump power was increased to 2.5 kW.

- The cost of zeolite 13X (VSA) of €1500 per tonne with a 5-year lifetime was adopted from [92], with instalment and replacement costs of €1500 retrieved from [94]. The same instalment cost was applied to zeolite 5A (TSA). The price of zeolite 5A was difficult to predict from the existing literature or obtain from reputable manufacturers, as they supply this adsorbent exclusively for laboratory use at uncompetitive prices. Thus, a potentially realistic price of €4750 per tonne of a decent-quality adsorbent was considered, representing the highest cost in the price range suggested by [153], which is still significantly below the manufacturer prices.

- The SCR direct cost is expressed as a function of catalyst cost, since no universal guide exists to estimate the SCR cost and the deployment is case-specific. The average price of the SCR catalyst is expected to be around $8000 per square metre, with a 5-year lifespan when processing natural gas emissions (about two years for coal emissions [154]) and a replacement cost of $10000, including installation within the SCR module [155]. This expectation aligns with the V_2O_5 catalyst price of about €7000 per square metre produced by *BASF SE* (type *O4-85*) [156], suggesting that the replacement cost of $10000 is likely relevant. According to internal information shared in this work, the investment cost of ready-to-operate SCR technology, including transport and deployment, is about 32 million CZK, with the catalyst price accounting for roughly 25 %. This is

slightly below a 30 - 50 % range when using V_2O_5/TiO_2 catalyst, as reported by [157]. This approach was compared with the SCR price operating in our laboratory and showed good agreement. Therefore, the catalyst share of 25 % in the total SCR direct cost was assumed.

Based on these assumptions, the following cost functions for individual components were adapted:

- ***Column***

  The costs of TSA (Equation (36)) and VSA (Equation (37)) columns were obtained from [158]:

$$C_{col}^{TSA}\ (\$_{2000}) = 4.92 \times 10^4 \left(\frac{m_{col}}{6000}\right)^{0.82} \tag{38}$$

$$C_{col}^{VSA}\ (\$_{2000}) = 19.68 \times 10^4 \left(\frac{m_{col}}{6000}\right)^{0.82} \tag{39}$$

  where m_{col} is the column weight, comprising shell and two heads (without a side ladder). The differences between Equations (38) and (39) reflect the use of carbon steel (CS, C: 0.05 - 0.25 %, Mn < 0.4 %; applied to all other CS) with a design temperature of 573 K for the TSA column (the highest operating temperature is 390 K), and high-grade stainless steel 316 [53, 109] (SS316, X5CrNiMo17-12-2; applied to all other SS316), and pressure correction up to 0.01 bar(a) (the lowest operating pressure is 0.061 bar(a)) for the VSA column with a design temperature of 273 - 373 K. The design of both columns follows the ASME standard and considers a mildly corrosive environment [151]. Both cylindrical columns are vertically placed and have a 25-year lifetime, which is typically considered for large vessels. However, it is worth noting that small pressure vessels with easy access and a volume of less than 11.3 m^3 may have a shorter lifetime around 10 years [159].

- ***Flue gas fan***

  Two types of fans were used based on their purchase costs and the required pressure rise. Higher gas compression can be achieved by using a centrifugal radial fan (up to 16 kPa):

$$C_{CR\ fan}\ (\$_{2001}) = F_M \cdot 10^{3.5391 - 0.3533 \log_{10}(\dot{V}_{fan}) + 0.4477 [\log_{10}(\dot{V}_{fan})]^2} + F_p \tag{40}$$

  A cheaper axial vane type allows gas compression up to 4 kPa:

$$C_{AV\ fan}\ (\$_{2001}) = F_M \cdot 10^{3.1761 - 0.1373 \log_{10}(\dot{V}_{fan}) + 0.3414 [\log_{10}(\dot{V}_{fan})]^2} + F_p \tag{41}$$

  where $\dot{V}_{fan}$ is inlet flow rate, F_M is the material factor that equals to about 2.75 for carbon steel, and F_p is the pressure factor being neglected for axial vane type, while added to the direct cost of

centrifugal fan as $F_{p,CR}(\$_{2001}) = 10^{0.20899\log_{10}(P_g) - 0.0328[\log_{10}(P_g)]^2}$, where P_g is the operating gauge pressure. The area of validity is given by the inlet volumetric flow rate of 1 - 100 $m^3.s^{-1}$ and the pressure rise of 0 - 0.04 bar for axial vane type and 0 - 0.16 bar for centrifugal radial type fans. Both fans are made of CS [160].

- ***Vacuum pump***

  A cost of a centrifugal vacuum pump made of CS supplied with a motor drive can be estimated as follows:

$$C_{VP}\ (\$_{2001}) = (1.89 + 1.35F_M F_P) \cdot 10^{3.3892 + 0.0536\log_{10}(P_{VP}) + 0.1538[\log_{10}(P_{VP})]^2} \quad (42)$$

  where P_{VP} is the vacuum pump shaft power retrieved from the 4-step VSA mathematical model, F_M is the material factor that equals to about 1.55 for CS, and F_P is the pressure factor that equals to 1. The area of validity is given by the vacuum pump shaft power of 1 - 300 kW. The centrifugal-type was selected due to its wide operating power range and less cost compared to alternatives such as reciprocating or positive displacement pumps [160].

- ***Water pump***

$$C_{WP}\ (\$_{2000}) = 1.97 \times 10^3\ (P_{WP})^{0.35} \quad (43)$$

  where P_{WP} is the water pump power. The area of validity is given by the water pump power of 1 - 10 kW. Equation (43) corresponds to the centrifugal-type pump and includes the price of electric motor with drive and assumes high-grade SS316, which is a recommended construction material for small industrial pumps up to 10 kW as it does not significantly increase cost at this scale. CS is typically used for larger pumps [158].

- ***Plate and fin heat-exchanger***

  The selection of plate and fin geometry allows for a larger heat transfer area within a compact casing, compared to plate geometries:

$$C_{H-E}\ (\$_{2011}) = 187.5 + 25A_{H-E} \quad (44)$$

  where A_{H-E} is the heat exchanger area (sum of cold-side and hot-side heat transfer areas). The original cost function was estimated for a counter-current flow regime heat exchanger made of aluminum with a 5-year operating period [161], which was maintained. The original heat-exchanger design was made in *Aspen Plus* for aluminum heat exchanger, with a constrained area range corresponding to the cost function used.

- **Condenser**

$$C_{cond}\ (\$_{1986}) = 2143A_{cond}^{0.86} \quad (45)$$

where A_{cond} is the condenser heat transfer area, which was determined by the *Aspen Plus* condenser designer. This cost estimate assumes shell and tube geometry with both made of CS [162]. Although its validity was not explicitly given, it is in line with *Aspen Plus* cost estimate. The reasons for using a cost function instead of *Aspen Plus* were twofold: (1) potential readers can apply it directly in their work; and (2) there is no comprehensive background on *Aspen Plus* economic evaluation. It should be noted that the currency exchange rate between the Euro and US Dollar was adjusted by the annual rate for 2021, after converting the Equation (45) to 2021 using CEPCI [163].

- ***Switching valves***

A fixed cost for solenoid-driven switching valves was considered:

$$C_{SV,VSA}\ (€_{2016}) = C_{SV,TSA}\ (€_{2016}) = 6000 \quad (46)$$

where $C_{SV,VSA}$ and $C_{SV,TSA}$ are the fixed costs for VSA and TSA, respectively. Depending on TSA and VSA configurations, the number of required switching valves per column varies: three per VSA column and four per TSA column. A basic TSA configuration without gas purge or direct heating may rely on two switching valves per column, but additional valves must be installed to control the heating medium (N_2 stream) coming from another pipeline [27, 92].

In case the CHP is located far from a water source, it may be necessary to instal a water tank may be necessary. Its purchase cost can be estimated using the following method:

- ***Water tank***

$$C_{WT}\ (\$_{2016}) \approx 1.003V_{WT}^{0.513} \quad (47)$$

where V_{WT} is the water tank volume in the validity range of 40 - 3800 m^3 and pressure of 1 - 1.3 bar(a). This tank is constructed from CS and has a cone roof, which ensures longevity and prevents the accumulation of water and waste matter on the top. An alternative lightweight option could be a fiberglass-reinforced plastic; however, this material could have size limitations due to its low durability without additional supporting structures, compared to steel-based construction materials [164]. This cost function was converted from its literature definition using Imperial units.

Table 14 shows each component considered, including its type, amount or number of units, cost scaling parameters and their values, and their cost functions. The costs of selected utilities, excluding electricity, are included. The TDC of four sub-systems along with the purchase costs of all individual components considered are displayed in Figure 22 as a cost share from the total TDC of the PCC chain proposed in Section 4.3. These sub-systems consist of the following components:

- ***Drying****:* TSA pressure vessels, switching valves, plate and fin heat-exchanger, and zeolite 5A requiring four replenishments.
- ***NO_X removal****:* SCR module, catalyst requiring four replacements, and NH_3 supply.
- ***PCC****:* VSA pressure vessels, switching valves, vacuum pumps, and zeolite 13X requiring four replenishments.
- ***Pipeline transport****:* all types of flue gas fans.

Although the result of the economic assessment should be considered with caution, the high cost of PCC capture via 4-step VSA is evident and accounts for about 69 % (Figure 22a) of all TDC throughout the CHP lifetime. Including electricity would likely accentuate its cost gap compared to other components. This finding can be attributed to the large number of columns, vacuum pumps, and complex gas streams control using switching valves, which are one of the most expensive components, as evidenced in Figure 22b. All these factors partly stem from the column dimensions defining the number of these components; however, scaling their size may require a practical approach or long-term experience with operating similar processes. The second most expensive component, drying, accounting for almost 20 %, demonstrates the drawback of using water-sensitive adsorbents. Condenser and TSA system cost three times the cost of zeolite 13X, including regular replenishments. Furthermore, this cost is achieved only by assuming that the cooling water is available at no charge. Supplying 270 $m^3.h^{-1}$ of cooling water, with prices of about 0.04 Euros per cubic metre squared [92], including make-up and chemical treatment if necessary, would alter the results. Conversely, removing trace amounts of NO_X appeared relatively cost-effective and accounted for about 9 %, as did the costs of the residual components (about 2 %) compensating for pressure drop occurrences and covering heat demands.

Table 14. Economy assessment summary of individual components and selected utilities purchase costs for CHP lifetime of 25 years.

Component	Type, material, note	Count	Cost function		Lifetime (year)	Direct cost (k€$_{2021}$/lifetime)
			Scaling parameter	Value[3]		
Catalyst	BASF O4-85, V_2O_5 honeycomb structure	8 blocks	Catalyst volume (m^3)	0.78	5	32.4
Column	Cylindrical pressure vessel, **TSA**: CS, **VSA**: SS316, vertically placed	**TSA**: 2 **VSA**: 15	Construction material weight (t)	**TSA**: 1.5 **VSA**: 0.5	25	**TSA**: 50.1 **VSA**: 650.8
Condenser	Shell and tube (U-tube design), CS, moderately corrosion-resistant	1	Heat transfer area (m^3)	98.9	25	43.3
Flue gas fan[1]	Centrifugal radial (CR), axial vane (AV), CS, sealed and electric driven	**CR**: 3 **AV**: 1	Gas flow rate ($m^3.h^{-1}$), pressure rise (kPa)	**CR**: (9634, 34); (8524, 17); (1330, 7) **AV**: (2000, 1)	25	102.1
Heat-exchanger	Plate and fin, aluminium, counter-current flow	3	Heat transfer area of cold and hot sides (m^2)	13, 286, 286	5	14.2
Switching valves	Solenoid-operated	**TSA**: 8 **VSA**: 45	Valve direct cost (k€$_{2016}$)	6	25	416.1
Vacuum pump	Centrifugal, CS, electric-driven	**BD**: 5 **Evac**: 5	Shaft power (kW)	**BD**: 23.0 **Evac**: 29.0	25	363.1
Water pump	Centrifugal, SS316, electric driven	1	Power (kW)	2.5	25	5.3
Utility	**Note**	**Amount**	**Cost parameter**	**Value**		
Adsorbent[2]	**TSA**: zeolite 5A **VSA**: zeolite 13X	**TSA**: 3.7 t **VSA**: 16.8 t	Cost per tonne (k€$_{2021}$)	**TSA**: 4.75 **VSA**: 1.50	5	**TSA**: 115.4 **VSA**: 251.6
NH_3	**Source**: Zhengzhou Sino Chemical Co., Ltd.	5.9 $t.yr^{-1}$	Cost per tonne (k$\$_{2020}$)	0.6	3.1	3.7

[1] Flue gas fans producing lower flow rate than 1 $m^3.s^{-1}$ are not considered due to their little significance in overall cost.

[2] Bed density: zeolite 5A: 750 $kg.m^{-3}$ (information obtained from *Sigma-Aldrich, Germany*), zeolite 13X: 712 $kg.m^{-3}$ [109].

[3] Value units are specified in the "Scaling parameter" column.

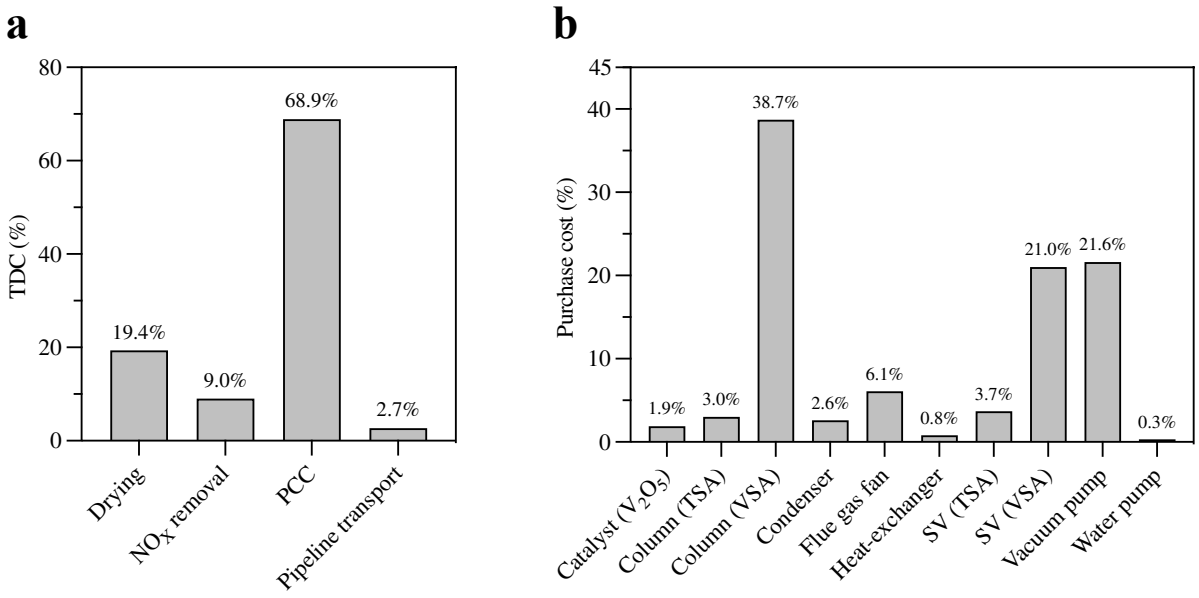

Figure 22. Results of economic assessment: **(a)** TDC of four sub-systems over 25 years of the CHP lifetime. **(b)** Basic purchase costs (without process contingency) of individual components forming the CHP PCC chain. *Note: SV = switching valve.*

Chapter 5

5 Conclusions

This thesis dealt with the feasibility of low-temperature adsorption technology for PCC in point emission sources by simulating the continuous operation of a 4-step VSA cycle. For this purpose, a mathematical model was developed in *MATLAB*. Its first simplified version was subsequently modified, tested, and improved to ultimately examine the performance and economy of 4-step VSA with zeolite 13X within the context of a district-scale CHP. A ready-to-operate flue gas cleaning was proposed as a consequence of the rigorous VSA process assessment.

The first two chapters provided the theoretical foundations for the research part. Chapter 1 introduced emerging CO_2 capture processes in the energy sector, focusing on PCC technologies with potential to compete with the most mature MEA absorption. Chapter 2 explored the physical nature of adsorption phenomena and the necessary elements of theoretical design and economic assessment of adsorption processes. Within this chapter, two literature reviews of PCC adsorption processes, including those using power plant as a case study, were carried out. The former review, summarised in Appendices A and B, suggested that using process simulation as a design tool, while considering a VSA cycle with zeolite 13X operating in four steps, are the best options, offering a good compromise between process performance and cost, straightforward scalability, and simple process control. The latter review highlighted areas within PCC, where VSA offers advantages over alternative technologies, and identified gaps in existing research. Consequently, a district-scale natural gas-fired CHP plant (4.3 MW) was selected to represent a small-scale point emission source in the industrial sector. This required several steps, which formed the main objectives of this thesis.

The research component of this thesis involved the development of a mathematical model in *MATLAB* to simulate the continuous 4-step VSA process.

In Chapter 3, a simplified mathematical model was designed to simulate the core step of any adsorption cycle, namely adsorption, by utilising mass transport equations within the gas and solid phases. This model accurately predicted experimentally measured CO_2 breakthrough experiments and demonstrated flexibility by fitting adsorption isotherm parameters, which were missing from the experimental data. Sensitivity analysis of mass transport equations and numerical approaches followed, aiming to deepen understanding acquired from the theoretical part. Finally, the mathematical model was combined with empirical process-design criteria and literature recommendations to establish an initial PCC process

design for the CHP. Here, it became apparent that the simplified model was inadequate, necessitating further refinements.

Chapter 4 addressed these refinements by including energy and momentum transport equations, which were converted into a non-dimensionless form, and implementing more efficient numerical scheme. The three remaining VSA steps for continuous simulation were also added. Next, essential flue gas treatment sub-systems and auxiliary components were proposed and determined to define practically achievable flue gas parameters and composition at the VSA inlet, placed as a tail-end unit. This process formed a ready-to-operate PCC downstream from the CHP. Potential operability was ensured by considering real operating parameters, efficiency ranges, and material constraints for all sub-systems and components involved. The mathematical model demonstrated that a 4-step VSA could achieve 90 % CO_2 purity, often required for its conditioning or repurposing, although it required lower evacuation pressure (0.07 bara) than initially estimated. To ensure continuous operation, the VSA process consisted of 15 columns placed in three parallel trains. The final Section of this thesis assessed basic economics, comparing the cost of the PCC adsorption system with established commercial sub-systems. It was determined that PCC is the most expensive process, accounting for nearly 70 % of the total direct costs throughout the CHP lifetime of 25 years.

5.1 Accomplishment of individual goals

This thesis explored the application of mathematical modelling to predict the behaviour of breakthrough experiments and low-temperature adsorption processes. Ultimately, the operation of a 4-step VSA processes for post-combustion CO_2 capture was simulated, and its theoretical concept was designed alongside other flue gas treating sub-systems and auxiliary components, forming a ready-to-operate PCC process downstream from the CHP.

The main objectives, specified in Section 2.5, have been addressed as follows:

1. **Development of a simplified non-linear dynamic mathematical model of adsorption phenomena. The reliability of the model will be verified using high-pressure breakthrough experimental data, and its robustness assessed through analysis of the numerical approach and balance equations, and application for process design.**
   I successfully developed a simplified non-linear mathematical model of adsorption phenomena for predicting experimentally measured high-pressure CO_2 breakthrough experiments in a fixed-bed column. This model was validated against these data, measured at two pressures (2 and 5 bar) and four temperatures (283 - 313 K). Model reliability and robustness were demonstrated by an accurate prediction of all CO_2 breakthrough curves and by fitting the missing adsorption isotherm parameters, respectively. Transport PDEs of mass in gas and solid phases were subjected to a sensitivity analysis, involving parameters that often need to be estimated. High-order flux limiters were also incorporated into this sensitivity analysis. Finally, the mathematical model was used in conjunction with process-design criteria and literature recommendations to establish an initial PCC process design. Detailed findings are presented in Chapter 3.

2. **Development of a complex non-linear dynamic mathematical model of 4-step VSA process, enabling simulation of various scenarios for different process parameters and configurations, and its application to experimental and theoretical studies.**
   I developed a 4-step VSA model based on an experimentally validated model in the literature, incorporating PDEs of mass, enthalpy, and momentum transfers. I drew on previous experience with FVM used in a simplified mathematical model of adsorption phenomena, which helped to implement more complex system of PDEs. The model was verified against various literature data (Appendix D) and applied for the theoretical design of a PCC adsorption process. The detailed description of model assumptions, PDEs, initial and boundary conditions, non-dimensionless scheme, including the determination of CSS and PIs, is provided in Appendix D.

3. **Design of adsorption PCC system integrated into an urban-scale energy system, including general economic assessment.**

   I approached the designing part in three steps: (1) establishing an initial VSA process design using a simplified model; (2) proposing essential sub-systems and auxiliary components to define flue gas properties at the VSA inlet; and (3) using a complex mathematical model to verify and revise an initial design. The resulting ready-to-operate process with adsorption PCC process was considered downstream from a 4.3 MW natural gas fired CHP, representing industrial point emission source. The main sub-systems included SCR-deNOx, a two-step dehydration combining condenser and TSA with zeolite 5A, and a 4-step VSA with zeolite 13X. The simulated 4-step VSA achieved a CO_2 purity and recovery of 90.4 % and 15.6 %, respectively, utilising 15 columns arranged into five parallel trains continuously processing 8524 $m_N^3.h^{-1}$ of dry flue gas containing 6.4 vol% CO_2 at 286 K and 1 bara. Economic assessment was limited to an estimate of the component purchase costs. PCC was determined to be the largest cost contributor, accounting for about 70 % of the total direct costs throughout the CHP lifetime.

5.2 Future perspectives

This thesis presented results in a previously unexplored area at the Department of Energy Engineering and established a theoretical foundation. The mathematical model was designed for a specific purpose and validated using experimental data from the literature on a single adsorbent and VSA process configurations, raising the question of universal applicability, which paves the way for opportunities for future research:

- Verification of the mathematical model reliability and the area of applicability by performing experimental measurements under various condition.
- Extension of the 4-step VSA concept by adding steps that transfer gas between the columns, which can improve process performance.
- Inclusion of water vapour and trace impurities (*e.g.* nitric or sulphuric oxides) as a secondary component to CO_2 or in a ternary mixture. This should be supported by experimentally obtained multicomponent adsorption isotherms, due to the lack of experimental data in the existing literature.
- Implementation of a process optimiser to determine the optimum process settings and scheduling.
- Following process optimisation, a priority should be to carry out detailed techno-economic analysis comparing adsorption with pilot PCC projects (*e.g.* chemical adsorption).
- With the rapid progress in neutral network models, exploring their potential may be worthwhile.

References

[1] DeConto RM, Pollard D, Alley RB, Velicogna I, Gasson E, Gomez N, et al. The Paris Climate Agreement and future sea-level rise from Antarctica. Nature 2021;593(7857):83-9. https://doi.org/10.1038/s41586-021-03427-0

[2] IPCC. In-depth Q&A: The IPCC's sixth assessment on how to tackle climate change. [cited 2023 17 January]. Available from: https://www.carbonbrief.org/in-depth-qa-the-ipccs-sixth-assessment-on-how-to-tackle-climate-change/.

[3] Gür TM. Carbon Dioxide Emissions, Capture, Storage and Utilization: Review of Materials, Processes and Technologies. Progress in Energy and Combustion Science 2022;89. https://doi.org/10.1016/j.pecs.2021.100965

[4] United Nations Framework Convention on Climate Change. The Paris Agreement. [cited 2023 16 January]. Available from: https://unfccc.int/process-and-meetings/the-paris-agreement/the-paris-agreement.

[5] Fuchs R, Brown C, Rounsevell M. Europe's Green Deal offshores environmental damage to other nations. Nature 2020;586(7831):671-3. https://doi.org/10.1038/d41586-020-02991-1

[6] García M, Chronopoulos T, Montañés RM. CO2 Capture - A Brief Review of Technologies and Its Integration. Engineering Solutions for CO2 Conversion 2021. p. 1-28. https://doi.org/10.1002/9783527346523.ch1

[7] Einbu A, Pettersen T, Morud J, Tobiesen A, Jayarathna CK, Skagestad R, et al. Energy assessments of onboard CO2 capture from ship engines by MEA-based post combustion capture system with flue gas heat integration. International Journal of Greenhouse Gas Control 2022;113. https://doi.org/10.1016/j.ijggc.2021.103526

[8] Kearns D, Liu H, Consoli C. Technology readiness and costs of CCS. Global CCS institute 2021.

[9] Leung DYC, Caramanna G, Maroto-Valer MM. An overview of current status of carbon dioxide capture and storage technologies. Renewable and Sustainable Energy Reviews 2014;39:426-43. https://doi.org/10.1016/j.rser.2014.07.093

[10] Creamer AE, Gao B. Overview of CO2 Capture Technology. Carbon Dioxide Capture: An Effective Way to Combat Global Warming. SpringerBriefs in Molecular Science 2015. p. 17-24. https://doi.org/10.1007/978-3-319-17010-7_2

[11] Cheng Z, Li S, Liu Y, Zhang Y, Ling Z, Yang M, et al. Post-combustion CO2 capture and separation in flue gas based on hydrate technology：A review. Renewable and Sustainable Energy Reviews 2022;154. https://doi.org/10.1016/j.rser.2021.111806

[12] Kawalkar R, Dubey HK, Lokhande S. Carbon Capture Technology a Sustainable Energy Production Technique: A Review. Advances in Systems Engineering. Lecture Notes in Mechanical Engineering 2021. p. 713-36. https://doi.org/10.1007/978-981-15-8025-3_69

[13] Hrdlicka J, Vodička M, Skopec P, Hrdlička F, Dlouhý T. CO2 Capture by Oxyfuel Combustion. CO2 Separation, Purification and Conversion to Chemicals and Fuels. Energy, Environment, and Sustainability 2019. p. 55-78. https://doi.org/10.1007/978-981-13-3296-8_5

[14] Liu Z, Zhang T. Pilot and Industrial Demonstration of Oxy-fuel Combustion. Oxy-Fuel Combustion 2018. p. 209-22. https://doi.org/10.1016/b978-0-12-812145-0.00010-4

[15] Wilcox J. Carbon Capture New York: Springer New York, NY; 2012. 324 p.

[16] Hashemi SM, Sedghkerdar MH, Mahinpey N. Calcium looping carbon capture: Progress and prospects. The Canadian Journal of Chemical Engineering 2022;100(9):2140-71. https://doi.org/10.1002/cjce.24480

[17] Khalifa O, Alkhatib III, Bahamon D, Alhajaj A, Abu-Zahra MRM, Vega LF. Modifying absorption process configurations to improve their performance for Post-Combustion CO2 capture - What have we

learned and what is still Missing? Chemical Engineering Journal 2022;430. https://doi.org/10.1016/j.cej.2021.133096
[18] Nessi E, Papadopoulos AI, Seferlis P. A review of research facilities, pilot and commercial plants for solvent-based post-combustion CO2 capture: Packed bed, phase-change and rotating processes. International Journal of Greenhouse Gas Control 2021;111. https://doi.org/10.1016/j.ijggc.2021.103474
[19] Romero-García AG, Mora-Morales C, Chargoy-Amador JP, Ramírez-Corona N, Sánchez-Ramírez E, Segovia-Hernández JG. Implementing CO2 capture process in power plants: Optimization procedure and environmental impact. Chemical Engineering Research and Design 2022;180:232-42. https://doi.org/10.1016/j.cherd.2022.02.023
[20] Liang X, Qader A, Chen L, Fu X, Huang D, Lin Q, et al. Regional: Integrated High Impact Innovation in Sustainable Energy Technology - Prefeasibility Analysis for Carbon Capture, Utilization and Storage (Subproject 2). Periodical Regional: Integrated High Impact Innovation in Sustainable Energy Technology - Prefeasibility Analysis for Carbon Capture, Utilization and Storage (Subproject 2) [Internet] 2022,
[21] Song C, Liu Q, Ji N, Deng S, Zhao J, Li Y, et al. Alternative pathways for efficient CO2 capture by hybrid processes - A review. Renewable and Sustainable Energy Reviews 2018;82:215-31. https://doi.org/10.1016/j.rser.2017.09.040
[22] Chao C, Deng Y, Dewil R, Baeyens J, Fan X. Post-combustion carbon capture. Renewable and Sustainable Energy Reviews 2021;138. https://doi.org/10.1016/j.rser.2020.110490
[23] Vaz S, Rodrigues de Souza AP, Lobo Baeta BE. Technologies for carbon dioxide capture: A review applied to energy sectors. Cleaner Engineering and Technology 2022;8. https://doi.org/10.1016/j.clet.2022.100456
[24] Baliga B, Bhujade R, Kar S, Magneschi G, Velan VK, Wattal D, et al. Integrated High Impact Innovation in Sustainable Energy Technology - Prefeasibility Analysis for Carbon Capture, Utilization and Storage (Subproject 2). Periodical Integrated High Impact Innovation in Sustainable Energy Technology - Prefeasibility Analysis for Carbon Capture, Utilization and Storage (Subproject 2) [Internet] 2021, 192 p.
[25] Hasan MMF, Baliban RC, Elia JA, Floudas CA. Modeling, Simulation, and Optimization of Postcombustion CO2 Capture for Variable Feed Concentration and Flow Rate. 1. Chemical Absorption and Membrane Processes. Industrial & Engineering Chemistry Research 2012;51(48):15642-64. https://doi.org/10.1021/ie301571d
[26] Hasan MMF, Baliban RC, Elia JA, Floudas CA. Modeling, Simulation, and Optimization of Postcombustion CO2 Capture for Variable Feed Concentration and Flow Rate. 2. Pressure Swing Adsorption and Vacuum Swing Adsorption Processes. Industrial & Engineering Chemistry Research 2012;51(48):15665-82. https://doi.org/10.1021/ie301572n
[27] Zanco SE, Pérez-Calvo J-F, Gasós A, Cordiano B, Becattini V, Mazzotti M. Postcombustion CO2 Capture: A Comparative Techno-Economic Assessment of Three Technologies Using a Solvent, an Adsorbent, and a Membrane. ACS Engineering Au 2021;1(1):50-72. https://doi.org/10.1021/acsengineeringau.1c00002
[28] Inc. S. Svante Inc. Our Innovative Carbon Capture Technology. [cited 2023 19 January]. Available from: https://svanteinc.com/carbon-capture-technology/.
[29] Zhou J, Van Den Assem D, Chalaturnyk R, Meikle G, Gray M, Dar S, et al. Carbon Capture Utilization, and Storage (CCUS). Periodical Carbon Capture Utilization, and Storage (CCUS) [Internet] 2022, 40 p.
[30] Lafarge. Lafarge. Project CO2MENT. [cited 20 January. 2023. Available from: https://www.lafarge.ca/en/project-co2ment.
[31] Ltd. SGC. Seibu Giken Co. Ltd. Products Under Development - CO2 Recovery System C-SAVE ®. [cited 2023 19 January]. Available from: https://seibu-giken.com/english/our-products/products-under-development.

[32] RITE. RITE Today Annual Report. Periodical RITE Today Annual Report [Internet] 2018;13, 65 p. https://www.rite.or.jp/en/results/today/pdf/rt2018_all_e.pdf
[33] Elliott JE, Copeland RJ, McCall PP, inventors. Rotary moving bed for CO2 separation and use of same. United States patent US 9,539,540 B2. 2017.
[34] Carbone C, Ferrario D, Lanzini A, Stendardo S, Agostini A. Evaluating the Carbon Footprint of Cement Plants Integrated With the Calcium Looping CO2 Capture Process. Frontiers in Sustainability 2022;3. https://doi.org/10.3389/frsus.2022.809231
[35] Ruthven DM. Principles of adsorption and adsorption processes: John Wiley & Sons; 1984.
[36] Thommes M, Kaneko K, Neimark AV, Olivier JP, Rodriguez-Reinoso F, Rouquerol J, et al. Physisorption of gases, with special reference to the evaluation of surface area and pore size distribution (IUPAC Technical Report). Pure and Applied Chemistry 2015;87(9-10):1051-69. https://doi.org/10.1515/pac-2014-1117
[37] Liu RS, Shi XD, Wang CT, Gao YZ, Xu S, Hao GP, et al. Advances in Post-Combustion CO2 Capture by Physical Adsorption: From Materials Innovation to Separation Practice. ChemSusChem 2021;14(6):1428-71. https://doi.org/10.1002/cssc.202002677
[38] Bulánek R. Povrchové jevy na pevných látkách. Univerzita Pardubice; 2015
[39] Gomes VG, Yee KWK. Pressure swing adsorption for carbon dioxide sequestration from exhaust gases. Separation and Purification Technology 2002;28(2):161-71. https://doi.org/10.1016/s1383-5866(02)00064-3
[40] Traegner UK, Suidan MT. Parameter Evaluation for Carbon Adsorption. Journal of Environmental Engineering 1989;115(1):109-28. https://doi.org/10.1061/(asce)0733-9372(1989)115:1(109)
[41] Valenzuela DP, Myers AL. Adsorption equilibrium data handbook: Prentice Hall; 1989.
[42] Technology NIoSa. NIST/ARPA-E Database of Novel and Emerging Adsorbent Materials. [1 February 2023]. Available from: https://adsorbents.nist.gov.
[43] Bobbitt NS, Shi K, Bucior BJ, Chen H, Tracy-Amoroso N, Li Z, et al. MOFX-DB: An Online Database of Computational Adsorption Data for Nanoporous Materials. Journal of Chemical & Engineering Data 2023. https://doi.org/10.1021/acs.jced.2c00583
[44] Cambridge Structural Database [Internet]. [cited 30 January 2023]. Available from: https://www.ccdc.cam.ac.uk/Community/csdcommunity/csd-mof-collection/.
[45] Dhoke C, Zaabout A, Cloete S, Amini S. Review on Reactor Configurations for Adsorption-Based CO2 Capture. Industrial & Engineering Chemistry Research 2021;60(10):3779-98. https://doi.org/10.1021/acs.iecr.0c04547
[46] Jones RL, Keller GE. Pressure-Swing parametric pumping - A new adsorption process. J Separ Proc Technol 1981;2(3):17-23.
[47] Fouladi N, Makarem MA, Sedghamiz MA, Rahimpour HR. CO2 adsorption by swing technologies and challenges on industrialization. Advances in Carbon Capture 2020. p. 241-67. https://doi.org/10.1016/b978-0-12-819657-1.00011-6
[48] Gemmingen Uv. Technical Adsorption - Modern Processes. Chemie Ingenieur Technik 2011;83(1-2):36-43. https://doi.org/10.1002/cite.201000151
[49] Hedin N, Andersson L, Bergström L, Yan J. Adsorbents for the post-combustion capture of CO2 using rapid temperature swing or vacuum swing adsorption. Applied Energy 2013;104:418-33. https://doi.org/10.1016/j.apenergy.2012.11.034
[50] Maruyama RT, Pai KN, Subraveti SG, Rajendran A. Improving the performance of vacuum swing adsorption based CO2 capture under reduced recovery requirements. International Journal of Greenhouse Gas Control 2020;93. https://doi.org/10.1016/j.ijggc.2019.102902
[51] Skarstrom CW, inventor Method and apparatus for fractionating gas mixtures by adsorption. US1960.
[52] Guérin de Montgareuil P, Domine D. Process for separating a binary gaseous mixture by adsorption. US Patent 3,155,468; 1964

[53] Haghpanah R, Nilam R, Rajendran A, Farooq S, Karimi IA. Cycle synthesis and optimization of a VSA process for postcombustion CO2 capture. AIChE Journal 2013;59(12):4735-48. https://doi.org/10.1002/aic.14192
[54] Ntiamoah A, Ling J, Xiao P, Webley PA, Zhai Y. CO2 capture by vacuum swing adsorption: role of multiple pressure equalization steps. Adsorption 2015;21(6-7):509-22. https://doi.org/10.1007/s10450-015-9690-8
[55] Erden H, Ebner AD, Ritter JA. Development of a Pressure Swing Adsorption Cycle for Producing High Purity CO2 from Dilute Feed Streams. Part I: Feasibility Study. Industrial & Engineering Chemistry Research 2018;57(23):8011-22. https://doi.org/10.1021/acs.iecr.7b05024
[56] Abd AA, Naji SZ, Hashim AS, Othman MR. Carbon dioxide removal through physical adsorption using carbonaceous and non-carbonaceous adsorbents: A review. Journal of Environmental Chemical Engineering 2020;8(5). https://doi.org/10.1016/j.jece.2020.104142
[57] You YY, Liu XJ. Modeling of CO2 adsorption and recovery from wet flue gas by using activated carbon. Chemical Engineering Journal 2019;369:672-85. https://doi.org/10.1016/j.cej.2019.03.118
[58] Wu J, Zhu X, Yang F, Wang R, Ge T. Shaping techniques of adsorbents and their applications in gas separation: a review. Journal of Materials Chemistry A 2022;10(43):22853-95. https://doi.org/10.1039/d2ta04352a
[59] Bae Y-S, Snurr RQ. Development and Evaluation of Porous Materials for Carbon Dioxide Separation and Capture. Angewandte Chemie International Edition 2011;50(49):11586-96. https://doi.org/10.1002/anie.201101891
[60] Modak A, Jana S. Advancement in porous adsorbents for post-combustion CO2 capture. Microporous and Mesoporous Materials 2019;276:107-32. https://doi.org/10.1016/j.micromeso.2018.09.018
[61] Subramanian Balashankar V, Rajagopalan AK, de Pauw R, Avila AM, Rajendran A. Analysis of a Batch Adsorber Analogue for Rapid Screening of Adsorbents for Postcombustion CO2 Capture. Industrial & Engineering Chemistry Research 2019;58(8):3314-28. https://doi.org/10.1021/acs.iecr.8b05420
[62] Kim SH, Landa HOR, Ravutla S, Realff MJ, Boukouvala F. Data-driven simultaneous process optimization and adsorbent selection for vacuum pressure swing adsorption. Chemical Engineering Research and Design 2022;188:1013-28. https://doi.org/10.1016/j.cherd.2022.10.002
[63] Singh G, Lee J, Karakoti A, Bahadur R, Yi J, Zhao D, et al. Emerging trends in porous materials for CO2 capture and conversion. Chemical Society Reviews 2020;49(13):4360-404. https://doi.org/10.1039/d0cs00075b
[64] Arora A, Iyer SS, Hasan MMF. Computational Material Screening Using Artificial Neural Networks for Adsorption Gas Separation. The Journal of Physical Chemistry C 2020;124(39):21446-60. https://doi.org/10.1021/acs.jpcc.0c05900
[65] Rahimi M, Moosavi SM, Smit B, Hatton TA. Toward smart carbon capture with machine learning. Cell Reports Physical Science 2021;2(4). https://doi.org/10.1016/j.xcrp.2021.100396
[66] Pai KN, Prasad V, Rajendran A. Generalized, Adsorbent-Agnostic, Artificial Neural Network Framework for Rapid Simulation, Optimization, and Adsorbent Screening of Adsorption Processes. Industrial & Engineering Chemistry Research 2020;59(38):16730-40. https://doi.org/10.1021/acs.iecr.0c02339
[67] Kikkinides ES, Yang RT, Cho SH. Concentration and Recovery of CO2 from Flue Gas by Pressure Swing Adsorption. Industrial & Engineering Chemistry Research 1993;32(11):2714-20. https://doi.org/10.1021/ie00023a038
[68] Kumita M, Watanabe F, Hasatani M, editors. Separation of Carbon Dioxide by Pressure Swing Adsorption Using Granular Molecular Sieving Carbon. Process Industries Power the Pacific Rim: Sixth Conference of the Asia Pacific Confederation of Chemical Engineering; Twenty-first Australasian Chemical Engineering Conference; Official Proceedings of Combined Conference 1993: Sixth Conference of the Asia Pacific Confederation of Chemical Engineering; Twenty-first Australasian

Chemical Engineering Conference; Official Proceedings of Combined Conference 1993; 1993: Institution of Engineers, Australia Barton, ACT.

[69] Chue KT, Kim JN, Yoo YJ, Cho SH, Yang RT. Comparison of Activated Carbon and Zeolite 13X for CO2 Recovery from Flue Gas by Pressure Swing Adsorption. Industrial & Engineering Chemistry Research 1995;34(2):591-8. https://doi.org/10.1021/ie00041a020

[70] Ishibashi M, Ota H, Akutsu N, Umeda S, Tajika M, Izumi J, et al. Technology for removing carbon dioxide from power plant flue gas by the physical adsorption method. Energy Conversion and Management 1996;37(6-8):929-33. https://doi.org/10.1016/0196-8904(95)00279-0

[71] Saji A, Takamura Y, Noda H, Watanabe F, Matsuda H, Hasatani M. Application of PSA to Separation of Carbon Dioxide from Flue Gas. Kagaku Kogaku Ronbunshu 1997;23(2):149-56. https://doi.org/10.1252/kakoronbunshu.23.149

[72] Liu B, Yu X, Shi W, Shen Y, Zhang D, Tang Z. Two-stage VSA/PSA for capturing carbon dioxide (CO2) and producing hydrogen (H2) from steam-methane reforming gas. International Journal of Hydrogen Energy 2020;45(46):24870-82. https://doi.org/10.1016/j.ijhydene.2020.06.264

[73] Webley PA, Qader A, Ntiamoah A, Ling J, Xiao P, Zhai Y. A New Multi-bed Vacuum Swing Adsorption Cycle for CO2 Capture from Flue Gas Streams. Energy Procedia 2017;114:2467-80. https://doi.org/10.1016/j.egypro.2017.03.1398

[74] Mondino G, Spjelkavik AI, Didriksen T, Krishnamurthy S, Stensrød RE, Grande CA, et al. Production of MOF Adsorbent Spheres and Comparison of Their Performance with Zeolite 13X in a Moving-Bed TSA Process for Postcombustion CO2 Capture. Industrial & Engineering Chemistry Research 2020;59(15):7198-211. https://doi.org/10.1021/acs.iecr.9b06387

[75] Gibson JAA, Mangano E, Shiko E, Greenaway AG, Gromov AV, Lozinska MM, et al. Adsorption Materials and Processes for Carbon Capture from Gas-Fired Power Plants: AMPGas. Industrial & Engineering Chemistry Research 2016;55(13):3840-51. https://doi.org/10.1021/acs.iecr.5b05015

[76] Schöny G, Dietrich F, Fuchs J, Pröll T, Hofbauer H. A multi-stage fluidized bed system for continuous CO2 capture by means of temperature swing adsorption - First results from bench scale experiments. Powder Technology 2017;316:519-27. https://doi.org/10.1016/j.powtec.2016.11.066

[77] Keller L, Lohaus T, Abduly L, Hadler G, Wessling M. Electrical swing adsorption on functionalized hollow fibers. Chemical Engineering Journal 2019;371:107-17. https://doi.org/10.1016/j.cej.2019.04.029

[78] Ribeiro RPPL, Grande CA, Rodrigues AE. Activated carbon honeycomb monolith - Zeolite 13X hybrid system to capture CO2 from flue gases employing Electric Swing Adsorption. Chemical Engineering Science 2013;104:304-18. https://doi.org/10.1016/j.ces.2013.09.011

[79] Voskian S, Hatton TA. Faradaic electro-swing reactive adsorption for CO2 capture. Energy & Environmental Science 2019;12(12):3530-47. https://doi.org/10.1039/c9ee02412c

[80] Yassin MM, Biti S, Afzal W, Fernández Martín C. A systematic analysis of the dynamics of microwave- and conventionally-assisted swing adsorption on zeolite 13X and an activated carbon under post-combustion carbon capture conditions. Journal of Environmental Chemical Engineering 2021;9(6). https://doi.org/10.1016/j.jece.2021.106835

[81] Luberti M, Oreggioni GD, Ahn H. Design of a rapid vacuum pressure swing adsorption (RVPSA) process for post-combustion CO2 capture from a biomass-fuelled CHP plant. Journal of Environmental Chemical Engineering 2017;5(4):3973-82. https://doi.org/10.1016/j.jece.2017.07.029

[82] El Fil B, Hoysall DC, Garimella S. Carbon Dioxide Capture Using Sorbent-Loaded Hollow-Fiber Modules for Coal-Fired Power Plants. Journal of Energy Resources Technology 2022;144(6). https://doi.org/10.1115/1.4051899

[83] Nikolaidis GN, Kikkinides ES, Georgiadis MC. An Integrated Two-Stage P/VSA Process for Postcombustion CO2 Capture Using Combinations of Adsorbents Zeolite 13X and Mg-MOF-74. Industrial & Engineering Chemistry Research 2017;56(4):974-88. https://doi.org/10.1021/acs.iecr.6b04270

[84] Joss L, Gazzani M, Mazzotti M. Rational design of temperature swing adsorption cycles for post-combustion CO2 capture. Chemical Engineering Science 2017;158:381-94. https://doi.org/10.1016/j.ces.2016.10.013

[85] Zanco SE, Mazzotti M, Gazzani M, Romano MC, Martínez I. Modeling of circulating fluidized beds systems for post - combustion CO2 capture via temperature swing adsorption. AIChE Journal 2017;64(5):1744-59. https://doi.org/10.1002/aic.16029

[86] Arora A, Hasan MMF. Flexible oxygen concentrators for medical applications. Scientific Reports 2021;11(1). https://doi.org/10.1038/s41598-021-93796-3

[87] Sazali N. Emerging technologies by hydrogen: A review. International Journal of Hydrogen Energy 2020;45(38):18753-71. https://doi.org/10.1016/j.ijhydene.2020.05.021

[88] ISO 27919-1:2018. Carbon dioxide capture. The British Standards Institution; 2018

[89] Feron PHM, Cousins A, Jiang K, Zhai R, Garcia M. An update of the benchmark post-combustion CO2-capture technology. Fuel 2020;273. https://doi.org/10.1016/j.fuel.2020.117776

[90] Rajagopalan AK, Avila AM, Rajendran A. Do adsorbent screening metrics predict process performance? A process optimisation based study for post-combustion capture of CO2. International Journal of Greenhouse Gas Control 2016;46:76-85. https://doi.org/10.1016/j.ijggc.2015.12.033

[91] Krishnamurthy S, Boon J, Grande C, Lind A, Blom R, Boer R, et al. Screening Supported Amine Sorbents in the Context of Post-combustion Carbon Capture by Vacuum Swing Adsorption Chemie Ingenieur Technik 2021;93(6):929-40. https://doi.org/10.1002/cite.202000172

[92] Subraveti SG, Roussanaly S, Anantharaman R, Riboldi L, Rajendran A. Techno-economic assessment of optimised vacuum swing adsorption for post-combustion CO2 capture from steam-methane reformer flue gas. Separation and Purification Technology 2021;256. https://doi.org/10.1016/j.seppur.2020.117832

[93] Subraveti SG, Roussanaly S, Anantharaman R, Riboldi L, Rajendran A. How much can novel solid sorbents reduce the cost of post-combustion CO2 capture? A techno-economic investigation on the cost limits of pressure-vacuum swing adsorption. Applied Energy 2022;306. https://doi.org/10.1016/j.apenergy.2021.117955

[94] Ward A, Pini R. Efficient Bayesian Optimization of Industrial-Scale Pressure-Vacuum Swing Adsorption Processes for CO2 Capture. Industrial & Engineering Chemistry Research 2022;61(36):13650-68. https://doi.org/10.1021/acs.iecr.2c02313

[95] Susarla N, Haghpanah R, Karimi IA, Farooq S, Rajendran A, Tan LSC, et al. Energy and cost estimates for capturing CO2 from a dry flue gas using pressure/vacuum swing adsorption. Chemical Engineering Research and Design 2015;102:354-67. https://doi.org/10.1016/j.cherd.2015.06.033

[96] Wawrzyńczak D, Majchrzak-Kucęba I, Srokosz K, Kozak M, Nowak W, Zdeb J, et al. The pilot dual-reflux vacuum pressure swing adsorption unit for CO2 capture from flue gas. Separation and Purification Technology 2019;209:560-70. https://doi.org/10.1016/j.seppur.2018.07.079

[97] Anselmi H, Mirgaux O, Bounaceur R, Patisson F. Simulation of Post-Combustion CO2 Capture, a Comparison among Absorption, Adsorption and Membranes. Chemical Engineering & Technology 2019;42(4):797-804. https://doi.org/10.1002/ceat.201800667

[98] Jiang L, Gonzalez-Diaz A, Ling-Chin J, Roskilly AP, Smallbone AJ. Post-combustion CO2 capture from a natural gas combined cycle power plant using activated carbon adsorption. Applied Energy 2019;245:1-15. https://doi.org/10.1016/j.apenergy.2019.04.006

[99] Mondino G, Grande CA, Blom R, Nord LO. Moving bed temperature swing adsorption for CO2 capture from a natural gas combined cycle power plant. International Journal of Greenhouse Gas Control 2019;85:58-70. https://doi.org/10.1016/j.ijggc.2019.03.021

[100] Riboldi L, Bolland O. Evaluating Pressure Swing Adsorption as a CO2 separation technique in coal-fired power plants. International Journal of Greenhouse Gas Control 2015;39:1-16. https://doi.org/10.1016/j.ijggc.2015.02.001

[101] Sjostrom S, Senior C. Pilot testing of CO2 capture from a coal-fired power plant - Part 2: Results from 1-MWe pilot tests. Clean Energy 2020;4(1):12-25. https://doi.org/10.1093/ce/zkz034
[102] Sjostrom S, Senior C. Pilot testing of CO2 capture from a coal-fired power plant - Part 1: Sorbent characterization. Clean Energy 2019;3(2):144-62. https://doi.org/10.1093/ce/zkz009
[103] . !!! INVALID CITATION !!! .
[104] Zhao R, Liu L, Zhao L, Deng S, Li S, Zhang Y, et al. Techno-economic analysis of carbon capture from a coal-fired power plant integrating solar-assisted pressure-temperature swing adsorption (PTSA). Journal of Cleaner Production 2019;214:440-51. https://doi.org/10.1016/j.jclepro.2018.12.316
[105] Chen X, Wang J, Ren T, Li Z, Du T, Lu X, et al. Novel exchanger type vacuum temperature swing adsorption for post-combustion CO2 capture: Process design and plant demonstration. Separation and Purification Technology 2023;308. https://doi.org/10.1016/j.seppur.2022.122837
[106] Farmahini AH, Krishnamurthy S, Friedrich D, Brandani S, Sarkisov L. Performance-Based Screening of Porous Materials for Carbon Capture. Chemical Reviews 2021;121(17):10666-741. https://doi.org/10.1021/acs.chemrev.0c01266
[107] Li S, Deng S, Zhao L, Zhao R, Lin M, Du Y, et al. Mathematical modeling and numerical investigation of carbon capture by adsorption: Literature review and case study. Applied Energy 2018;221:437-49. https://doi.org/10.1016/j.apenergy.2018.03.093
[108] Shafeeyan MS, Wan Daud WMA, Shamiri A. A review of mathematical modeling of fixed-bed columns for carbon dioxide adsorption. Chemical Engineering Research and Design 2014;92(5):961-88. https://doi.org/10.1016/j.cherd.2013.08.018
[109] Haghpanah R, Majumder A, Nilam R, Rajendran A, Farooq S, Karimi IA, et al. Multiobjective Optimization of a Four-Step Adsorption Process for Postcombustion CO2 Capture Via Finite Volume Simulation. Industrial & Engineering Chemistry Research 2013;52(11):4249-65. https://doi.org/10.1021/ie302658y
[110] Glueckauf E. Theory of chromatography. Part 10.- Formulæ for diffusion into spheres and their application to chromatography. Trans Faraday Soc 1955;51(0):1540-51. https://doi.org/10.1039/tf9555101540
[111] Sircar S. Adsorbate mass transfer into porous adsorbents - A practical viewpoint. Separation and Purification Technology 2018;192:383-400. https://doi.org/10.1016/j.seppur.2017.10.014
[112] Ahn H, Hong S-H, Zhang Y, Lee C-H. Experimental and Simulation Study on CO2 Adsorption Dynamics of a Zeolite 13X Column during Blowdown and Pressurization: Implications of Scaleup on CO2 Capture Vacuum Swing Adsorption Cycle. Industrial & Engineering Chemistry Research 2020;59(13):6053-64. https://doi.org/10.1021/acs.iecr.9b05862
[113] Rečka L, Máca V, Ščasný M. Green Deal and Carbon Neutrality Assessment of Czechia. Preprints 2023. https://doi.org/10.20944/preprints202301.0556.v1
[114] Danaci D, Webley PA, Petit C. Guidelines for Techno-Economic Analysis of Adsorption Processes. Frontiers in Chemical Engineering 2021;2. https://doi.org/10.3389/fceng.2020.602430
[115] Nedoma M, Staf M, Hrdlička J. Experimental and simulation study of CO2 breakthrough curves in a fixed-bed adsorption process. Acta Polytechnica 2022;62(3):370-85. https://doi.org/10.14311/ap.2022.62.0370
[116] Wilkins NS, Rajendran A, Farooq S. Dynamic column breakthrough experiments for measurement of adsorption equilibrium and kinetics. Adsorption 2020;27(3):397-422. https://doi.org/10.1007/s10450-020-00269-6
[117] Xiao P, Zhang J, Webley P, Li G, Singh R, Todd R. Capture of CO2 from flue gas streams with zeolite 13X by vacuum-pressure swing adsorption. Adsorption 2008;14(4-5):575-82. https://doi.org/10.1007/s10450-008-9128-7
[118] Poling BE, Prausnitz JM, O'Connell JP. The properties of gases and liquids. 5th ed. New York: McGraw-Hill; 2001.

[119] Malek A, Farooq S, Rathor MN, Hidajat K. Effect of velocity variation due to adsorption-desorption on equilibrium data from breakthrough experiments. Chemical Engineering Science 1995;50(4):737-40. https://doi.org/10.1016/0009-2509(94)00245-m
[120] Ribeiro A, Neto P, Pinho C. Mean porosity and pressure drop measurements in packed beds of monosized spheres: side wall effects. International Review of Chemical Engineering 2010;2(1):40-6.
[121] Delgado JMPQ. Longitudinal and Transverse Dispersion in Porous Media. Chemical Engineering Research and Design 2007;85(9):1245-52. https://doi.org/10.1205/cherd07017
[122] Langer G, Roethe A, Roethe KP, Gelbin D. Heat and mass transfer in packed beds - III. Axial mass dispersion. International Journal of Heat and Mass Transfer 1978;21(6):751-9. https://doi.org/10.1016/0017-9310(78)90037-6
[123] Ruthven DM, Post MFM. Chapter 12 Diffusion in zeolite molecular sieves. Introduction to Zeolite Science and Practice. Studies in Surface Science and Catalysis 2001. p. 525-77. https://doi.org/10.1016/s0167-2991(01)80254-8
[124] Ciahotný K, Vagenknechtová A, Netušil M, Ditl P, Prokopová O. Adsorption Drying of Natural Gas under High Pressure. Oil Gas European Magazine 2014;40(2):91-5.
[125] Hu X, Mangano E, Friedrich D, Ahn H, Brandani S. Diffusion mechanism of CO2 in 13X zeolite beads. Adsorption 2013;20(1):121-35. https://doi.org/10.1007/s10450-013-9554-z
[126] Hefti M, Marx D, Joss L, Mazzotti M. Adsorption equilibrium of binary mixtures of carbon dioxide and nitrogen on zeolites ZSM-5 and 13X. Microporous and Mesoporous Materials 2015;215:215-28. https://doi.org/10.1016/j.micromeso.2015.05.044
[127] Pai KN, Prasad V, Rajendran A. Practically Achievable Process Performance Limits for Pressure-Vacuum Swing Adsorption-Based Postcombustion CO2 Capture. ACS Sustainable Chemistry & Engineering 2021;9(10):3838-49. https://doi.org/10.1021/acssuschemeng.0c08933
[128] Javeed S, Qamar S, Ashraf W, Warnecke G, Seidel-Morgenstern A. Analysis and numerical investigation of two dynamic models for liquid chromatography. Chemical Engineering Science 2013;90:17-31. https://doi.org/10.1016/j.ces.2012.12.014
[129] Javeed S, Qamar S, Seidel-Morgenstern A, Warnecke G. Efficient and accurate numerical simulation of nonlinear chromatographic processes. Computers & Chemical Engineering 2011;35(11):2294-305. https://doi.org/10.1016/j.compchemeng.2010.10.002
[130] Sircar S, Kumar R, Anselmo KJ. Effects of column nonisothermality or nonadiabaticity on the adsorption breakthrough curves. Industrial & Engineering Chemistry Process Design and Development 2002;22(1):10-5. https://doi.org/10.1021/i200020a002
[131] Berdenova B, Pal A, Saha BB, Kaltayev A. Non-isothermal pore change model predicting CO2 adsorption onto consolidated activated carbon. International Journal of Heat and Mass Transfer 2021;177. https://doi.org/10.1016/j.ijheatmasstransfer.2021.121480
[132] Bollini P, Brunelli NA, Didas SA, Jones CW. Dynamics of CO2 Adsorption on Amine Adsorbents. 1. Impact of Heat Effects. Industrial & Engineering Chemistry Research 2012;51(46):15145-52. https://doi.org/10.1021/ie301790a
[133] Roušar I, Ditl P. Numerical Simulation of Multicomponent Isobaric Adsorption in Fixed Bed Columns. Adsorption Science & Technology 1986;3(2):49-59. https://doi.org/10.1177/026361748600300201
[134] Delgado JMPQ. A critical review of dispersion in packed beds. Heat and Mass Transfer 2005;42(4):279-310. https://doi.org/10.1007/s00231-005-0019-0
[135] Dixon AG. Correlations for wall and particle shape effects on fixed bed bulk voidage. The Canadian Journal of Chemical Engineering 1988;66(5):705-8. https://doi.org/10.1002/cjce.5450660501
[136] Wakao N, Funazkri T. Effect of fluid dispersion coefficients on particle-to-fluid mass transfer coefficients in packed beds. Chemical Engineering Science 1978;33(10):1375-84. https://doi.org/10.1016/0009-2509(78)85120-3

[137] Silcox GD, Noble JJ, Saforim AF, Wankat PC, Knaebel KS. In: Green DW, Southard MZ, editors. Perry's Chemical Engineers' Handbook. 9th Edition ed. New York: McGraw-Hill Education; 2019.
[138] Khurana M, Farooq S. Integrated Adsorbent Process Optimization for Minimum Cost of Electricity Including Carbon Capture by a VSA Process. AIChE Journal 2019;65(1):184-95. https://doi.org/10.1002/aic.16362
[139] Purdue MJ, Qiao Z. Molecular simulation study of wet flue gas adsorption on zeolite 13X. Microporous and Mesoporous Materials 2018;261:181-97. https://doi.org/10.1016/j.micromeso.2017.10.059
[140] Son KN, Weibel JA, Knox JC, Garimella SV. Calibration and uncertainty analysis of a fixed-bed adsorption model for CO2 separation. Adsorption 2018;24(8):781-802. https://doi.org/10.1007/s10450-018-9982-x
[141] Jeníková J, Michaliková K, Hrdlička F, Hrdlička J, Pilař L, Vodička M, et al. Applicability of Secondary Denitrification Measures on a Fluidized Bed Boiler. Acta Polytechnica 2022;62(3):341-51. https://doi.org/10.14311/ap.2022.62.0341
[142] Skopec P, Jeníková J, Vodička M, Hrdlička J, Pilař L, Michaliková K. NOx Reduction Using Pilot-Scale SCR Under Oxyfuel Conditions. SSRN Electronic Journal 2021. https://doi.org/10.2139/ssrn.3820592
[143] . Fakta o klimatu. Průměrná roční teplota v ČR. [cited 2023 4 April]. https://faktaoklimatu.cz/infografiky/teplota-cr]. Available from: https://faktaoklimatu.cz/infografiky/teplota-cr.
[144] Chloupková R. Analysis of stream thermal regime and effects on macroinvertebrate communities. Brno: Masaryk University; 2016.
[145] Chenoweth JM. Final Report of the HTRI/TEMA Joint Committee to Review the Fouling Section of the TEMA Standards. Heat Transfer Engineering 1990;11(1):73-107. https://doi.org/10.1080/01457639008939724
[146] Metrane A, Delhali A, Ouikhalfan M, Assen AH, Belmabkhout Y. Water Vapor Adsorption by Porous Materials: From Chemistry to Practical Applications. Journal of Chemical & Engineering Data 2022;67(7):1617-53. https://doi.org/10.1021/acs.jced.2c00145
[147] Xin F, Yuan ZX, Wang WC, Du CX. Experimental comparison of adsorption characteristics of silica gel and zeolite in moist air. Heat and Mass Transfer 2016;53(2):387-94. https://doi.org/10.1007/s00231-016-1829-y
[148] Gandhidasan P. Dehydration of natural gas using solid desiccants. Energy 2001;26(9):855-68. https://doi.org/10.1016/s0360-5442(01)00034-2
[149] Kumar S. Gas Production Engineering. Houston: Gulf Publishing Company, Book Division; 1987.
[150] Association GPS. GPSA engineering data book. 12th ed. Tulsa, Oklahoma: Gas Processors Suppliers Association; 2004.
[151] Towler G, Sinnott R. Design of pressure vessels. Chemical Engineering Design 2022. p. 441-95. https://doi.org/10.1016/b978-0-12-821179-3.00014-5
[152] Engineering C. Economic Indicators. Chemical Engineering. 2022:60.
[153] de Oliveira LH, Pereira MV, Meneguin JG, de Barros MASD, do Nascimento JF, Arroyo PA. Influence of regeneration conditions on cyclic CO2 adsorption on NaA zeolite at high pressures. Journal of CO2 Utilization 2023;67. https://doi.org/10.1016/j.jcou.2022.102296
[154] Jeníková J. Návrh opatření pro snížení emisí NOx kotlů Teplárny Otrokovice: České vysoké učení technické v Praze. Vypočetní a informační centrum.; 2017.
[155] Zhang G, Yan H, Li T, Zhu Y, Zhou S, Feng Y, et al. Relation analysis on emission control and economic cost of SCR system for marine diesels. Science of The Total Environment 2021;788. https://doi.org/10.1016/j.scitotenv.2021.147856
[156] Kučera J. Technology to remove nitrogen oxides (NOx) from flue gases for large combustion plants. Brno: Vysoké učení technické v Brně; 2020.

[157] Zhang Q, Wu Y, Yuan H. Recycling strategies of spent V2O5-WO3/TiO2 catalyst: A review. Resources, Conservation and Recycling 2020;161. https://doi.org/10.1016/j.resconrec.2020.104983
[158] Smith R. Process Economics. Chemical Process Design and Integration. 2nd ed: John Wiley & Sons, Ltd; 2016. p. 19-36.
[159] Stewart M. Materials selection for pressure vessels. Surface Production Operations 2021. p. 93-116. https://doi.org/10.1016/b978-0-12-803722-5.00004-5
[160] Turton R, Shaeiwitz J, Bhattacharyya D, Whiting W. Analysis, Synthesis, and Design of Chemical Processes. 5th ed. Boston: Pearson Education, Inc.; 2018. 1520 p.
[161] Najafi H, Najafi B, Hoseinpoori P. Energy and cost optimization of a plate and fin heat exchanger using genetic algorithm. Applied Thermal Engineering 2011;31(10):1839-47. https://doi.org/10.1016/j.applthermaleng.2011.02.031
[162] Guo-Yan Z, En W, Shan-Tung T. Techno-economic study on compact heat exchangers. International Journal of Energy Research 2008;32(12):1119-27. https://doi.org/10.1002/er.1449
[163] Vatavuk WM. Updating the CE plant cost index. Chemical Engineering 2002;109(1):62-70.
[164] Seider WD, Lewin DR, Seader JD, Widagdo S, Gani R, Ng KM. Cost Accounting and Capital Cost Estimation Product and Process Design Principles: Synthesis, Analysis and Evaluation. 4th ed. United States of America: John Wiley & Sons, Inc.; 2016. p. 426-97.

Publications of the Author

Articles

[MN1] Nedoma, M., & Netušil, M. (2021). CO_2 Separation from Flue Gases by Adsorption. *Chemical Engineering Transactions, 88*, 421-426. https://doi.org/10.3303/CET2188070

[MN2] Nedoma, M., Netušil, M., & Ditl, P. (2022). Experimental Investigation and Modelling of PSA Oxygen Generator in Context of Oxy-fuel Combustion. *Chemical Engineering Transactions*, *94*, 283-288. https://doi.org/10.3303/CET2294047

[MN3] Nedoma, M., Staf, M., & Hrdlička, J. (2022). Experimental and simulation study of CO_2 breakthrough curves in a fixed-bed adsorption process. *Acta Polytechnica*, *62*(3), 370-385. https://doi.org/10.14311/ap.2022.62.0370

[MN4] Nedoma, M., Netušil, M., & Hrdlička, J. (2023). Integration of adsorption based post-combustion carbon dioxide capture for a natural gas-fired combined heat and power plant. *Accepted for publication in Fuel (ISSN 0016-2361) on 29. 07. 2023.*

Conference contributions

(1) [MN1] Nedoma, M., & Netušil, M. (2021). CO_2 Separation from Flue Gases by Adsorption. In 24th Conference Process Integration, Modelling and Optimisation for Energy Saving and Pollution Reduction, PRES'21 - Brno.

(2) [MN2] Nedoma, M., Netušil, M., & Ditl, P. (2022). Experimental Investigation and Modelling of PSA Oxygen Generator in Context of Oxy-fuel Combustion. In *25th Conference Process Integration, Modelling and Optimisation for Energy Saving and Pollution* Reduction, PRES'22 - Croatia.

(3) Nedoma, M., Azzan, H., Yio, M. H. N., Danaci, D., Pini, R., & Petit, C. (2023). The effect of adsorbent shaping on the equilibrium and kinetic CO_2 adsorption properties of ZIF-8. In *6th Annual UKPorMat Conference*, Sheffield.